INVESTIGATION OF PROTEIN – PROTEIN INTERACTIONS UNDERLYING ALPHA-SYNUCLEIN AGGREGATION IN PARKINSON'S DISEASE

By

XUE YANG

A dissertation submitted to the

School of Graduate Studies

Rutgers, The State University of New Jersey

In partial fulfillment of the requirements

For the degree of

Doctor of Philosophy

Graduate Program in Chemistry & Chemical Biology

Written under the direction of

Jean Baum

And approved by

_____

_____

_____

_____

New Brunswick, New Jersey

January 2020

ABSTRACT OF THE DISSERTATION

Investigation of Protein – Protein Interactions Underlying Alpha-Synuclein Aggregation in Parkinson's Diseases

By XUE YANG

Dissertation Director:

Jean Baum

Alpha-synuclein (αSynuclein) accumulation and aggregation is related to many neurodegenerative diseases like Alzheimer's diseases, Parkinson's diseases, and dementia with Lewy bodies. However, the mechanism of αSynuclein aggregation and the relationship between aggregation pathways and toxicity are still unclear. Beta-synuclein (βSynuclein) is a homologue protein of αSynuclein with high sequence similarity but plays a different role in neurodegenerative diseases. βSynuclein has shown anti-Parkinson capacity in mouse models. In this work, we used βSynuclein as a comparison to answer why αSynuclein fibrils are good templates for seeding aggregation and what kind of interactions promote aggregate formation or inhibition. The work in this thesis explores

structure, toxicity, dynamic and seeding aggregation capacity of different αSynuclein oligomers and fibrils which provide critical information for therapeutic targets and designs.

By characterizing and comparing αSynuclein, βSynuclein and α/β co-incubated fibrils, we suggest that the stability and dynamics of the fibrils play an important role in controlling the fibril seeding aggregation ability. However, both αSynuclein and βSynuclein fibrils show similar cellular toxicity which suggest that seeding monomer aggregation is not the only contribution for fibril toxicity. Using solution NMR, we show that the initial step for fibril seeding is through interactions at the first 40 residues of the N-terminus. The interactions between αSynuclein stable oligomers and monomers are primarily located at the first 12 residues which results in inhibiting fibril seeding aggregation processes through competing interactions. Coupling these facts together suggests that peptides or small molecular targets that interact with the N-terminus of αSynuclein may be a good approach to inhibit αSynuclein seeding processes and increase the dynamics of fibril packing interfaces can be novel strategies to reduce amyloid toxicity.

Acknowledgements

I would like to thank all the people who helped me pursuing this degree. First and foremost, I would like to thank Prof. Jean Baum for giving me the opportunity to be her student and involving in the αSynuclein project. With her guidance and help, I can grow as a scientist and make contribution for understanding neurodegenerative diseases. I'm grateful that she is supporting me all the time and giving me the chances to work on the questions I'm interested in. Without her encouragement and advice, my graduate research would have never been completed.

I would also like to thank all the past and present group members. I want to thank Dr. Maria Janowska and Dr. Gina Moriarty trained me all the lab techniques and helped me to start my research. They are also my models in scientific area during these years. I appreciate Dr. Ana Monica Nunes and Dr. Cody Hoop's thoughtful suggestions; Dr. Jie Zhu's helpful discussion and Dr. Jonathan K. Williams and Dr.Baifan Wang's help in NMR. I would like to thank other lab mates for making the working environment full of joy – Tamr Atieh, Jonathan Roth, Jonathan Stoeber, Caitlyn Tobita and Ben Ashamole.

I thank all my committee members, Prof. Sagar Khare and Prof. Andrew Nieuwkoop help me finish my research and provide valuable suggestions. Special thanks to my outside committee member Dr. Maral Mouradian and postdoc from her lab Dr. Run Yan and Dr. Jie Zhang's help for cell culture.

Thank you to Dr. Seho Kim and Dr. Nagarajan Murali for keeping the NMR running and join my group meetings. Thank you to Dr. Alexei Emerakov's helping with lab equipment and sharing the knowledge about MS. Thank you to Prof. Vikas Nanda giving us the access to his lab equipment.

Thank you to my friends at Rutgers Dr. Wen Wu, Dr. Yingfu Lin and Dr. Yuanyuan Wang who make the graduate school life exciting. Special thanks to Dr. Mengjun Li's accompany and love for these years. Thank you to my middle school teacher Mr. Xuezhu Wang and high school teacher Ms. Xiangrong Liu who makes science so interesting and build up my confidence for majoring in science. Thank for Dr. Xinhui Liu as my undergraduate research advisor helped me understand what research is. I also want to thank Mr. Yanbin Hu who is a role model for me, and his music encouraged me all the time.

Lastly, I would like to thank my parents who give me unconditionally love. Without their support, I could study abroad and finish this thesis. I'm so proud to be their child.

Table of Contents

List of Figures

Chapter 1 – Introduction to the thesis

Neurodegenerative diseases are associated with different protein misfolding and aggregation processes. Up to date, no efficient diagnostic methods and cures have found for neurodegenerative diseases. The trigger for protein aggregation in these diseases is not well understood, but aging, environment and genes are believed to be the three main factors. Among all these factors, aging is the primary trigger. With longer life span, increasing populations are suffering from Alzheimer's disease, Parkinson's diseases and others. The mechanism and relationship between protein aggregation and neurodegenerative diseases is still unclear which make the therapeutic design more difficult. More information is needed to understand the mechanism of amyloid aggregate formation, their structures, dynamics and inter- or intra- interactions which will provide critical information for therapeutic design.

In this thesis, the focus is to investigate the aggregation of αSynuclein which is main protein component deposit in Lewy bodies – the hallmark of Parkinson's diseases (PD). βSynuclein, the homologue protein of αSynuclein which has a high sequence similarity but play a different role in PD is delaying or inhibiting the aggregation process of αSynuclein. Charactering the interactions between these two proteins and comparing the aggregate formation will provide valuable information. The questions include 1. How does βSynuclein influence αSynuclein aggregation and its toxicity? 2. What kind of interactions promote seeding of amyloid formation and what interactions inhibit or delay

the seeding processes. 3. What makes αSynuclein fibrils good template for seeding aggregation.

The anti-parkinsonian role of βSynuclein has been found for almost 20 years in mouse models and extensive work has been done to understand the interactions between α and β Synuclein at different aggregation stages. However, the molecular level understanding for how βSynuclein inhibits αSynuclein aggregation and reduces the toxicity is still unknown. In Chapter 2, we have a review about the interactions between αSynuclein and its aggregation inhibitors – βSynuclein. First, we briefly introduce the relationship between αSynuclein aggregation and synucleinopathies and summarize the interaction partner of αSynuclein which may affect the aggregation pathway. Then we focus on βSynuclein where βsynuclein monomer can interact with αSynuclein at different stages – monomer, oligomers and fibrils. These different interactions can result in different influences on cellular activities.

Based on the information about αSynuclein and βSynuclein interactions in the literature, we set out to understand how βSynuclein influences αSynuclein amyloid fibril formation and toxicity. In Chapter 3, we characterized and compared αSynuclein fibrils and amyloid fibrils formed in the presence of βSynuclein. Amyloid fibril formed with βSynuclein showed reduced cytotoxicity and seeding aggregation ability which may result from the increased dynamics in the fibril filament packing interface. For future therapeutic design, molecules or interactions which can increase the flexibility of amyloid

fibrils may be a new approach to reduce the seeding aggregation ability and cytotoxicity of amyloid fibrils. We also characterized how βSynuclein influences αSynuclein oligomer formation by western blot and AFM which suggestS that βSynuclein can inhibit certain types of αSynuclein oligomer formation. Chapter 3 indicates that βSynuclein is not only influences αSynuclein monomers or certain aggregates, that can influence the whole aggregation pathway.

After investigating the interactions between α and β synuclein, we focus on αSynuclein oligomers. We try to understand what the role of stable αSynuclein oligomers play during aggregation processes or how stable αSynuclein oligomers influence the fibril formation. We made two types of stable oligomers under physiological fibril forming conditions. Our data suggest that these stable oligomers are on the off-fibril formation pathway and also inhibit fibril seeding processes. By comparing the interaction between monomers and stable oligomers or fibrils, we found that a competing interaction with monomers is one of the reasons for the inhibition seeding effect. The interaction between monomers and stable oligomers and monomers and fibrils are very similar, but fibrils can seed monomers to form more amyloid fibrils while stable oligomers cannot. By comparing the differences in interactions between monomers and stable oligomers, and monomers and fibrils may shed light on the interactions that contribute to seeding processes.

Stable oligomers and fibrils are formed in different pathways, and fibrils have the intrinsic ability to recruit monomers to form fibrils while stable oligomers do not have these properties. In order to understand why fibrils have this unique seeding ability, we

use solution NMR to characterize the dynamic nature of these aggregates in chapter 5. It has been shown in the literature that amyloid fibrils are dynamic species in solution, they are in equilibration with monomers. The interaction between fibril and its own equilibrium monomer is a critical biological process which may be the first step for seeding process. By comparing the equilibrium in fibrils and stable oligomers, we provide valuable information for the dynamics of different aggregates and interactions that contribute to seeding processes.

In chapter 6, we continue to understand the seeding process of αSynuclein fibrils. We used amyloid fibrils formed by βsynuclein as comparison to get the information about what makes αSynuclein fibril a good seeding template. By comparing the seeding ability, cytotoxicity, stability and structure of these two amyloid fibrils, we found that stable structures may be essential for seeding. βSynuclein fibrils do not have a good seeding ability as αSynuclein fibrils, but they can induce the same level of cell viability decrease which suggest that seeding aggregation is not the only reason for amyloid fibril toxicity but that other properties of amyloid fibrils contribute to their cytotoxicity.

In this PhD research, we characterized different aggregates formed by αSynuclein or βSynuclein and their dynamics. Our goal is to understand the aggregation process of αSynuclein and investigate the interactions which can inhibit the aggregation to provide critical information for therapeutic design.

Chapter 2 – A review of interactions between α-synuclein and β-synuclein

2.1 Publication information

2.1.1 Title

Interactions between the Intrinsically Disordered Proteins β-Synuclein and α-Synuclein

2.1.2 Author Information

Jonathan K. Williams, Xue Yang and Jean Baum

Department of Chemistry and Chemical Biology, Rutgers University, Piscataway, New Jersey 08854

Corresponding author: Jean Baum; Dept. of Chemistry and Chemical Biology, Rutgers University, 610 Taylor Rd., Piscataway, NJ 08854; Tel.: 848-445-5284; Email: baum@chem.rutgers.edu

2..1.3 Abstract

Several intrinsically disordered proteins (IDPs) have been implicated in the process of amyloid fibril formation in neurodegenerative disease and developing approaches to inhibit the aggregation of these IDPs is critical for establishing effective therapies against disease progression. The aggregation pathway of the IDP alpha-synuclein (αS), is implicated in several neurodegenerative diseases known as synucleinopathies and has been extensively characterized. Less attention has been leveraged on beta-synuclein (βS), a homologous IDP that co-localizes with αS and is known to delay αS fibril formation. In this review, we focus on βS and the molecular-level interactions between αS and βS that underlie the delay of fibril formation. We highlight studies that begin to define αS and βS

interactions at the monomer, oligomer, and surface levels, and suggest that βS plays a role in regulation of inhibition at many different stages of αS aggregation.

2.1.4 Abbreviations

IDP, intrinsically disordered protein; αS, alpha synuclein; βS, beta synuclein; PD, Parkinson's disease; DLB, dementia with Lewy bodies; MSA, multiple-system atrophy; LB, Lewy body; CD, circular dichroism; AAV, adeno-associated virus; PRE, paramagnetic relaxation enhancement; MTSL, *S*-(1-oxyl-2,2,5,5-tetramethyl-2,5-dihydro-1H-pyrrol-3-yl)methyl methanesulfonothioate; ThT, thioflavin T; PMF, potential of mean force; DMPS, 1,2-dimyristoyl-*sn*-glycero-3-phospho-L-serine.

2.1.5 Keywords

alpha synuclein; beta synuclein; intrinsically disordered protein; protein-protein interaction.

2.2 Introduction: Synucleinopathies and Aggregation

The role and actions of intrinsically disordered proteins (IDPs) have become an area of intense interest, with IDPs now being identified to play important roles in many biological processes including cellular signaling,(*1*) phase separation,(*2, 3*) and transcription and translation.(*4, 5*) But beyond their normal physiological functions, IDPs have also been found to contribute to several human neurodegenerative diseases (e.g. Parkinson's disease (PD), Alzheimer's disease, Huntington's disease, spongiform encephalopathies, dementia with Lewy Bodies (DLB)) and non-neuropathic amyloidoses (e.g. type II diabetes, ApoAI amyloidosis, atrial amyloidosis),(*6*) which are characterized by the accumulation, misfolding, aggregation and deposition of an IDP into amyloid

plaques. While the amyloid diseases involving IDPs are relatively well-known by the general public, it is also true that natively folded proteins also misfold and aggregate to cause human amyloid diseases.(*7*) It has been found that folded proteins on-average contain more amyloidogenic sequences than IDPs.(*8*) Understanding the mechanism of amyloid plaque formation beginning from the native IDP or folded protein, and developing approaches to inhibit aggregation, is critical for establishing effective therapies against disease progression. In the case of PD, DLB, and multiple system atrophy (MSA), the aggregation of the 140-residue IDP alpha-synuclein (αS) has been implicated in the disease etiology.(*9-13*) A second member of the synuclein family, beta-synuclein (βS), is a 134-residue IDP that is co-expressed and co-localizes with αS,[*14-16*] and has been found to inhibit αS fibril formation and reduce the formation of LBs.(*17, 18*) The molecular mechanisms of the interaction between βS and αS, and the stages of the aggregation pathway at which these interactions arise, has been the subject of recent investigations. In this review, after a brief introduction of αS and known modulators of its aggregation, we discuss the nature of βS and its interaction with αS along the aggregation pathway to highlight how the IDP βS modulates αS aggregation.

A large body of work exists on trying to understand the conformational preferences of monomeric IDPs, and in establishing conformational ensembles from experimental parameters and computational modelling that accurately reflect the intrinsic disorder.(*19-23*) For αS and βS in particular, an irregular distribution of charged residues allows for different domains of the IDPs to be described as polyampholyte or polyelectrolyte,(*24*) which can influence the conformational preferences of the IDP ensemble.(*25*) The N-

terminal domains of αS and βS exhibit a slight net-positive charge, while the C-terminal domains are negatively charged, with βS more so than αS (**Fig. 1**). These domains can participate in intra-chain, as well as inter-chain, electrostatic interactions.(*18, 26*) The synucleins have been observed to transiently adopt both compact and extended structures, with the N-terminal domain displaying a higher propensity to form α-helices, especially in the presence of membranes, while the C-terminal domain tends to adopt more extended structure, likely due to the higher proportion of proline residues present (**Fig. 1**).(*27-34*)

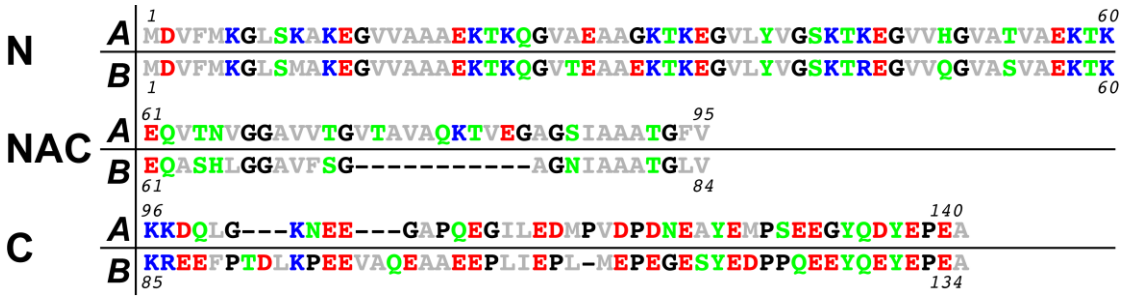

Figure 1. Comparison of the aligned(35) primary sequences of aS (A) and bS (B). Residues are colored by hydrophobic (gray), positively charged (blue), negatively charged (red), and polar-uncharged (green) residues.

The aggregation pathways of many of the disease implicated IDPs, *in vitro*, can be described by a general mechanism of amyloid formation. IDP partners interact and nucleate directly from monomers to form primary nuclei, which can immediately undergo elongation, secondary nucleation and fragmentation to proliferate and grow.(*36-39*) These molecular processes occur during all three phases (lag phase, growth phase, plateau phase) of the detected macroscopic aggregation profile, with rates and activities that vary with time.(*40, 41*) Several factors have been found to modulate the rate of αS

aggregation, including pH, temperature, post-translational modifications, agitation, salt concentration, surfaces, and chaperone proteins.(*36, 37, 42, 43*) Post-translational modifications may play a role in disease progression, with hyperphosphorylation of Ser129(*44*) and small ubiquitin-related modifiers (SUMOylation) at K96 and K102 found in LBs.(*45*) Various small molecules, peptides, and proteins have been shown to inhibit αS at various stages of the aggregation process. The antibiotic rifampicin was shown to inhibit fibril formation and disaggregate existing fibrils *in vitro*,(*46*) while a mouse model of MSA showed marked reductions in monomeric, oligomeric, and S129 phosphorylated forms of αS with rifampicin treatment.(*47*) Nortriptyline, an antidepressant, was found to delay the onset of fibril formation *in vitro* and showed some efficacy *in vivo* in protecting from αS neurotoxicity, and was suggested to bind directly to the αS monomer.(*48*) The natural product squalamine reduced αS aggregation both *in vitro* and *in vivo*, by displacing αS from the surfaces of lipid vesicles.(*49*) Small heat shock proteins (Hsps) have been found in LBs, and may play roles in directing αS folding and aggregation. Although the interactions between αS and Hsps was found to be weak and transient,(*50*) several (HspB8, Hsp27, Hsp70, α-crystallin) were found to prevent or reduce the formation of mature αS fibrils *in vitro* and provide neuroprotection *in vivo*.(*50-54*)

Targeting an intrinsically disordered protein with a small molecule, peptide or a second IDP differs from the traditional approach to drug design, in which the drug molecule typically targets a well-defined protein fold. Instead, for targeting an IDP, the promiscuity of interactions and the ensemble of interconverting IDP conformers must be considered,(*55*) a field which is still in development.(*56*) Interestingly, a few examples of direct IDP-IDP

interactions have been identified recently, including the histone H1/prothymosin-α high affinity complex(*57*) and the 4.1G/NuMA proteins,(*58*) bringing up the possibility of utilizing a second IDP to target αS monomers in the earliest stages of aggregation. The remainder of this review will focus on the intrinsically disordered βS and its interactions with αS, its own potential cytotoxicity, and its potential utility as a therapeutic intervention to inhibit αS aggregation.

2.3 The Curios Case of β-Synuclein: Natural Inhibitor or Cytotoxic Homologue?

The IDP sequences of αS and βS contain ~78% sequence similarity and are described by an N-terminal region that contains several imperfect KTKEGV repeats, a hydrophobic NAC region, and a highly negatively charged C-terminal region (**Fig. 1**). Despite their similarities, the sequences differ significantly in the NAC region due to a 11-residue deletion, and βS contains more negatively charged residues and prolines than αS in the C-terminal region (**Fig. 1**). Studies of average secondary structure by circular-dichroism (CD) and hydrodynamic radius indicated that βS adopts a more unfolded conformation relative to αS at neutral pH.(*42*) NMR measurements of the residual structural ensembles of these two IDPs in solution also found that βS had a reduced propensity for α-helical secondary structure in the N-terminal region compared to αS, while the C-terminus of βS adopted extended conformations.(*28, 30*) Unlike αS, βS does not aggregate to form fibrils under normal physiological conditions;(*42*) instead, fibrillation can be induced under a variety of conditions, including acidic pH,(*59*) metal ions and certain pesticides,(*60*) and in the presence of lipid vesicles at elevated temperatures.(*61*) We have recently found that a single-residue mutation located between the N-terminal and NAC domains (E61A) is sufficient to remove the pH-dependence of βS fibril formation, and allows it to form fibrils

at a rate comparable to αS fibril formation at neutral pH.(*59*) Despite its sequence similarity to αS, wild-type βS is not known to contribute to any of the synucleinopathies in humans, and instead has been found to provide some neuroprotective effects *in vivo*,(*17, 62*) and acts as an inhibitor of αS aggregation *in vitro*.(*17, 18, 42, 63-65*) However two missense mutations of βS, V70M and P123H, have been linked to DLB,(*66*) and P123H βS can produce neurodegeneration in a transgenic mouse model;(*67*) these have been proposed as "toxic gain-of-function" mutations that may occur in sporadic or familial synucleinopathies.(*68*) The conformational ensemble of P123H βS was found to be more αS-like (i.e. more flexible), which allows for this mutated βS to aggregate. Conformational differences of IDP monomers which effect their aggregation propensities have also recently been identified with the tau protein.(*69*) The normal inhibitory properties of βS were also lost with the P123H mutation, and suggests that the extended structure of the proline-rich C-terminus is important for inhibiting αS fibril formation.(*70*)

Recently, the notion that wild-type βS may itself cause neurodegeneration has been proposed in the literature. Overexpression of βS in cultured primary cortical neurons led to cell loss and signs of metabolic impairment, but to a lesser extent than overexpressing αS neurons.(*71*) A further *in vivo* rat model showed slower signs of neurodegeneration upon infection with βS containing adeno-associated virus (AAV) vectors consistent with the cultured neurons, but eventually reached the same level of dopaminergic cell loss as αS (8 weeks βS vs. 2 weeks αS).(*71*) When expressed in *Saccharomyces cerevisiae* (yeast), βS was found to form toxic cytosolic inclusions in a similar manner to αS.(*72*) Even more interestingly, when βS and αS were co-expressed in yeast the cytotoxicity increased, even

though hetero-dimers of αS and βS were found to exist, which were previously implicated as an important step in inhibition of αS aggregation by βS.(*18*) Upregulation of SUMOylation machinery in yeast provided a protective effect to βS toxicity.(*73*) These results warrant more study in the future to determine the basis of βS toxicity in yeast, and whether it is applicable to the synucleinopathies in humans.

2.4 The Interactions Between α-Synuclein and β-Synuclein

The interactions between βS and αS have been found to occur at three levels: through the formation of hetero-dimers (i.e. monomer-monomer interactions), through the formation of hetero-oligomers, and by influencing secondary nucleation processes (e.g. competition for binding on surfaces).

Monomer-monomer Interactions Between βS and αS

Mapping the interactions between IDPs is an inherently difficult task due to their transient nature, and is amenable to characterization by only a few experimental techniques.(*21, 74-76*) To investigate monomer-monomer interactions between αS and βS, one approach has been to use solution-state NMR paramagnetic relaxation enhancement (PRE) measurements to probe weak and transient inter-chain interactions.(*77, 78*) In the PRE experiment, a paramagnetic probe is incorporated into the sequence of one protein that is not isotopically labeled with $^{15}N/^{13}C$ (NMR-invisible), and its effect on the relaxation parameters of another $^{15}N/^{13}C$ isotopically labeled protein (NMR-visible) is recorded. For synuclein, to probe the interaction between αS and βS monomers, cysteine mutations to residues 11, 44, 90 and 132 on αS and 11, 44, 80, and 134 on βS were introduced in order to incorporate a paramagnetic nitroxide spin label (MTSL); then NMR spectra were

recorded of combinations of wild-type ^{15}N labeled αS or βS (NMR-visible) and ^{14}N MTSL labeled αS or βS (NMR-invisible) protein.(*18*) This allowed for the observation of αS/αS, βS/βS and αS/βS interchain interactions. It was found that αS homo-dimer interactions exhibit both transient head-to-head and head-to-tail orientations, while αS/βS hetero-dimer interactions were only found to have weak and transient head-to-tail oriented interactions. NMR PRE titration experiments found that residue specific K_d's for the αS/βS hetero-dimer were ~100 μM (range 40-350 μM), while the αS/αS homo-dimer K_d's were ~500 μM (range 90-1200 μM).(*18*) Brown et. al. also found the interaction between the αS and βS monomers to be very weak. When equimolar amounts of βS monomer and αS monomer were incubated together in the presence of pre-formed αS seed-fibrils under quiescent conditions, no change in the aggregation behavior of αS was observed, suggesting that direct αS and βS interactions are extremely weak and indicating that βS does not interfere with αS fibril elongation.(*64*) Homo-dimer interactions between βS monomers were not detected, indicating that any such interactions are extremely weak, consistent with βS's propensity to not form fibrils.(*18*) The NMR data suggest that the sampling of transient dimer conformations promotes the very earliest stages of aggregation or inhibition. In this model, homotypic head-to-head interactions of αS dimers prefer aggregation, while the heterotypic head-to-tail interactions of αS/αS and αS/βS complexes prevent misfolding of αS by having to undergo conformational rearrangement to form the parallel arrangements of monomers in mature fibrils.(*79*)

In a separate, more indirect approach to probe αS and βS interactions, a small library of domain-swapped αS/βS chimeras were used to isolate the contributions of the N-terminal,

NAC, and C-terminal sequence domains to the inhibitory interaction between αS and βS.(*80*) Thioflavin-T (ThT) fluorescence assays showed the greatest degree of inhibition of fibril formation when αS was incubated in the presence of chimeras containing both the N-terminal and C-terminal primary sequence domains of βS simultaneously; having only the βS N-terminal or C-terminal domain (relative to a fixed NAC domain) resulted in a lesser degree of inhibition.(*80*) This suggests that the inhibitory interactions are spread over multiple locations, at both the N- and C-termini, and may be cooperative. Taken together, these PRE and fluorescence measurements suggest that head-to-tail conformations, which exist in both the αS homo-dimer and αS/βS hetero-dimer complexes and are mediated by interactions between the N- and C-termini, may provide a regulatory role in slowing down the conformational rearrangements needed to form aggregation-promoting head-to-head conformations.

A recent molecular dynamics and potential of mean force (PMF) computational study was conducted to better understand the strength of the association between αS and βS.(*81*) Since there is no PDB structure of βS, the authors created a starting structure of βS by using the I-TASSER server, which aims to predict protein structures by using templates from the PDB in combination with iterative template fragment assembly simulations.(*82*) The starting structure for βS that was created by the I-TASSER server is very similar to that of the micelle-bound αS (PDB ID: 1XQ8(*83*)) that the authors chose to use as a starting point; namely, that there is a kinked α-helix in the N-terminus of each of the starting αS and βS structures. The authors found the atomic contact energy of the αS/βS dimer to be more negative relative to the αS/αS dimer, indicating a larger contact surface area of the

heterodimer. The PMF calculations showed that the energy barrier for dissociation was twice as high for the αS/βS hetero-dimer complex than for the αS/αS homo-dimer. Taken together, the authors conclude that it is more favorable for αS to complex with βS to form hetero-dimers, rather than a second αS to form homo-dimers.(*81*)

A second molecular dynamics study, again using structures derived from micelle-bound synuclein, found more favorable electrostatic energies of formation for αS/βS head-to-tail hetero-dimer complexes relative to αS/αS dimers, leading to the formation of stable αS/βS non-propagating complexes.(*84*) It was also observed that binding of a βS monomer to a preformed αS homo-dimer was stronger than the binding of an additional αS monomer to the homo-dimer. These experimental NMR and computational studies show the ability of βS to interact with and interrupt αS aggregation very early in the process, at the point where αS and βS monomers interact in both a solution state and in surface-associated conformations.

βS Interactions with αS Oligomers

The trending hypothesis for the IDP-misfolding diseases now favors an oligomer-centric model as the cause of neurodegeneration,(*85*) with the oligomers causing membrane disruption or providing seeding activity for propagation of aggregation cell-to-cell.(*86, 87*) As the αS aggregation process continues, higher order oligomers of both an amorphous and ordered “proto-fibril” nature are formed, and it becomes crucial to understand the potential for βS to interact with αS oligomers and how this may affect the mechanism by which βS alters the kinetics of αS fibril formation. Single-molecule fluorescence measurements of

αS/βS interactions in a cell-free expression system showed that βS inhibits αS aggregation at the earliest stages, by preferentially incorporating into small oligomers.(*65*) Two-color coincidence fluorescence assays, where αS is tagged with sGFP and βS is tagged with mCherry, showed that βS replaces αS in small oligomers as the ratio of βS:αS increases, suggesting that βS is able to shield αS/αS homotypic interactions and inhibit further self-oligomerization.(*65*) The ability of βS to inhibit aggregation of pathological mutations of αS, associated with familial forms of PD (A30P, G51D, E46K, H50Q, A53T), were also investigated. In the cell-free system, the mutants A30P and G51D were found to form small oligomers while E46K, H50Q and A53T formed larger aggregates and fibrils. Interestingly, βS was observed to efficiently inhibit aggregation of A30P and G51D mutants, while it did not efficiently interfere with aggregation of the other three mutants, although βS has previously been observed to delay the lag time of A53T proto-fibril and fibril formation.(*63*) Taken together, these single-molecule fluorescence measurements provide evidence that βS interacts with early stage oligomers to inhibit aggregation of αS.

βS Influence on αS Surface Interactions

The normal physiological function of αS is not well understood, but it is thought to play a role in membrane remodeling and presynaptic vesicle release;(*88*) during disease progression, αS oligomers are thought to disrupt cell membranes.(*89*) Recent experimental evidence has provided several examples of αS and βS interactions with lipid membranes,(*64, 84, 89-91*) and both αS and βS have been found to interact with micelle and lipid-bilayer surfaces, with the N-terminal region adopting an α-helical secondary

structure(*29, 92*) and the charge composition and curvature of the membranes significantly affecting the degree of binding.(*91*)

Assessment of the binding affinity of βS to lipid vesicles found that βS has a 5-fold lower affinity for DMPS (1,2-dimyristoyl-*sn*-glycero-3-phospho-L-serine) vesicles relative to αS, and does not show any lipid-induced increase in amyloid formation compared to the increase in αS amyloid formation.(*64*) However, more recently βS has been found to form DMPS lipid-induced protofibrils and mature fibrils when at an elevated temperature (60°C).(*61*) In the former study, βS was found to decrease the rate of αS amyloid formation in a dose-dependent fashion, indicating that βS is inhibitory in the presence of lipid membranes.(*64*) Further investigation determined that βS inhibited αS aggregation by competing for binding to the surface of the liposomes, and by a similar mechanism, βS also inhibited the auto-catalytic surface interactions(*37*) of αS monomers by competing for binding to the surface of αS fibrils.(*64*) The auto-catalytic surface interactions are described as a secondary-nucleation process, whereby already formed αS fibrils are able to template the nucleation of free monomers, which can then go on to form fibrils and further template nucleation and so on. This results in a significantly faster fibril growth profile relative to only growth by elongation of fibrils.(*36, 37, 93*) It should be noted that the mechanism of inhibition proposed by Brown et. al. does not rely on direct interaction between αS and βS, but is rather a competition between αS and βS for binding sites on surfaces,(*64*) and is therefore distinct from the inhibition mechanisms discussed in the previous sections which rely on direct αS and βS interactions.(*18, 65*)

Inhibition of proteasomal degradation has been implicated as a contributing factor in Parkinson's disease, and there is evidence that αS binds to and inhibits a component of the 26S proteasome.(*94*) Further, βS was shown to prevent proteasomal inhibition of αS by either interacting directly with αS monomers and aggregates or by competition with the binding interface on the proteasome.(*95*)

2.5 Perspectives

While it is established that βS can reduce or inhibit the formation of αS fibrils *in vitro*, and is able to provide some neuroprotective effect *in vivo*, the mechanisms by which this arises are still not well understood. Here we have reviewed recent work on the different stages at which αS is inhibited by βS, and begin to provide a molecular description of the key interactions between αS and βS that arise in the early and later stages of αS assembly (**Fig. 2**). The aggregation of αS has been well characterized, and αS is known to adopt an intrinsically disordered conformation in solution (**Fig. 2**, *top row*). It can transiently form homotypic head-to-head interactions, leading to further aggregation, or off-pathway head-to-tail interactions. As more monomers are added to the initial aggregation nucleus, oligomers of a disordered, amorphous nature are formed; eventually a conformational change occurs, and the β-sheet content of these oligomers increases, transforming into "proto-fibrils." These proto-fibrils can undergo elongation to become mature amyloid fibrils, as well as participate in various secondary nucleation processes to seed new fibril growth. On the other hand, the aggregation process of βS has been less extensively characterized (**Fig. 2**, *middle row*). βS is intrinsically disordered in its monomeric state in solution, but no homotypic monomer-monomer interactions have been observed. It can

form unstructured oligomers, but does not continue to aggregate to form fibrils unless mutations are introduced or non-physiologically neutral conditions are used.

The mechanisms of inhibition of αS by βS are just beginning to be understood and indicate that βS interacts with αS at several different levels in the aggregation pathway (**Fig. 2**, *bottom row*). αS/βS can form transient dimeric complexes of heterotypic head-to-tail interactions, form hetero-oligomeric complexes, and interact with the surface of αS fibrils to disrupt secondary nucleation processes. Further and more detailed characterization of the different intermediates along the aggregation pathways will help determine possible targets for therapeutic intervention. However, the difficulties of characterization here often stem from the inability to isolate and purify a specific oligomer out of a complex mixture of species along the aggregation pathway, or the amorphous nature of the oligomer itself, which preclude high resolution structural characterization. Further development and optimization of methods and techniques designed to purify and characterize this oligomer continuum, as well as methods to better define, simulate and model these ensembles, are needed in order to provide atomic-resolution detail on these important components of amyloid pathology, and bring light to one corner of this dark proteome. The studies reviewed here begin to provide a fundamental mechanistic understanding of how βS inhibits aggregation of αS, and highlight how interactions between βS and αS at the different stages of aggregation may create novel opportunities for developing therapeutic strategies to combat Parkinson's disease.

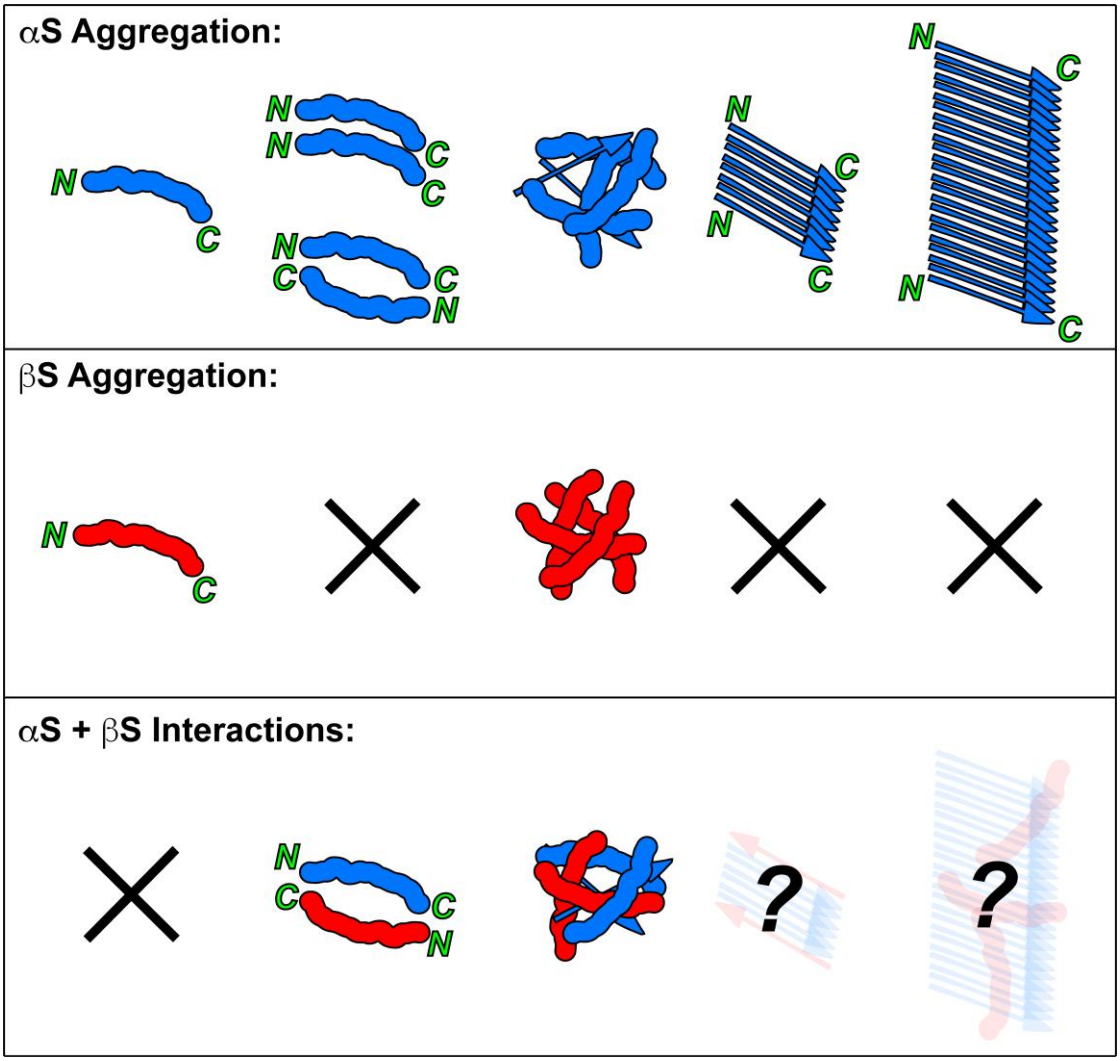

Figure 2. Summary of the species observed along the aggregation pathways of αS (top row), βS (middle row), and αS/βS together (bottom row). αS can exist as a monomer, dimer, amorphous oligomer, proto-fibril, and mature fibril. βS exists primarily as a monomer, but can aggregate to form disordered oligomers. βS may delay αS aggregation by forming head-to-tail dimer complexes, hetero-oligomers, or by altering secondary nucleation properties.

Chapter 3 Characterization oligomers and fibrils formed by co-incubation of α and βSynuclein

3.1 Publication information

3.1.1 Title

Increased Dynamics of α-Synuclein Fibrils by β-Synuclein Leads to Reduced Seeding and Cytotoxicity

3.1.2 Author Information

Xue Yang[1$], Jonathan K. Williams[1$], Run Yan[2], M. Maral Mouradian[2], and Jean Baum[1*]

[1]Department of Chemistry and Chemical Biology, Rutgers University, Piscataway, New Jersey 08854

[2]RWJMS Institute for Neurological Therapeutics, Rutgers Biomedical and Health Sciences, and Department of Neurology, Robert Wood Johnson Medical School, Rutgers University, Piscataway, New Jersey, 08854

[$]These authors contributed equally to this work.

Corresponding author: Jean Baum; Dept. of Chemistry and Chemical Biology, Rutgers University, 123 Bevier Rd., Piscataway, NJ 08854; Tel.: 848-445-5284; Email: baum@chem.rutgers.edu

3.1.3 Abstract

Alpha-synuclein (αS) fibrils are toxic to cells and contribute to the pathogenesis and progression of Parkinson's disease and other synucleinopathies. β-Synuclein (βS), which co-localizes with αS, has been shown to provide a neuroprotective effect, but the

molecular mechanism by which this occurs remains elusive. Here we show that αS fibrils formed in the presence of βS are less cytotoxic, exhibit reduced cell seeding capacity and are more resistant to fibril shedding compared to αS fibrils alone. Using solid-state NMR, we found that the overall structure of the core of αS fibrils when co-incubated with βS is minimally perturbed, however, the dynamics of Lys and Thr residues, located primarily in the imperfect KTKEGV repeats of the αS N-terminus, are increased. Our results suggest that amyloid fibril dynamics may play a key role in modulating toxicity and seeding. Thus, enhancing the dynamics of amyloid fibrils may be a strategy for future therapeutic targeting of neurodegenerative diseases.

3.2 Introduction

Parkinson's disease (PD) is a progressively debilitating neurodegenerative disorder that is estimated to affect 1% of the world's population over the age of 60(*96*). Amyloid fibril deposits of the protein alpha-synuclein (αS) are found in Lewy bodies (LB) and Lewy neurites (LN)(*97, 98*) in the substantia nigra and other brain regions of PD patients. Myriad evidence shows that αS fibrils are toxic to cells(*99-102*), yet the precise role of αS in the pathology of PD and other synucleinopathies is still unclear.

Several hypotheses have been proposed to explain the experimentally observed cellular toxicity of the fibrils. Among these, seeding-propagation is a proposed mechanism to explain the observed cytotoxicity of the fibrils and the progressive nature of the disease. This process involves the release of mature αS amyloid seeds from the cell(*103-105*) that can then be taken up by a neighboring cell(*86, 105*); these seeds then template the further misfolding and aggregation of endogenous monomeric αS in the recipient cell(*102, 106*).

Fibril polymorphism and protofilament packing have been shown to play an important role in seeding capacity and toxicity(*101, 107-110*), while the ability of the fibrils to "shed" oligomer and protofibril species may also contribute to cellular toxicity and propagation(*111, 112*). Previous studies have identified some of the cellular-level details of the internalization, seeding, and propagation of αS fibrils(*86, 105, 113-121*). However, these studies lack the information needed to understand the molecular details of how fibrils can template further aggregation, and critically, the mechanisms by which αS fibril seeding of endogenous αS is affected by inhibitors of αS aggregation.

Beta-synuclein (βS), a homologous protein which is co-localized with αS and is expressed at variable levels relative to αS in different synucleinopathies(*122, 123*), has been recognized as a natural inhibitor of αS aggregation(*124*). A transgenic mouse model that simultaneously expresses both human αS and βS had fewer inclusions and less neurodegeneration compared with only αS-expressing transgenic mice(*124*). Interestingly, no detectable amount of βS has been found in LB(*125, 126*) even though βS can be over-expressed in certain parts of the PD brain(*122*), begging the question of how exactly βS interacts with αS to provide neuroprotection and influence αS fibril-induced cellular toxicity.

We have previously investigated the sequence and domain level interactions that mediate the influence of βS on the aggregation and fibril formation of αS(*59, 80*). We have found that head-to-tail transient complexes between βS and αS(*127*), mediated by multi-pronged N- and C-terminal interactions(*80*), provide enough of a kinetic trap at the earliest stages

of αS aggregation to slow down the assembly of αS into fibrils. However, even though βS slows down αS aggregation and reduces the overall αS fibril load in a concentration dependent manner(*127, 128*), it does not fully abolish αS fibril formation. Therefore, a detailed understanding of the conformational properties and cytotoxicity of αS fibrils formed in the presence of βS will provide us with a deeper understanding of the mechanisms underlying fibril toxicity.

Here, we show that co-incubation of the monomeric intrinsically disordered αS with the monomeric intrinsically disordered βS results in unique "co-incubated αS/βS" fibrils that show a significant reduction in cellular toxicity, a reduction in seeding capacity, and are more resistant to fibril shedding. Solid-state NMR experiments revealed that while the overall structure of the core of αS/βS fibrils is minimally perturbed, the imperfect KTKEGV consensus motif repeats of αS in the preNAC N-terminus become dynamic and more water accessible. Our results offer insight into the mechanism of amyloid fibril toxicity and highlight that increased dynamics of co-incubated αS/βS fibrils may interfere with their templating ability, thereby reducing their seeding capacity. Targeting amyloid fibrils by enhancing their dynamics may be a new strategy in designing therapeutics against neurodegenerative diseases.

3.3 Results

Co-incubation with βS Induces Subtle Differences in αS Fibril Morphology.

We studied the differences in the morphology of αS fibrils formed from the incubation of monomeric N-terminally acetylated αS, and αS fibrils formed by co-incubation of

monomeric N-terminally acetylated αS with monomeric N-terminally acetylated βS at a 1:3 ratio (called αS/βS co-incubated fibrils). We have used the N-terminally acetylated forms of αS and βS, since this post-translational modification is constitutively present in the native forms of these intrinsically disordered proteins(*129, 130*). Consistent with our previous work(*80, 127*), βS delays αS fibril formation in the Thioflavin T (ThT) aggregation assay (**Fig. 4**), whereby the co-incubation of αS with βS results in a longer lag time and slower growth kinetics compared with αS by itself. Fibrils formed as the end products of these two monomer aggregation assays display differences in their polymorph composition. Atomic force microscopy (AFM) images show that αS by itself (**Fig. 3a**) forms long straight or twisted fibril polymorphs, similar to previous reports(*107, 131, 132*), while co-incubated αS/βS forms fibril polymorphs that are shorter and straight (**Fig. 3b**), with no discernable twisting pattern. On average, the height of αS fibrils (6.0 ± 1.1 nm) tends to be shorter than αS/βS fibrils (7.9 ± 1.7 nm) (**Fig. 3c**), while the length of αS/βS fibrils (0.3 ± 0.2 μm) tend to be shorter than αS fibrils (0.5 ± 0.4 μm) (**Fig. 3d**).

We quantified the monomer composition of the co-incubated αS/βS fibrils to try to ascertain whether these morphological changes could be induced by incorporation of βS into the protofilaments that make up the fibril. Mature fibrils were solubilized in 4M guanidine hydrochloride and analyzed by ESI-MS. Surprisingly, the co-incubated αS/βS fibrils are composed of less than 6% βS (**Fig. 4**).

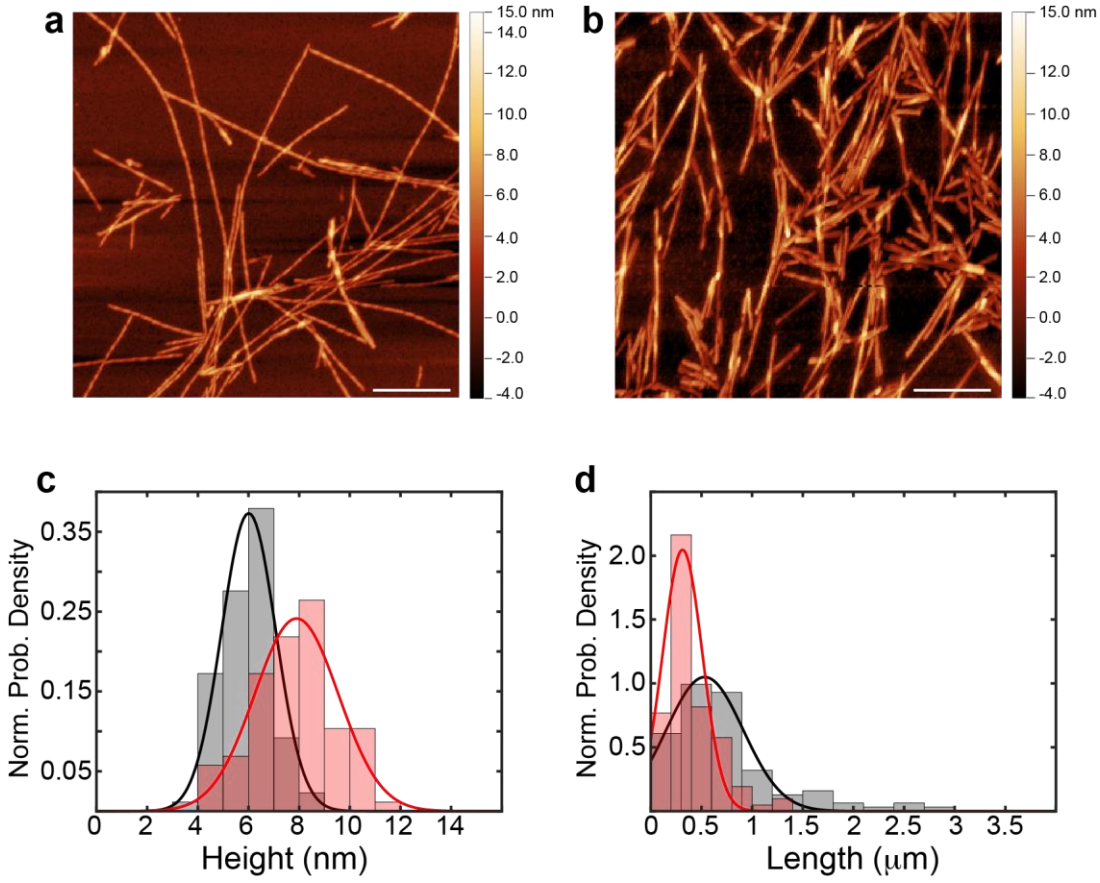

Figure 3. Morphological differences between αS and co-incubated αS/βS fibrils. (a,b) Amplitude modulated (AM) AFM images of fibrils formed from (a) 70 μM monomeric αS and (b) 70 μM monomeric αS co-incubated with 210 μM monomeric βS. The x-y axes length scale bar is 500 nm. Assessment of the height (c) and length (d) of αS (black) versus co-incubated αS/βS (red) fibrils. Histograms of height and length data are presented as normalized probability densities, and the best-fit probability density function is overlaid to better visualize the distributions.

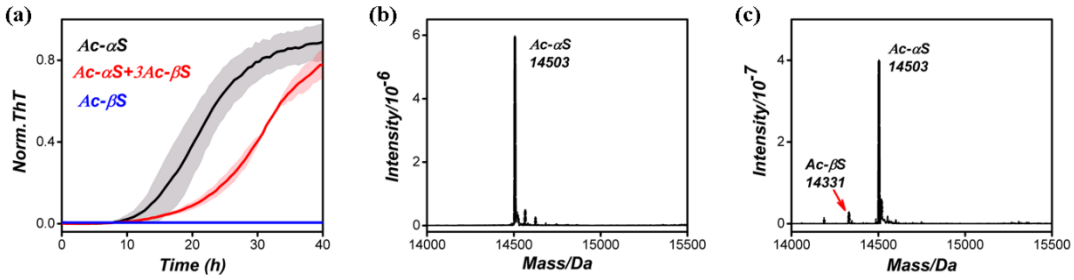

Figure 4. (a) Normalized change in ThT fluorescence signal of 70 µM Ac-αS (black), 210 µM Ac-βS (blue), or a mixture of 70 µM Ac-αS + 210 µM Ac-βS (1:3) (red) incubated at 37°C in 10 mM PBS with Teflon beads and shaking. (b,c) ESI-MS data showing the protein composition of αS fibrils and co-incubated αS/βS fibrils.

αS/βS co-Incubated Fibril Core Structure is Maintained while the N-Terminal Dynamics are Increased.

We investigated the conformational and dynamics properties of the αS fibril when co-incubated with βS utilizing solid-state NMR (ssNMR) spectroscopy. We first assessed the secondary structure of our fibrils from 2D ^{13}C-^{13}C and ^{15}N-^{13}C correlation spectra. **Figure 5a** shows the 2D ^{13}C-^{13}C 100 ms DARR spectra and **Fig. 8** the 2D ^{15}N-^{13}C correlation spectra of αS fibrils in black overlaid with co-incubated αS/βS fibrils in red. This experiment utilizes a cross-polarization period to transfer ^{1}H to ^{13}C magnetization, which preferentially detects the rigid residues that make up the core of the fibril and does not detect the dynamic or disordered residues that make up the bulk of the N- and C-terminal regions. The ^{13}C chemical shifts, ^{13}C-^{13}C cross peaks, and ^{15}N-^{13}C cross peaks of the spectra do not show marked differences between αS and αS/βS fibrils, indicating that the core structure of the fibril does not change even when formed in the presence of a

stoichiometric excess of βS (**Fig. 5a**). To ascertain whether our fibrils maintain the common Greek-key motif core structure previously identified(*107, 131-133*), without conducting a full structure determination by ssNMR, we compared our spectra with the ^{13}C chemicals shifts of αS fibrils deposited into the Biological Magnetic Resonance Data Bank(*134*) (BMRB). Out of 15 total entries in the BMRB of αS fibril chemical shifts (8 human WT, 6 human mutants, 1 mouse WT) only one is associated with a high-resolution 3D structural model of human WT αS fibrils (BMRB 25518, PDB 2N0A)(*133*). Using the ^{13}C chemical shifts from BMRB 25518 we created a ^{13}C-^{13}C chemical shift correlation map, shown in green in **Fig. 5c**, and overlaid it with our αS fibril ^{13}C-^{13}C spectrum; we observe relatively good agreement between the published chemical shifts and our αS spectrum. In addition, we created a ^{13}C-^{13}C chemical shift correlation map using an average of the ^{13}C chemical shifts from the core residues (44-96) in the 8 human WT entries in the BMRB (Entries: 16939 (*135*), 17498 (*136*), 17910 (*137*), 18243 (*138*), 18860 (*136*), 25518 (*133*), 25535 (*139*), 26890 (*140*)) (**Fig. 5d**). When overlaid with our αS fibril spectrum, we again find relatively good agreement between the two spectra. This comparison between the previously published ^{13}C chemical shifts, in particular the ^{13}C chemical shifts from PDB 2N0A, and our own ^{13}C spectra suggests that the secondary structure of our αS fibril core is consistent with a Greek-key topology. A full structure determination and peak assignment is currently underway to confirm this assessment.

While the core of our αS and co-incubated αS/βS fibrils are unchanged, there are some subtle differences in peak intensities between αS and αS/βS fibrils. The Cβ-Cα, Cβ-Cγ and Cβ-CO cross-peaks of the threonine residues show marked intensity decreases in the

co-incubated fibril (**Fig. 5b**). We also observed intensity decreases in the cross peaks of lysine Cε-γ and Cβ-γ of N65 of the co-incubated fibril (**Fig. 5b**); the N65 Cβ-γ assignment is tentative, and could also plausibly be from I88 Cβ-CO or F94 Cβ-CO. The loss of intensity of these peaks could be caused by increased dynamics of these residues in the co-incubated fibril. To further investigate this point we measured the ^{13}C $T_{1\rho}$ relaxation time(*141*), which reports on μs timescale dynamics, of the threonine Cβ, since these peaks are well resolved from chemical shift overlap of any other residue in the region from ~65-70 ppm (**Fig. 5a** and **Fig. 7a,b**). We found that the ^{13}C $T_{1\rho}$ relaxation time of the Thr Cβ's from co-incubated αS/βS fibrils decreased relative to the Thr Cβ's from αS fibrils (**Fig. 7c**), indicating an increase in dynamics of these residues.

To further characterize any differences between αS and co-incubated αS/βS fibrils, we probed the changes in water accessibility and hydration between the two fibrils. **Figure 6** shows the water-edited 2D ^{13}C-^{13}C correlation spectra(*142, 143*) of ^{13}C,^{15}N-labeled αS fibrils (**Fig. 6a**) and co-incubated αS/βS fibrils where only αS is uniformly labeled with ^{13}C and ^{15}N (**Fig. 6b**). The basic premise of this experiment is to observe how the transfer of water ^{1}H magnetization varies across the fibril. The long water ^{1}H spin-diffusion (SD) mixing time (100 ms, black) spectra represent a state where the water ^{1}H magnetization has fully equilibrated across each fibril, while the short water ^{1}H SD mixing time (3 ms, red) spectra illustrate the fibril residues that are in closest proximity to water. The relative proximity or accessibility of a residue to water is then most easily compared by taking the ratio between these two intensities (Int_{3ms}/Int_{100ms}). Due to sample sensitivity and time constraints, in lieu of obtaining residue specific full SD build up curves, the reason for

using the ratio between the short and long mixing times is to provide normalization of the intensities measured in the short mixing time experiment and allow for a relative comparison of the initial spin-diffusion buildup rates between different samples. For example, residues that are far from water or are located in the center of the fibril core will have smaller water-accessibility ratios, while residues that are on the surface of the fibril will have larger water-accessibility ratios. This approach has been used previously to probe the differential hydration environments of amyloid fibrils and other biomolecules(*143-147*).

Slices from the water edited 2D ^{13}C-^{13}C spectra show decreases in the relative intensities of several of the threonine and lysine cross-peaks of the αS/βS fibrils compared to αS fibrils, while those lysine cross-peaks that remain in the αS/βS fibril spectra have increased water spin-diffusion (i.e. larger Int_{3ms}/Int_{100ms} ratios) relative to αS fibrils (**Fig. 6c**). The increase in water spin-diffusion of the αS/βS fibril lysine peaks indicates that these residues are more water accessible. Conversely, the water spin diffusion ratios of the hydrophobic alanine and valine residues do not change between αS and co-incubated αS/βS fibrils (**Fig. 6c**), indicating that the hydration environment of these residues does not significantly change between the two fibrils.

Co-Incubated Fibrils are More Sensitive to Proteinase K Digestion.

Proteasomal impairment has been implicated in several neurodegenerative diseases(*148*), including PD(*149*), and as proteasome activity decreases with age cells become more vulnerable to deleterious protein aggregation(*150*). Therefore, an understanding of how synuclein fibrils and aggregates undergo protease degradation and clearance may shed

critical light on PD progression. In order to understand the differences in protease degradation and fibril stability between αS fibrils and co-incubated αS/βS fibrils, we carried out a series of digestion assays with increasing concentrations of proteinase K (**Fig. 6c**). We observed that co-incubated αS/βS fibrils are more sensitive to proteinase K digestion at a concentration of 5 μg/ml. The co-incubated fibrils display an enhanced propensity to be degraded to low molecular weight species (i.e. intense band at ~5 kDa only) compared to αS fibrils, which have a larger proportion of high molecular species (i.e. intense bands at ~10 and ~15 kDa).

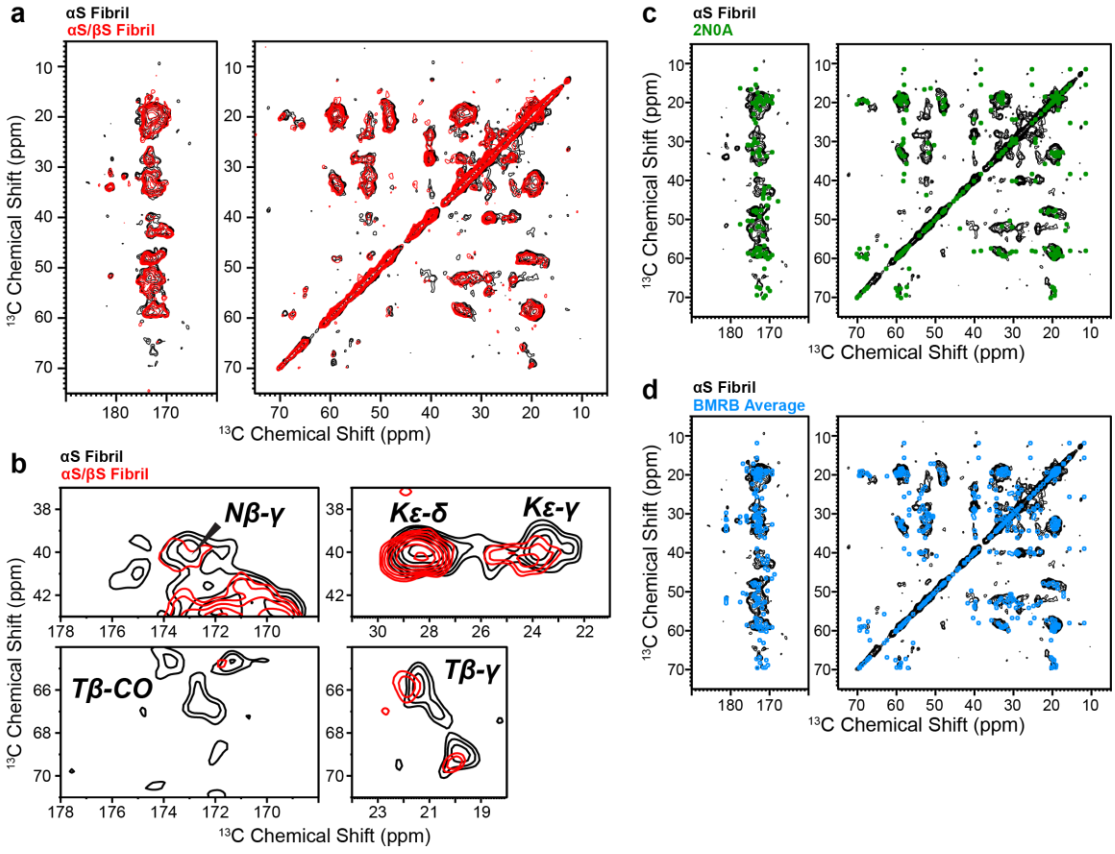

Figure 5. Characterization of the Fibril Core. (a) Overlay of αS fibril (black) and co-incubated αS/βS fibril (red) 2D ^{13}C-^{13}C correlation spectra (100 ms DARR), showing that the conformation of the core does not differ significantly between these two fibrils.

(b) Expansion of select regions of the 2D ^{13}C-^{13}C spectra in (a) that show the major cross peak intensity differences, which are the Lys, Thr and a tentatively assigned Asn residues. (c,d) Overlays of the αS 2D ^{13}C-^{13}C correlation spectrum in (a) with chemical shift maps derived from (c) the published solid-state NMR structure of αS fibrils (green, PDB: 2N0A, BMRB: 25518 (*133*)) and (d) an average of the ^{13}C chemical shifts of αS fibrils deposited into the BMRB (BRMB: 16939 (*135*), 17498 (*136*), 17910 (*137*), 18243 (*138*), 18860 (*136*), 25518 (*133*), 25535 (*139*), 26890 (*140*)).

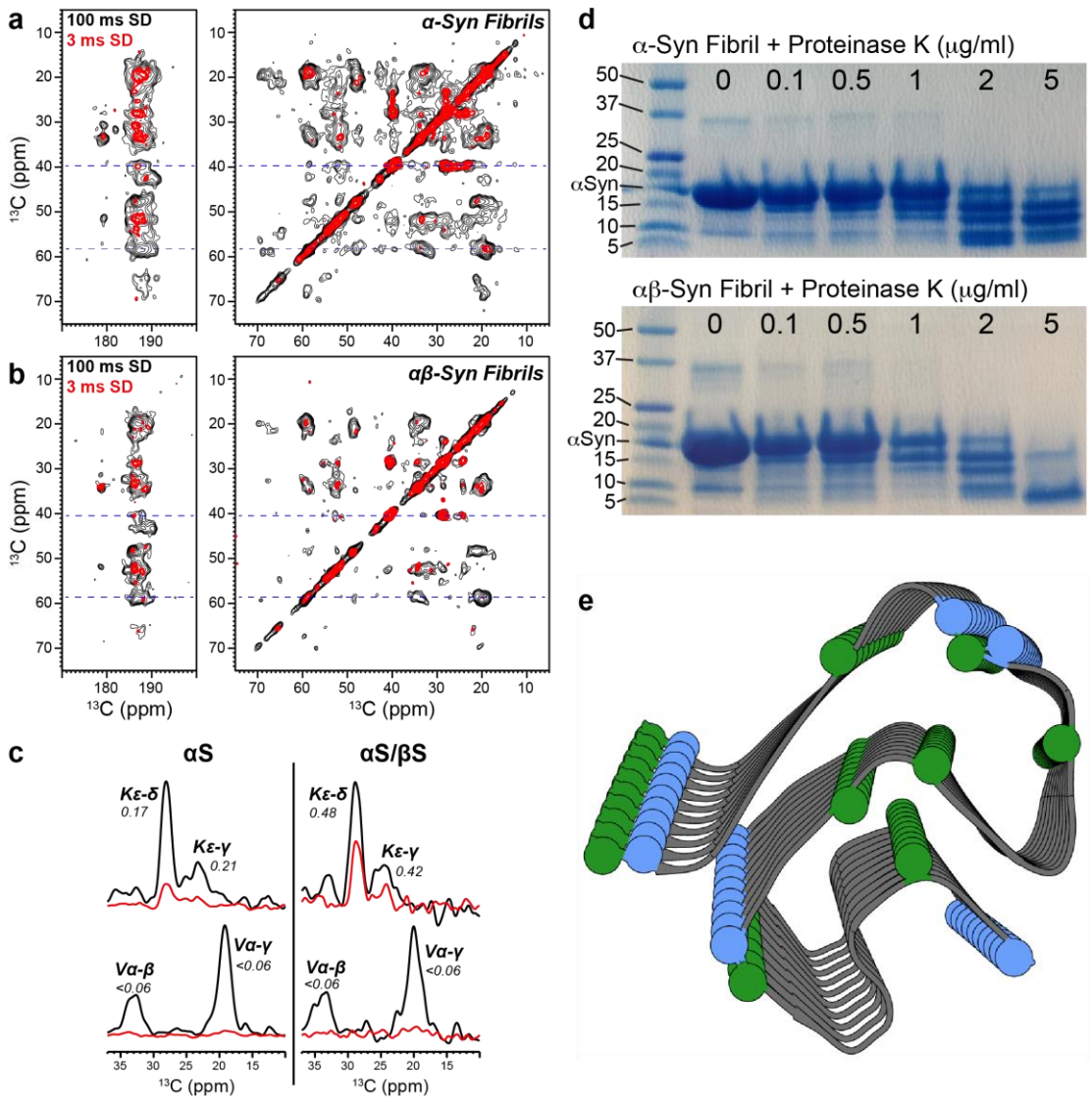

Figure 6. Changes in fibril water accessibility and fibril degradation. (a-c) Water-edited solid-state NMR ^{13}C-^{13}C correlation spectra of (a) αS and (b) co-incubated αS/βS fibrils. Magnetization was equilibrated at long water spin-diffusion times (100 ms, *black*) compared with the initial water-protein magnetization transfer at short spin-diffusion times (3 ms, *red*). (c) 1D slices taken at the blue dashed lines in (a) and (b) of αS fibrils (left side) and αS/βS fibrils (right side), showing the intensities of cross-peaks to lysine (top) or valine (bottom) side chains. The ratio of the cross-peak intensities at long and short spin diffusion times (Int_{3ms}/Int_{100ms}) indicates the relative proximity of water on a

residue-specific basis. (d) Digestion of αS and αS/βS fibrils at various concentrations of proteinase K. Full-length gels are presented in Supplementary Figure 6. (e) Map of the residues that show the largest degree of change in water accessibility between αS and αS/βS fibrils, lysine (blue) and threonine (green), on the core-residues (44-96) of PDB structure 2N0A.

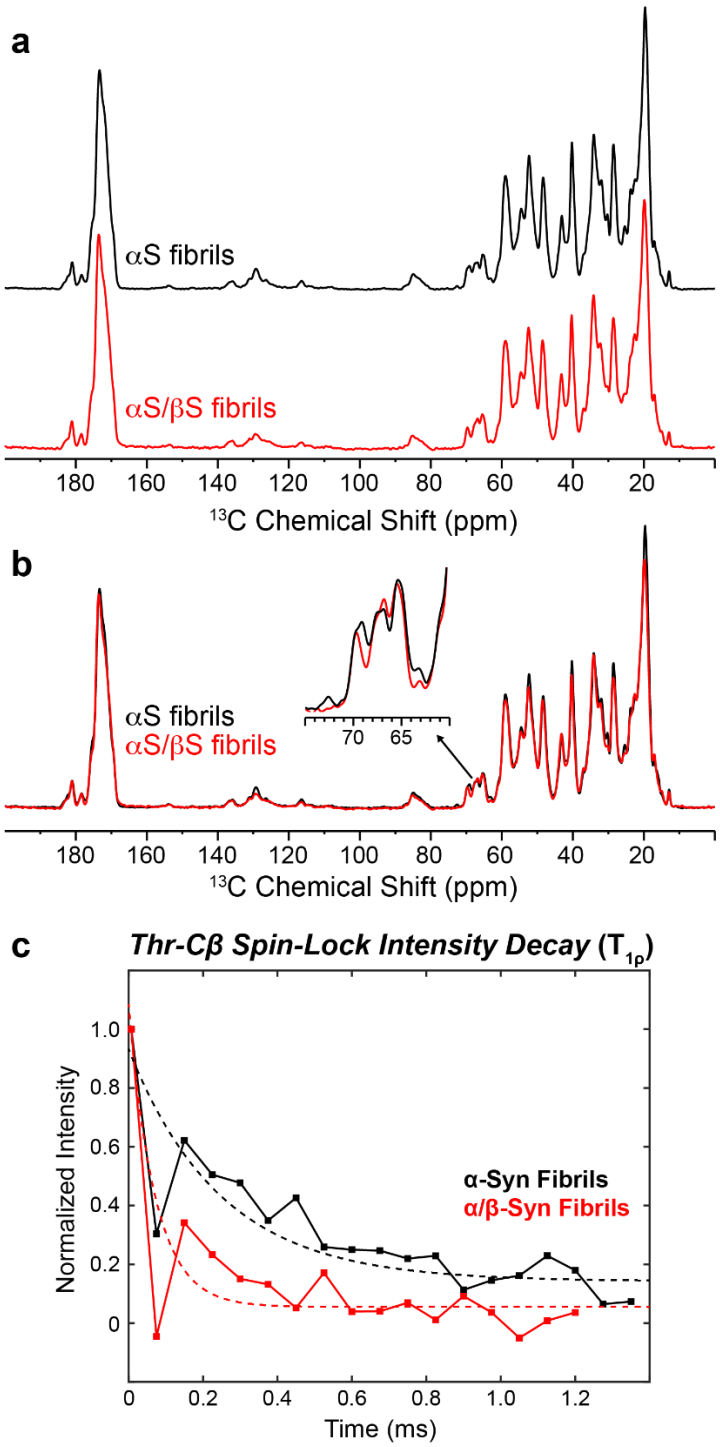

Figure 7. **(**a) One-dimensional (1D) ^{13}C cross-polarization (CP) spectra of αS fibrils (black) and co-incubated αS/βS fibrils (red). (b) Overlay of the spectra in (a), with the intensity of the carbonyl region matched. The inset shows the zoomed in region of the Thr Cβ from 60-75 ppm. (c) Intensity decay of the Thr Cβ region under spin-lock, with a

^{13}C ω_1 field of $2.25\omega_r$ applied on resonance with the Thr Cβ (70 ppm) during the spin-lock period. Several different ω_1 rf strengths were tested. The $\omega_1 = 2.25\omega_r$ condition was found to be optimal, as we observed that it minimized the oscillations of the magnetization due to coherent evolution while providing agreeable RF power levels for our probe. The $T_{1\rho}$ values were observed to maintain their trend for the RF strengths tested. A best-fit simple exponential decay (dotted line) is overlaid to guide the eye. Spectra were recorded at a MAS rate of 13.333 kHz, and temperature was controlled at 25 °C.

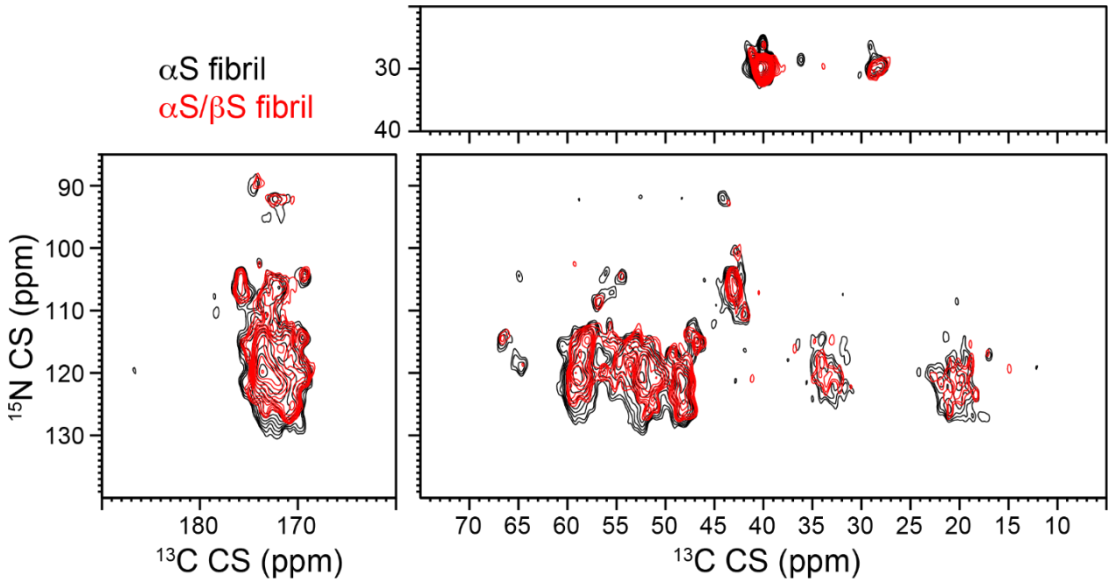

Figure 8. Two-dimensional (2D) ^{15}N-^{13}C heteronuclear correlation spectra of αS fibrils (black) and co-incubated αS/βS fibrils (red). Spectra were recorded using a REDOR based pulse sequence with a REDOR period of 1.35 ms, at a MAS rate of 13.333 kHz, and temperature was controlled at 25 °C.

Co-Incubated αS/βS Fibrils are Less Toxic and Exhibit Reduced Seeding and Proliferation Capacity Compared to αS Fibrils in Neuroblastoma Cells.

Having now characterized the conformational and polymorphic differences between αS and co-incubated αS/βS fibrils, we investigated how these changes in protofilament packing and dynamics affects the cytotoxicity of the fibrils. It is common practice to sonicate amyloid fibrils directly before use in cell toxicity assays, in order to obtain a more uniform distribution of fibril lengths and size. However the sonication process also produces smaller aggregates and oligomers(*151*), with an unknown distribution of shapes and sizes, that show different toxicities, fibril seeding abilities, and cell incorporation capacities(*113*). In order to avoid forming these additional oligomers, we have elected to use un-sonicated fibrils in our assays of cell toxicity and seeding, with polymorph compositions (**Fig. 3a,b**) and size distributions (**Fig. 3c,d**) illustrated in our AFM images. As a consequence of using long un-sonicated fibrils, the concentration of fibrils used in our assays (~1 μM) is higher than the nM concentrations used previously for smaller sonicated fibrils, since these smaller sonicated species are more easily incorporated into cells(*152, 153*). However, our fibril preparations are internalized similarly to sonicated fibrils, showing the characteristic fluorescent punctate-like structures (**Fig. 10**).

Fibrils of αS or αS/βS were added to cultures of human SH-SY5Y neuroblastoma cells and incubated for 24 hours, at which time cellular viability was assessed by the ability of the cells to reduce 3-(4, 5-dimethylthiazol-2-yl)-5-(3-carboxymethoxyphenol)-2-(4-sulfophenyl)-2H-tetrazolium (MTS). Compared with untreated cells, or cells treated with monomeric αS, fibrils of αS induced a 30% reduction in cell viability (***$p < 0.001$),

whereas αS/βS fibrils had no significant impact on cell viability (**Fig. 9a**).

We also investigated the ability of αS and αS/βS fibrils to seed aggregation in vitro using a quiescent thioflavin-T (ThT) fluorescence assay. **Figure 11** shows that while preformed seeds of both αS and αS/βS fibrils have the ability to induce fibril formation in the presence of αS monomers, the time for the ThT fluorescence curve to plateau takes longer with αS/βS fibril seeds. This indicates that αS/βS fibrils have a reduced capacity to seed further αS aggregation. We confirmed these observations of αS and αS/βS fibril seeding capacity in cell, by assessing the ability of these fibrils to seed aggregation of endogenous αS in SH-SY5Y cells through the analysis of the fluorescence intensities of dyes that specifically bind to αS and amyloid structures (**Fig. 9b**). Cells were treated with monomeric αS, αS fibrils or αS/βS fibrils for 24 hours before being fixed and stained with purified mouse anti-αS (anti-α-synuclein) antibody, thioflavin S (ThioS), and 4',6-diamidino-2-phenylindole (DAPI). Cells were then imaged by confocal fluorescence microscopy, where the anti-αS antibody fluoresces red and indicates the presence of any synuclein species present, ThioS fluoresces green and indicates the formation of amyloid species, and DAPI stains the cell nucleus blue (**Fig. 9b**). Compared with cells treated with monomeric αS (**Fig. 9b**, bottom row), cells treated with αS fibrils showed an increase in anti-αS antibody fluorescence of 7.3x (**Fig. 9b**, top row), while cells treated with αS/βS fibrils showed a smaller increase of 4.4x (**Fig. 9b**, middle row). ThioS staining indicating amyloid formation showed a similar trend with a 4.8x increase with αS fibrils vs a 3.4x increase with αS/βS fibrils.

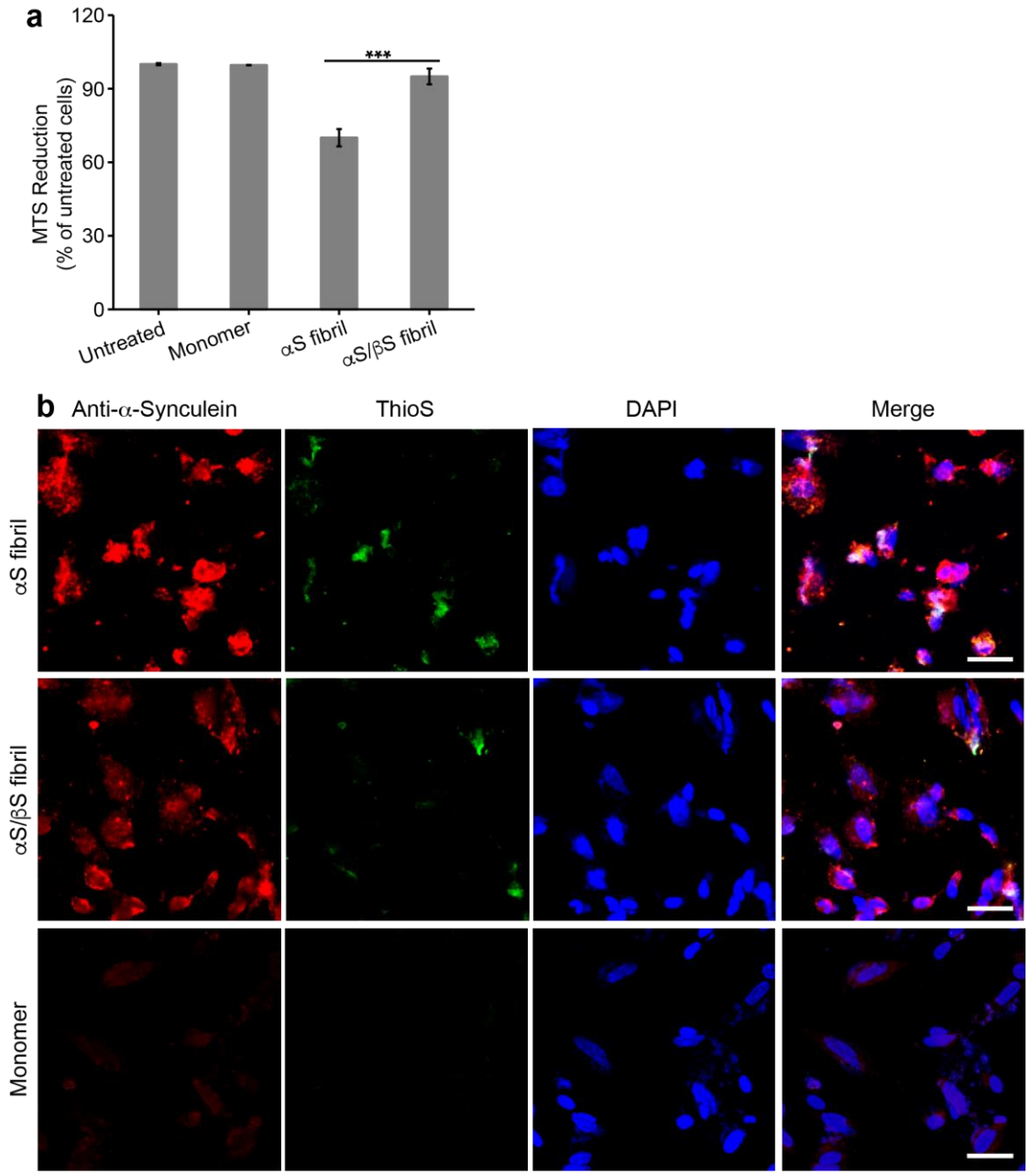

Figure 9. Cellular toxicity of αS and co-incubated αS/βS fibrils and their seeding potential. (a) Viability of SH-SY5Y cells assessed by MTS assay after treatment with αS or αS/βS fibrils (1.3 μM monomer equivalents), or monomeric αS (1.3 μM) as control, for 24 hours. Data shown are means and standard errors of the mean (SEM) of 3 independent experiments run in triplicates. ***ANOVA $p < 0.001$. (b) Confocal

fluorescence microscopy images of SH-SY5Y cells treated with 1.3 μM αS fibril (top), αS/βS fibril (middle), or αS monomer (bottom) for 24 hours before fixing and staining. Separate channels are presented showing the presence of all αS species (anti-αS antibody, red), all amyloid species (ThioS, green), and cell nuclei (DAPI, blue), along with the three channels overlaid (merge). The scale bar is 40 μm.

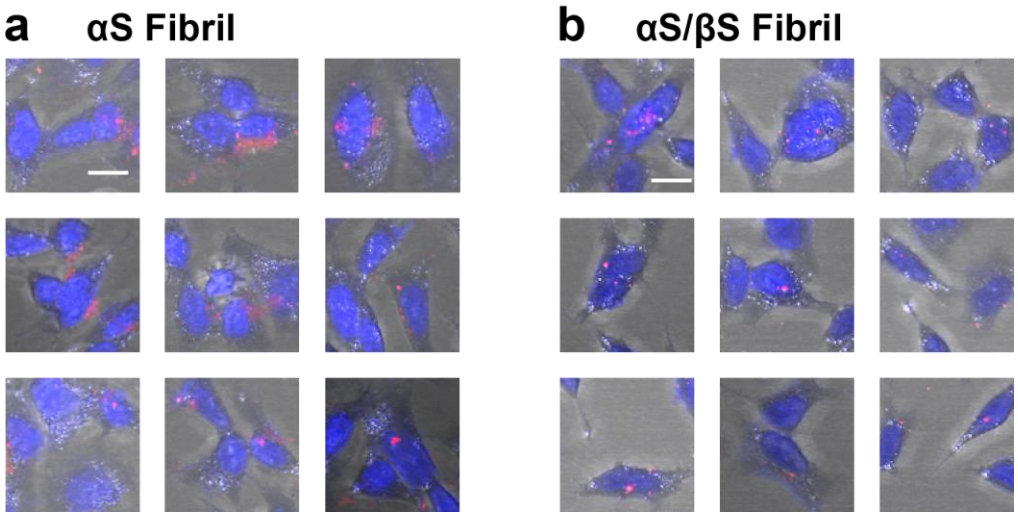

Figure 10. Confocal images showing internalized (a) αS fibrils and (b) co-incubated αS/βS fibrils into SH-SY5Y cell. Fibrils were made as described in the main text, labelled with ATTO-550 (red), and incubated with SH-SY5Y cells for 24h followed by fixing and staining with DAPI (blue).

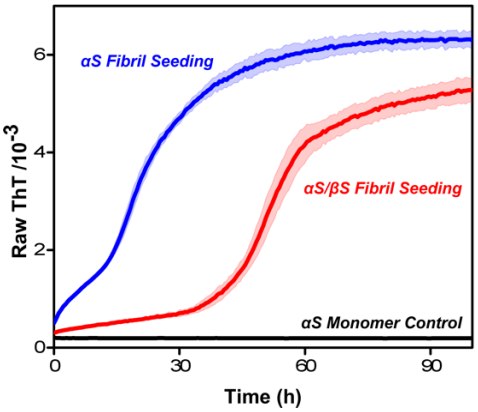

Figure 11. ThT fluorescence assay of seeded aggregation. 0.9 μM preformed αS (blue) or αS/βS (red) fibrils were added to a 70 μM αS monomer solution (10 mM PBS pH 7.4) and incubated at 37°C under quiescent conditions (i.e. no shaking). Under the same quiescent conditions, αS monomers alone (black) do not form fibrils.

Oligomers Shed from αS or αS/βS Fibrils Have Different Morphologies, Toxicities and Seeding Capacities.

It has been hypothesized that as the endpoint of misfolding and aggregation of several neurodegenerative disease associated proteins, amyloid fibrils might act as a "sink" to sequester misfolded toxic species(*154*). However, amyloid fibrils do not represent a completely stable species in solution, rather they exist in a dynamic equilibrium between fibril and oligomer forms. Indeed, toxic oligomers have even been observed to shed from mature αS fibrils over time(*112*). To understand the effect of βS on the stability and equilibrium of αS fibrils, we sought to determine the morphology, toxicity and cell seeding capacities of the oligomers that are shed from αS fibrils and αS/βS fibrils.

We first measured the thermostability of the two fibrils using far-UV circular dichroism

(CD) spectroscopy. The CD spectra show that both αS and αS/βS fibrils have the characteristic spectral minimum at 218 nm, indicating the presence of β-sheet structure (**Fig. 13**). We monitored the change in ellipticity of the 218 nm signal as a function of temperature, and found that change in ellipticity of co-incubated αS/βS fibrils is less than that of αS fibrils as temperature increased, indicating that αS/βS fibrils are more thermostable than αS fibrils (**Fig. 13**). AFM images show that the oligomers that are shed from αS fibrils (**Fig. 12a**) primarily adopt small globular morphologies, while oligomers shed from αS/βS fibrils tend to adopt short proto-fibril morphologies with some larger globular species also present (**Fig. 12b**). We next measured the toxicity of the shed oligomers in SH-SY5Y cells. After a 48 hour period of incubation with shed oligomers from either αS or αS/βS fibrils, we found that oligomers shed from αS reduced cell viability by 17% compared to the untreated cells and cells treated with monomeric αS, whereas oligomers shed from αS/βS did not (**Fig. 12c**). We also assessed the ability of shed oligomers to seed further aggregation in cells, using confocal fluorescence microscopy. Compared with cells treated with monomeric αS (**Fig. 12d**, bottom row), cells treated with oligomers shed from αS fibrils showed an increase in anti-synuclein antibody fluorescence of 1.6x (**Fig. 12d**, top row), while cells treated with oligomers shed from αS/βS fibrils showed an increase of 1.3x (**Fig. 12d**, middle row). ThioS staining indicates that amyloid formation increased by 1.6x in cells treated with oligomers shed from αS fibrils and by 1.3x in cells treated with oligomers shed from αS/βS fibrils.

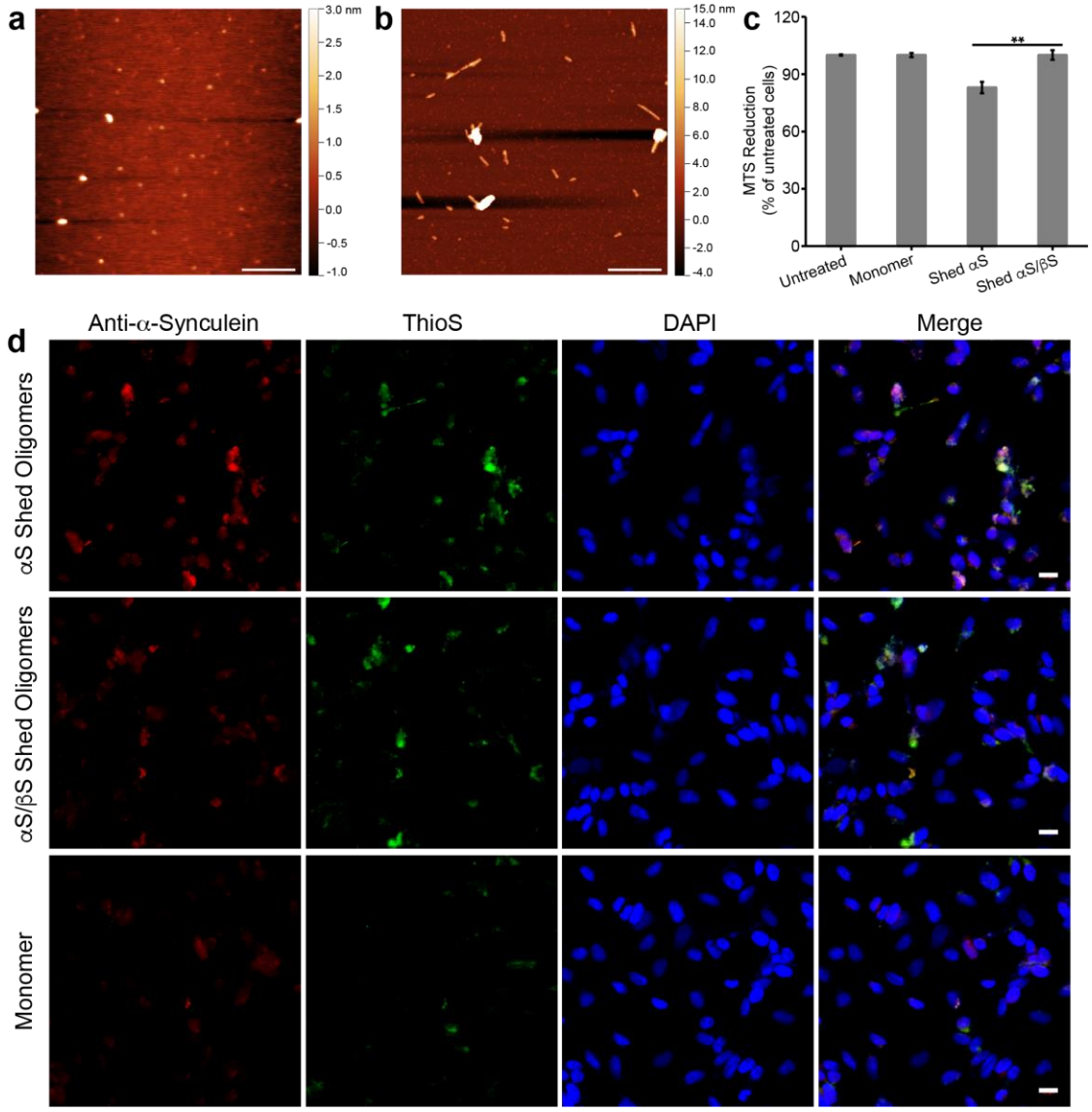

Figure 12. Morphology and toxicity of oligomeric species that are shed from mature fibrils. (a,b) AM-AFM images of the oligomeric species that are shed from mature αS fibrils (a) and mature αS/βS fibrils (b). The length scale bar is 500 nm. (c) Viability of SH-SY5Y cells assessed by MTS assay after treatment for 48 hours with the shed oligomers from αS fibrils or shed oligomers from αS/βS fibrils (0.7 μM monomer equivalents), or with monomeric αSyn (0.7 μM) as a control. Data shown are means ± SEM of 3 independent experiments run in triplicates. ** ANOVA $p < 0.01$. (d) Confocal

fluorescence microscopy images of SH-SY5Y cells treated with oligomers shed from αS fibrils (top), oligomers shed from αS/βS fibrils (middle), or with αS monomer (bottom) for 48 hours before fixing and staining. Separate channels are presented showing the presence of all αS species (anti-αS antibody, red), all amyloid species (ThioS, green), and cell nuclei (DAPI, blue), along with the three channels overlaid (merge). The scale bar is 16 μm.

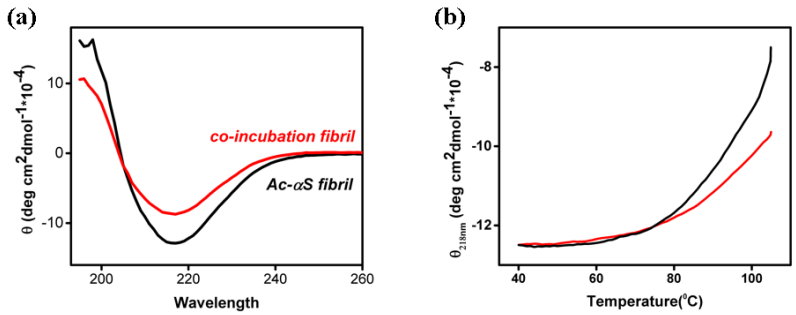

Figure 13. (a) Far-UV CD wavelength scan spectrum of αS fibril (black) and co-incubated αS/βS fibril (red) showing similar secondary structure. (b) Thermal stability curve of αS fibril (black) and co-incubation αS/βS fibril (red), monitored by CD signal change at 218nm.

3.4 Discussion

Amyloid fibrils of αS are key pathologic features of PD and have been recognized as contributing to the progression of the disease. These fibrils are thought to contribute to cellular toxicity through their ability to seed further aggregation of endogenous αS, and the ability of the fibrils to "shed" oligomer and protofibril species that may be toxic. The αS fibrils studied in this work should be distinguished from fibrils that are contained within

aggresome-like LBs. Fibrils that are formed as the end product of the aggregation pathway of αS (either *in vivo* or *in vitro*), and are not yet collected into LBs, exist in a dynamic equilibrium with oligomers, as evidenced by the ability of fibrils to "shed" smaller molecular species(*112, 155*). Here we have demonstrated that αS fibrils formed in the presence of the natural inhibitor βS, while maintaining similar core structures as αS fibrils alone, exhibit reduced toxicity to neuroblastoma cells, reduced seeding properties, and are in dynamic equilibrium with oligomers that also share reduced toxicity and seeding (**Fig. 14**).

We have utilized ssNMR and the changes in ^{13}C chemical shifts to probe how the core residues and dynamics of αS fibrils and co-incubated αS/βS fibrils differ from one another. While we have not yet completed a full assignment and structure determination of our fibrils, ^{13}C chemical shifts are very sensitive reporters of amino acid type and secondary structure(*156*). The cross-polarization based ssNMR experiments used in this work preferentially detect molecules and domains that are rigid, and dynamic and disordered domains are not detected. The dynamic regions of αS fibrils are the very N-terminal (residues ~1-43) and C-terminal (residues ~97-140) domains; what we detect in our spectra are the relatively rigid core of the amyloid fibrils (residues ~44-96). The ^{13}C resonances observed in our spectra show characteristic β-sheet chemical shifts. Comparison of our spectra with the chemical shift lists (BMRB Entry 25518) and spectra reported by Rienstra and coworkers(*133*), who have previously determined the core fibril structure of full-length αS by ssNMR, show relatively good agreement (**Fig. 5c**). Since we have prepared our fibrils in a similar manner to those used for the published αS fibril structure(*133*), we can

reasonably assume that our fibrils adopt a similar core structure. αS has a 140 amino acid primary sequence generally described by 3 domains: a 60 residue polyampholyte N-terminal domain, a 35 residue hydrophobic NAC domain, and a 45 residue highly negatively-charged polyelectrolyte C-terminal domain. Lysine and threonine (**Fig. 6e**) are almost exclusively located in the N-terminal and NAC regions of the αS sequence, where they are clustered into imperfect KTKEGV repeats. These two regions form the "Greek-key" motif of the αS fibril core structures, roughly spanning residues 44-96. Of particular note is the preNAC domain (44-60), which makes up the packing interface between two αS protofilaments(*107, 131, 132*), and contains two full KTK repeats.

While the overall fold of the core residues does not change between αS and αS/βS fibrils, and is similar to previously determined αS structures, based on the assignments of the Thr and Lys cross-peaks in our 2D ^{13}C-^{13}C spectra of the co-incubated αS/βS fibril we do find changes to these residues that make up the preNAC domain's final two KTKEGV repeats. First, from the loss of intensity in our 2D spectra and measurements of $T_{1\rho}$ relaxation, we have found an increase in the local dynamics of the Thr and Lys residues of co-incubated αS/βS fibrils relative to αS fibrils alone. Second, we observed that the water accessibility of the Lys residues increases in the co-incubated αS/βS fibrils relative to αS fibrils. Our ssNMR measurements of the fibril core structure (residues 44-96), and residue dynamics and water-accessibility highlight that βS does not perturb the core structure of αS fibrils, but instead may have an impact on the residues at the protofilament packing interface.

Recent structures of αS fibrils determined by cryo-electron microscopy have begun to show the importance of protofilament packing to the observed differences in fibril

polymorphism, rather than a change in the conformation of the protofilament core(*107, 131, 132*). Our AFM images indicate that the primary distinctions between αS and αS/βS fibrils lie in the average height and length, although these parameters are widely distributed (**Fig. 6c, d**). The more subtle distinction lies with the change in polymorph composition of the fibrils: αS fibrils show a mixture of twisted and straight polymorphs (**Fig. 6a**) while αS/βS fibrils appear to only have straight polymorphs (**Fig. 6b**). These observations suggest that βS modulates the packing of the protofilaments in the mature fibril, and is less likely to be incorporated into the cross-beta structure of the individual protofilament. A change in protofilament packing is also supported by the proteinase K digestion profiles, which indicate that αS/βS fibrils are more easily accessible to cleavage by proteinase K, suggesting that the co-incubated αS/βS fibrils might be more susceptible to degradation in vivo (**Fig. 6d**). These profiles resemble those from previous work by Miake and coworkers, who established that proteinase K digestion of αS preferentially cleaves the N- and C-terminal portions of αS and leaves the fibril core from residues 31-109 intact(*157*). In addition, our results demonstrate that while αS fibrils are indeed toxic to neuroblastoma cells (**Fig. 9a**), co-incubated αS/βS fibrils are not (**Fig. 9a**) and have a lesser tendency to cause the formation of synuclein aggregates and amyloid species compared with αS fibrils (**Fig. 9b**). Therefore, co-incubation of βS with αS results in fibrils that are not toxic to cells and have reduced ability to seed further aggregation in a cellular environment. The reduced seeding ability also suggests that βS interferes with the ability of αS fibrils to catalyze secondary nucleation processes on the fibril surface, proposed previously by Knowles and coworkers(*158*). Taken together with our earlier results, these results again suggest that βS is associated with the N-terminal domain and protofilament packing interface along αS

fibrils, inducing more dynamic flexibility in the N-terminal portions of the αS fibrils, and may suggest that N-terminal domain dynamics and packing may play a role in this seeding process.

We have also found that αS fibrils are less thermostable (**Fig. 13**) and shed primarily small globular and amorphous oligomers (**Fig. 12a**), while co-incubated αS/βS fibrils are more thermostable (**Fig. 13**) and shed primarily short proto-fibril aggregates (**Fig. 12b**). The proto-fibril species shed from αS/βS fibrils also show reduced seeding propensity compared to the small globular and amorphous αS oligomer species (**Fig. 12d**). This finding suggests that the dynamic equilibrium is shifted away from the formation of small toxic oligomers towards less toxic proto-fibrils in the presence of βS (**Fig. 12c**). Taken together in the context of our previous observations, the protofilament-packing of co-incubated αS/βS fibrils appears to be more stable than αS fibrils, while increasing the local dynamics of the N-terminal domain. This results in a reduced capacity for seeding and shedding of toxic oligomeric species.

βS has previously been identified in studies of transgenic mice as a natural anti-Parkinsonian factor which has the ability to reduce αS inclusion formation(*124*). Yet, even though it reduces αS positive inclusions, it does not completely abolish the formation of αS fibrils. We propose that the role of βS as an inhibitor is multifaceted, influencing αS aggregation at multiple points along its fibril-formation pathway. In the earliest stages of αS aggregation, βS can stabilize αS in αS-βS heterodimers(*127*), which help to slow down the conversion of αS into higher order aggregates. As αS continues to aggregate, βS has

been found to stabilize and eliminate the formation of toxic oligomers(*65, 159*). In this work, we have now shown that in the last stage of αS aggregation, co-incubation with βS minimizes the toxicity and seeding ability of αS fibrils, and furthermore alters the fibril-oligomer equilibrium. Our findings demonstrate that βS can reduce the effects of toxic αS fibrils in cells without changing the core structure of αS fibrils and provide insight into how the dynamics and the surface of these fibrils may directly contribute to their toxicity and seeding ability. The multi-pronged targeting of αS by βS highlights the potential of βS as a lead for the future design of inhibitors that provide therapeutic intervention in synucleinopathies at multiple stages of αS aggregation.

The misfolding and aggregation of endogenous αS monomers due to seeding by fibrils is believed to be critical to the progression of synucleinopathies. The mechanism by which mature αS fibrils seed further aggregation is believed to proceed by surface-mediated secondary nucleation(*160-162*), where the surface properties of αS fibrils govern their interaction with endogenous αS monomers and template further aggregation. The exact details of how additional αS monomers undergo templated conversion are not yet known, but the present work provides some clues. The recent cryo-EM structures of αS fibrils show that a steric-zipper motif in the N-terminal domain mediates the interface between two protofilaments and stabilizes the mature fibril morphology(*107, 132*). Our results show that co-incubated αS/βS fibrils have increased dynamics and water accessibility of residues in the N-terminal domain, particularly in the KTKEVG repeats in the preNAC region, and allow for enhanced protease degradation of the fibril, suggesting that the protofilament interface may be altered and more dynamic. These observations also highlight the

importance of dynamics in mediating the seeding ability of αS fibrils: increased dynamics of the N-terminal domain may lead to reduced seeding, as secondary nucleation may necessitate a rigid N-terminal domain for proper templating of αS aggregation. Our results suggest that enhancing amyloid fibril dynamics at templating domains may be an approach for future therapeutic intervention for neurodegenerative diseases.

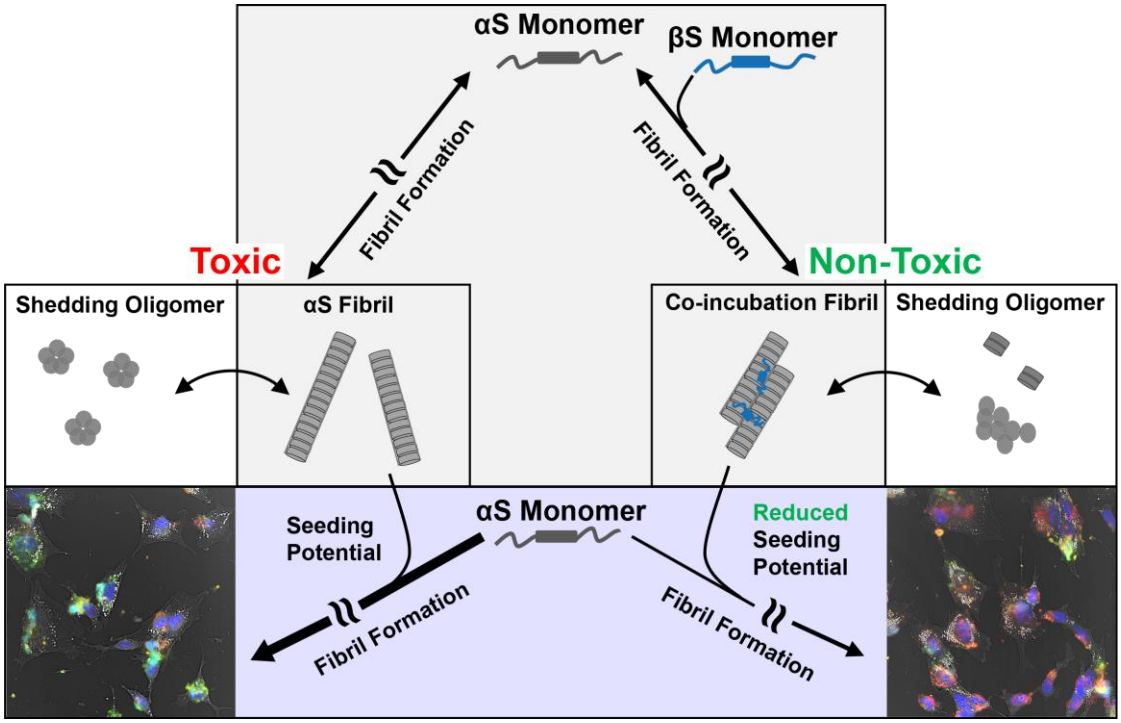

Figure 14. αS and αS/βS fibril toxicities and seeding potentials. αS aggregates and misfolds along a nucleation-dependent fibril formation pathway, generating various oligomeric species before finally adopting a characteristic repeating cross-beta amyloid fibril structure. When αS aggregates on its own (*left pathway*), the resulting fibrils are toxic to cultured human neuroblastoma cells, and the oligomeric species that shed from these fibrils are also toxic to cells. However, if αS is co-incubated with βS and allowed to aggregate (*right pathway*), then the resulting fibrils are no longer toxic to cells, and oligomer species that shed from these fibrils are also non-toxic. The αS and αS/βS fibrils

also display differential seeding capacities (*confocal images, bottom*). αS fibrils are able to efficiently seed amyloid formation, while co-incubated αS/βS fibrils have reduced propensity to seed further aggregation, as evidenced by the difference in green intensity in confocal images.

3.5 Materials and Methods

Protein Expression and Purification

Expression of N-terminally acetylated human αS and βS proteins was performed via co-expression with pNatB plasmid (Addgene #53613) in *E. coli* BL21(DE3) cells, and protein purification was performed as described previously(*163*). Uniformly ^{13}C, ^{15}N isotopically labeled αS for ssNMR experiments was expressed in M9 minimal media supplemented with ^{13}C-glucose and ^{15}N-ammonium chloride as the sole carbon and nitrogen sources, respectively. Protein molecular weight and purity were assessed by ESI-MS, and stored at -20 °C as a lyophilized powder until use.

Fibril Sample Preparation

Lyophilized acetylated αS or βS was dissolved in 10 mM PBS (pH 7.4), and large aggregates were removed by centrifuge filtration (50 kDa MWCO, Millipore Sigma, St. Louis, MO). The dissolved protein was concentrated in 3 kDa centrifuge units (Millipore Sigma, St. Louis, MO) to 1 mg/mL (αS) or 3 mg/mL (βS). To create fibrils, 100 uL of each sample mixture was loaded into 96-well clear bottom plates (Corning, Corning, NY) with a single Teflon bead (3 mm, Saint-Gobain N.A., Malvern PA). The plates were sealed with Axygen sealing tape (Corning, Corning, NY) and shaken at 600 rpm and 37 °C in a

POLARstar Omega fluorimeter (BMG Labtech, Cary, NC). Fibrils were allowed to form for at least 72 hours. Samples used for AFM, ESI-MS, ssNMR, and cell toxicity and shedding experiments were collected by centrifugation at 14k rpm for 2 hours, and washed through multiple rounds of re-suspension in 10 mM PBS (pH 7.4) and centrifugation at 14k rpm for 2 hours in order to remove residual soluble and non-fibrillar components.

Preparation of Oligomer Species Shed from Fibrils

Fibril samples were re-suspended in 1 mL of 10 mM PBS (pH 7.4) and incubated at 37 °C for 72 h, followed by removal of mature fibrils by using 0.22 μm filter (Millipore Sigma, St. Louis, MO). Samples were concentrated with 3 kDa centrifuge units (Millipore Sigma, St. Louis, MO), and protein concentration was measured using a bicinchoninic acid (BCA) assay (Thermo Scientific, Waltham, MA).

Proteinase K Digestion

Fibrils at a concentration of 1 mg/mL were incubated with various concentrations (0.1, 0.5, 1.0, 2.0, 5.0 μg/mL) of proteinase K (Sigma Aldrich, St. Louis, MO) in 10 mM PBS (pH 7.4) at 37 °C for 1 h. The digestion reaction was quenched by the addition of a 1200:1 molar excess of phenylmethane sulfonyl fluoride (Sigma Aldrich, St. Louis, MO) followed by the addition of 2 M guanidine thiocyanate (Sigma Aldrich, St. Louis, MO) and incubation at room temperature for 4 h. The results of the degradation reaction were mixed with 4x SDS-PAGE loading buffer (Invitrogen, Carlsbad, CA), loaded onto precast gels (Bio-Rad, Hercules, CA), and run at 120 V for 50 min.

Atomic Force Microscopy (AFM)

Samples (20 μL) were placed onto freshly cleaved mica (Ted Pella Inc., Redding, CA) and incubated for 15 min at room temperature, followed by 3 washes of 200 μL each deionized water as described previously(*59*). All images were collected on a NX-10 instrument (Park Systems, Suwon, South Korea) using non-contact mode tips (PPP-NHCR, 42 N/m, 330 kHz; Nanosensors, Neuchatel, Switzerland). Image processing and analysis were carried out in the Gwyddion software package(*164*).

Solid-State Nuclear Magnetic Resonance Experiments

All MAS ssNMR experiments were carried out on an Avance III HD 600 MHz (14 T) spectrometer (Bruker BioSpin, Billerica, MA) using a 1.6 mm triple resonance MAS probe (Phoenix NMR, Loveland, CO) tuned to $^{1}H/^{13}C/^{15}N$ frequencies. Typical radiofrequency (rf) field strengths were 118 kHz for ^{13}C, 74 kHz for ^{15}N, and 100-145 kHz for ^{1}H. ^{13}C chemical shifts were referenced to the $^{13}CH_2$ signal of adamantane at 38.48 ppm on the tetramethylsilane (TMS) scale, and ^{15}N chemical shifts were referenced to the ^{15}N signal of N-acetylvaline at 122.0 ppm on the liquid ammonia scale. All experiments utilized a MAS rate of 13.333 kHz, and sample temperature was controlled to 25 °C, unless otherwise noted. One-dimensional (1D) ^{13}C MAS spectra were recorded using a conventional cross-polarization (CP) sequence. Two-dimensional (2D) ^{13}C-^{13}C dipolar-assisted rotational-resonance (DARR) experiments(*165*) utilized a mixing period of 100 ms. A 2D water-edited DARR(*142*) experiment, with a DARR mixing period of 100 ms, a T_2-filter of 6 ms, and a ^{1}H spin-diffusion period of either 3 ms or 100 ms, was used to measure the water-protein ^{1}H spin diffusion differences between the two fibril samples. 2D ^{15}N-^{13}C correlation

spectra were measured using a REDOR-based pulse sequence(*166*), utilizing a REDOR period of 1.35 ms to observe long range correlations. A standard Bruker CP based pulse sequence was used to measure the ^{13}C $T_{1\rho}$ relaxation of the Thr Cβ(*141*). A ^{13}C ω_1 field of $2.25\omega_r$ was applied on resonance with the Thr Cβ (70 ppm) during the spin-lock period.

Analysis of Fibril Composition by ESI-MS

Mature fibril samples were dissolved in 4 M guanidine hydrochloride overnight, then buffer exchanged with 50 mM ammonium acetate with 0.1% formic acid. Samples were concentrated to 10 μM for ESI-MS analysis.

Neuroblastoma Cell Culture

Human SH-SY5Y neuroblastoma cells (ATCC, Manassas, VA) were cultured in DMEM/F12 (GE Healthcare, Boston, MA) with 10% fetal bovine serum (Gibco Co., Dublin, Ireland) and kept in a 37 °C, 5% CO_2 humidified atmosphere. Before cell viability assays or immunocytochemistry, cells were plated into 96-well (Corning, Corning, NY) or 12-well plates (Cellvis, Mountain View, CA), and allowed to grow for 24 h.

Cell Viability MTS Reduction Assay

SH-SY5Y cells were treated with 1.3 μM fibril (24 h), 0.7 μM shed species (48 h), or an equivalent concentration of monomer as a control (24 h or 48 h). Cell viability was assessed by adding 20 μL MTS per 100 μL cell culture (Promega, USA) and incubating for 2.5 h at 37 °C, before measuring absorbance at 490 nm.

Immunocytochemistry

SH-SY5Y cells were treated with 1.3 μM fibril (24 h), 0.7 μM shed species (48 h), or an equivalent concentration of monomer as a control (24 h or 48 h). Cells were fixed with 10% formalin (Sigma Aldrich, St. Louis, MO) and permeabilized with 0.5% Triton in PBS (Sigma Aldrich, St. Louis, MO). Cells were then blocked by incubation with 5% Donkey Serum solution (Sigma Aldrich, St. Louis, MO) for 30 min at 37 °C. Cells were incubated with 0.01% thioflavin S (Acros Organics, Waltham, MA) for 10 min at 37 °C and then washed with PBS, followed by incubation with purified mouse anti-α-synuclein primary antibody (BD Biosciences, Franklin Lakes, NJ; Cat.# 610786, RRID: AB_398107) at 4 °C overnight in the dark. Cells were washed with PBS 3 times and incubated with fluorophore-conjugated secondary antibody TRITC (Sigma Aldrich, St. Louis, MO; Cat.# T5393, RRID: AB_261699) for 1 h, then washed again 3 times with PBS. Cells were incubated with DAPI for 1.5 min at room temperature and then washed with PBS, to visual cell nuclei. All samples were imaged using a Zeiss LSM 780 confocal laser scanning microscope with 20x objective (Zeiss, Oberkochen, Germany), and images were processed using the Fiji distribution of ImageJ(*167*). To analyze the anti-αS-antibody and ThioS stained fluorescence images in a more quantitative manner, Fiji was used to filter and threshold each channel based on the DAPI-stained nuclei to extract the raw intensity per cell for each channel. These intensities were then normalized by the intensity per cell of the monomer treated cells, to give the relative increase in intensity reported in the results section.

Preparation of ATTO-550 Labelled Fibrils

Fibrils were labeled with the fluorescent ATTO550-NHS-ester (ATTO-TEC GmbH) per the manufacturer's procedure. In brief, fibrils formed as described above were incubated with a 2 M excess of ATTO550-NHS-ester in labeling buffer (pH 8.3 PBS/sodium bicarbonate solution) for 1 hour at room temperature. Conjugated ATTO550-fibrils were then separated from unreacted fluorophore by centrifugation at 16k rpm for 30min and resuspension of the ATTO550-fibril pellet in pH 7.4 PBS; this centrifugation/resuspension wash was repeated twice.

Statistical Analysis

All cell viability experiments were performed in triplicate, and each assay was repeated at least three times. Statistical significance was determined by one-way ANOVA with post-hoc Bonferonni analysis (GraphPad Prism).

3.6 Co-incubation βSynuclein with αSynuclein can reduce SDS-resistant oligomer formation.

In order to understand how βsynuclein influence αSynuclein aggregation on oligomer stage, we characterized αSynuclein, βSynuclein and both proteins incubated for different time by western blot and AFM. αSynuclein incubated with increasing time, more high molecular weight SDS-resistant oligomers have formed. For βSynuclein sample, the amount of SDS-resistant oligomer doesn't change a lot between different incubation time. When co-incubation αSynuclein and βSynuclein together no SDS-resistant oligomers were detected by western blot (except dimer) (**Figure. 15**). We also used FAM to characterize the total oligomers species in each sample (**Figure. 16**). During 12h

incubation time, no fibril was formed for βSynuclein sample, different sizes oligomers shown on AFM images. αSynuclein and co-incubation sample both stared to show fibril species after 9h incubation and after 12h mature fibril become the predominant species in samples. For 2h and 6h incubation time, co-incubation sample showed more oligomers than αSynuclein itself sample which may suggest that βSynuclein influence stable oligomers formation or convert stable oligomers into unstable oligomers. For western blot analysis, samples at appropriate concentration were run on 4-15% Mini Protean TGX Precast Gel (Bio-Rad, Hercules, CA) and transfer to nitrocellulose membranes which then blocked unspecific binding by using Odyssey Blocking Buffer (LI-COR Bioscience, Lincoln, NE) for 30 mins. Membranes were incubated with primary antibody at 4°C overnight followed by washing 3 time with TBS buffer with 0.01% Tween20 to remove unbound antibodies. IRDye® 800CW Goat anti-Mouse secondary antibody (LI-COR Bioscience, Lincoln, NE) was used for detection by LI-COR Odyssey image system.

For future work, structure and dynamic analysis should be done on different types of oligomers. Comparing the differences of αSynuclein, βSynuclein and co-incubation oligomers, we may have more information about the aggregation process of αSynuclein and how to inhibit them.

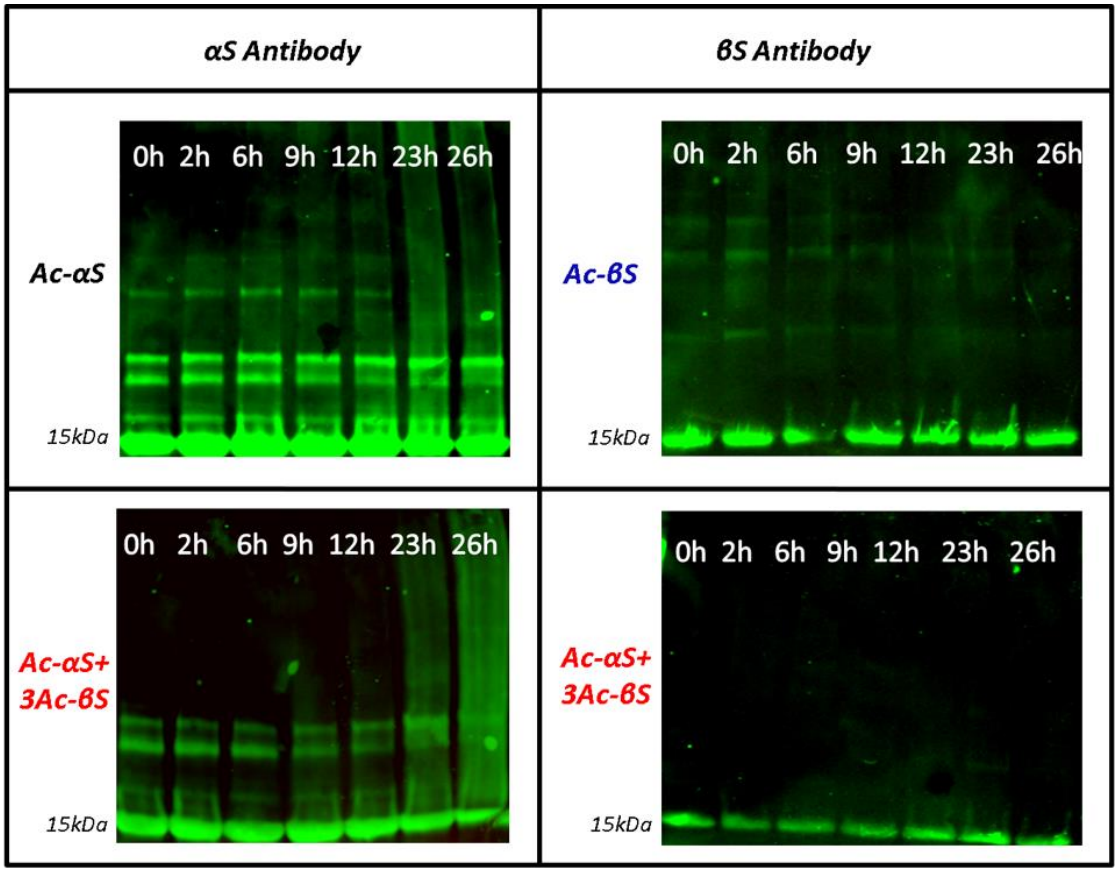

Figure 15. Western blot characterization of αSynuclein, βSynuclein and αSynuclein + 3βSynuclein incubated for different time point. Sample was stained by αSynuclein or βSynuclein antibodies. Reduced SDS-resistant oligomers were shown in co-incubation sample.

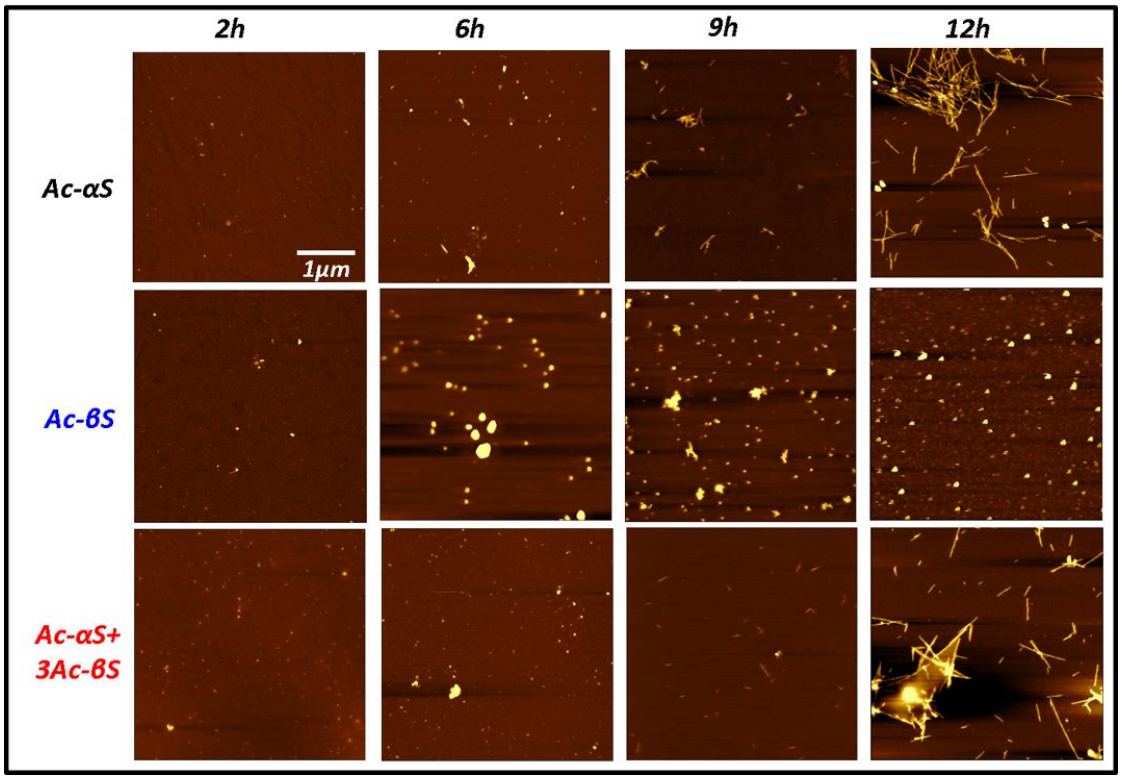

Figure 16. AFM characterization of aggregates formed by αSynuclein, βSynuclein and αSynuclein + 3βSynuclein incubated for different time. Within 12h incubation time, oligomer is the only species shown for βSynuclein incubation sample. Fibrils are formed for both αSynuclein and co-incubation sample. More oligomers have shown on co-incubation samples than αSynuclein self-incubation sample.

Chapter 4 – Stable oligomers inhibit fibril seeding amyloid formation through multi-interaction

4.1 Introduction

Neurodegenerative diseases including Alzheimer's, Parkinson's, and Huntington's disease affect millions of people all over the world(*168*). With the increased life span of people, these illnesses have become one of the most threatening diseases which not only influence the quality of people's lives but also lead to death. To date, no efficient therapies or even straightforward diagnostics have been established for these diseases(*169*). The wide variety of phenotypes and groups of symptoms make it even harder to understand neurodegenerative diseases. Protein aggregation appears to be the origin and shared common phenomenon for them. Understanding aggregation processes will provide critical information for finding cures for neurodegenerative diseases.

Protein aggregation is a process in which soluble proteins misfold and deposit insoluble aggregates, one example being amyloid fibrils. For Parkinson's disease, the soluble pre-synaptic protein α-synuclein aggregates into amyloid fibrils which is the main component of Lewy bodies – the hallmark of PD(*170*). The aggregation process of α-synuclein is believed to be the source for producing toxic species in PD. α- synuclein fibrils are shown to have various toxic effect in cell, mouse, and monkey models(*171-173*). The autocatalytic seeding of α-synuclein monomer aggregation and the propagation ability of α-synuclein fibrils make them one of the primary toxic species in PD(*174*). Eliminating fibril seeding ability is one of the most efficient approaches to stop the progression of PD. A lot of

research has been done to understand fibril seeding processes, but we still do not know the key factors that influence the seeding efficiency and how to diminish it(*175-177*).

αSynuclein oligomers are another targeted aggregate in PD which are in a metastable stage between monomers and fibrils. The classification of oligomers can be based on toxicity, stability, size, and on/off fibril formation pathway(*178*). Some types of oligomers are thought to be the intermediates between monomers and energy-favorable fibrils which will convert into fibrils with time. Because of their ability to convert into fibrils, this type of oligomer is often called on-fibrillar pathway oligomers and can usually disrupt certain cellular activities. Some oligomers have been made in vitro which show a degree of stability and ability to interfere with monomer aggregation and are thought to be off-fibrillar pathway(*179*). The diversity of sizes, shapes, and properties of oligomers makes studying them difficult. The unstable and low population nature of oligomers also limit the methods that can be used to characterize them. The information about oligomeric structure and the interactions between monomers -oligomers, or even oligomers – fibrils is missing which is the foundation for the design of any drug or therapy.

In this chapter, we set out to understand the role of two type of oligomers in fibril seeding processes and also characterize the interactions between monomers, oligomers, and fibrils at the individual residue level. Data from Circular Dichroism (CD), Transmission Electron Microscope (TEM), and limited proteinase K digestion experiments suggest these oligomers are different in size but share similar secondary structure and PK resistance. Because these oligomers are different from αS fibrils, they can not induce SH-SY5Y cells

thus lowering cell viability. By analyzing a series of Thioflavin T (ThT) experiments, we find these two types of oligomers can not convert into fibrils or seed monomer aggregation and they can efficiently inhibit fibril seeding monomer aggregation processes. NMR studies reveal that both oligomers and fibrils interact with monomers, primarily through the first 20 residues, which may result in competing interactions between monomer - oligomers and monomer - fibrils.

4.2 Result

Characterization of Stable Oligomers.

Stable oligomers are prepared by incubating 10 mg/mL of monomeric αS at 37ºC for 5h and separated by size exclusion column (SEC). While under these fibril formation conditions, after 5h incubation the majority of the protein is still in the monomeric form, around 2% of the protein is converted into oligomers. Two oligomer populations are detected by SEC – big oligomers and small oligomers (**Figure 17a**). TEM images show that small oligomers are generally in spherical shape and big oligomers have more diversity in shapes (**Figure 17c, d**). Consistent with the SEC profile, big oligomers have an overall larger size than small oligomers. Circular Dichroism (CD) was used to estimate the secondary structure component of the stable oligomers. Big and small oligomers show similar CD profiles which are remarkably different from fibrils or monomers. αS monomers show a signature minimum at 200nm indicating random coil structure and fibrils have a minimum at 217nm which indicates β-sheet structure. For stable oligomers, the absence of a signature minimum at 217 nm, 208 nm, or 222 nm suggest that stable oligomers are not predominantly one type of structure (**Figure 17b**).

After reinjection of freshly made stable oligomers into the SEC, small amount of monomer was observed which indicates stable oligomers are in equilibration with monomers. After keeping stable oligomers on ice for a month, their SEC profile still show at the oligomers' elution position but with an increased amount of monomer (**Figure 18**).

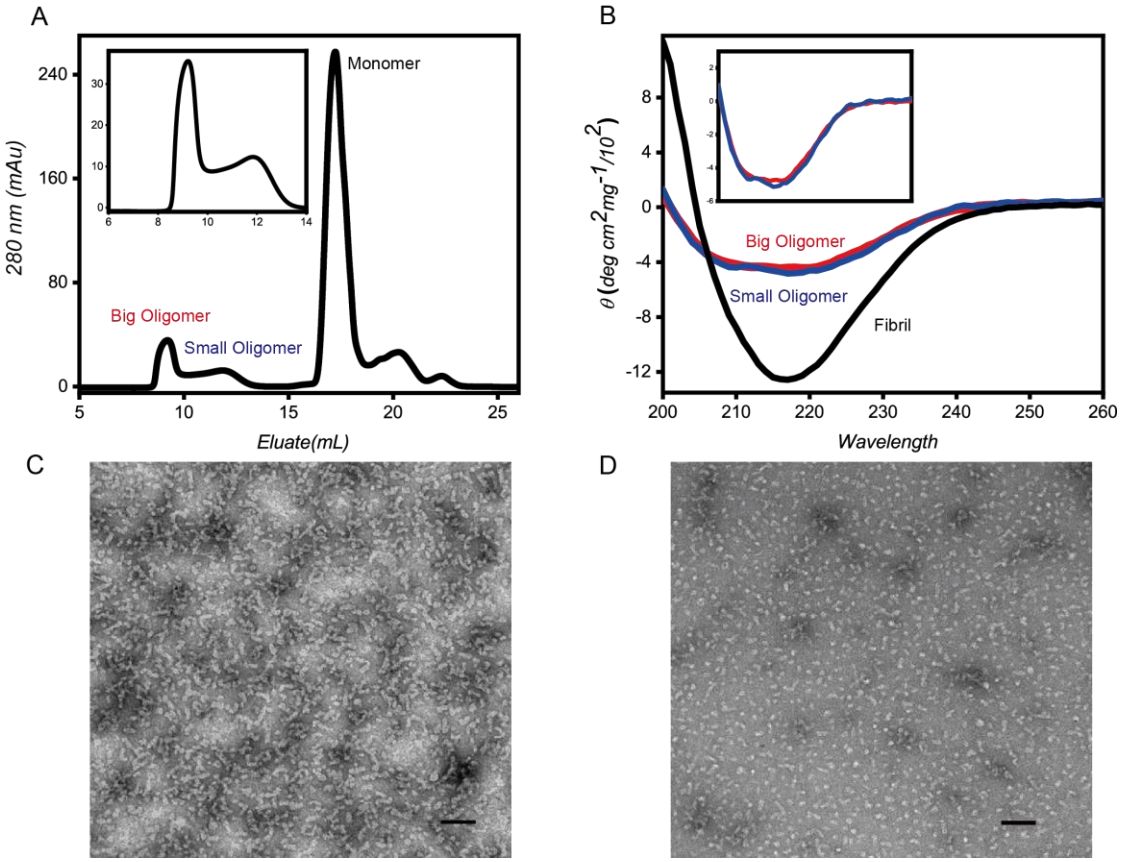

Figure 17. Characterization of purified stable alpha-synuclein oligomers. (A) SEC profile of separated big oligomers, small oligomers, and monomers. Majority species in the sample are still monomer. (B) Secondary structures of big oligomers (red), small oligomers (blue), and fibril (black) characterized by circular dichroism (CD). Big and small oligomers show similar secondary structures which are quite different from fibril secondary structure. TEM images show the morphology of big oligomers (C) and small oligomers (D). Scale bar is 100 nm.

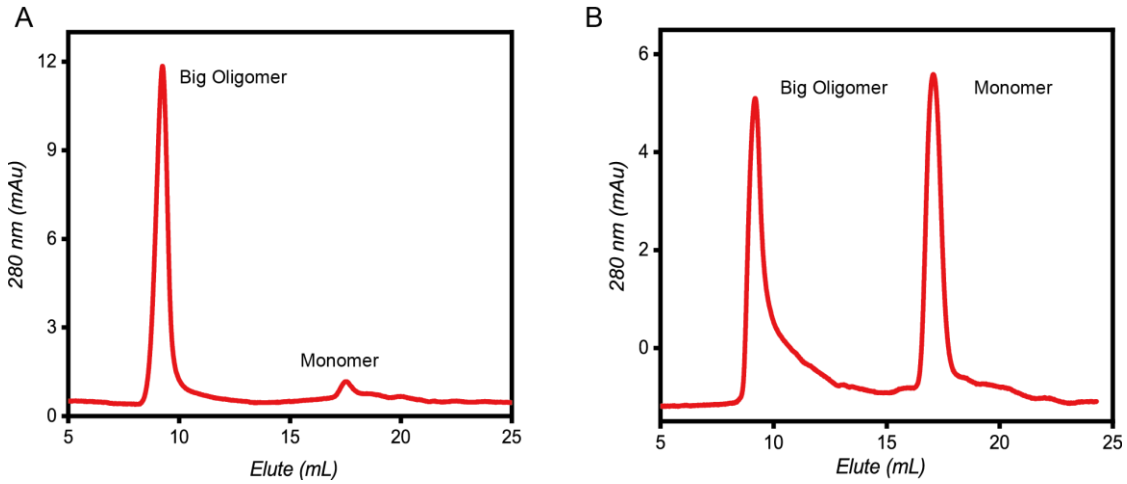

Figure 18. Reinjection of freshly made big oligomers into SEC show small amount of monomer equilibration (A), Reinjection of big oligomers which has been at 4^{O}C for one-month; monomer concentration increased to around 50% of total protein (B).

Both Oligomers are partially Proteinase K Degradation Resistant.

αS fibrils are highly resistant to proteinase K (PK) digestion, while αS monomer can be digested because of its IDP nature. Here, we did time dependent PK digestion experiments on stable oligomers and fibrils. Consistent with the literature, the intensity of αS fibrils' high molecular bands (can't run through the gel) does not change with time, equilibration of monomers in the fibril sample was gradually digested by PK(*180*). Big and small oligomers show similar molecular weights on SDS-gel (over 260kDa), and both oligomer samples show monomer band on the gel which may be the equilibration of monomers or the shedding of monomer from oligomers because of the presence of SDS. By adding PK into sample, both stable oligomers show smaller molecular weight bands (Over 120kDa) compared with the control but the oligomer bands remain the same with increase incubation

time which suggest that stable oligomers are partially resistant to PK degradation. The intensity of the monomer band in the stable oligomer samples is decreased with longer incubation time which suggest it is coming from the equilibration of monomer (**Figure 19**).

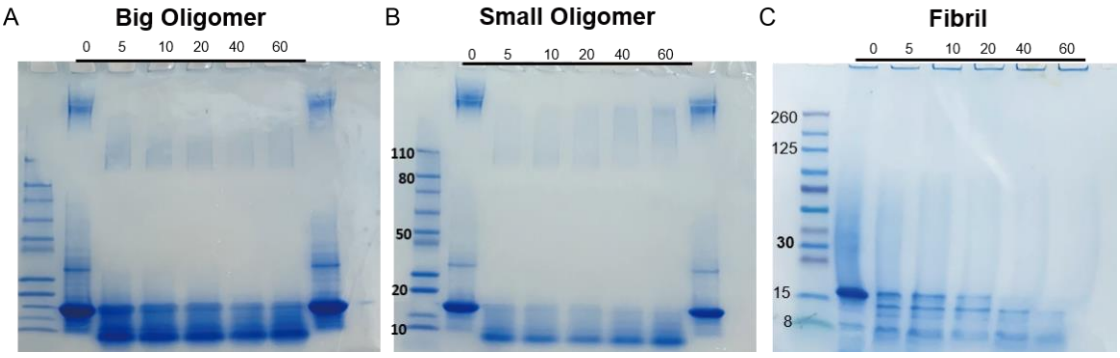

Figure 19. Time dependence proteinase K(PK) digestion experiments of big oligomers (A); small oligomers (B), and fibrils (C). The gel lanes to the right of time 60 on the big oligomer and small oligomer gels are oligomers that were incubated at 37°C for 60 mins as a control. Both big and small oligomers show PK resistant.

Stable oligomers show off- fibril formation pathway properties.

Stable oligomers used in this work are obtained by incubating monomer for 5h, we also explored how monomer incubation time influence the stable oligomers formation. After incubation of the monomer for 24h and 48h, we can still detect similar amounts of big and small oligomer by SEC as 5h incubation time. With incubation times that are longer than 3 days, the fibrils become the major component in the sample, but stable oligomers are still present as seen by SDS-gel (**Figure 20**). Stable oligomers present from lag time to plateau for the fibril formation pathway which suggest that the formation of stable oligomers may undergo a different pathway than fibril formation. Thioflavin T (ThT) is a fluorescence dye which binds to amyloid structure. Stable oligomers bind ThT much less compared to fibrils

but more than monomers. In order to understand the role of stable oligomers in the fibril formation process, we carried out a series of experiments to test if stable oligomers can convert into fibrils. We did not detect any fibril formation by stable oligomers alone or by the addition of excess monomer under fibril formation conditions for up to two months (**Figure 21**). TEM images confirm that stable oligomers are still roundly shaped after two months of incubation and no fibrillar-like structure is observed by the gel (**Figure 22**). It has been known that adding fibril seeds into αS monomer will abolish the lag time and lead to rapid fibril formation. When we add fibril seeds with stable oligomers, we did not observe any increased ThT signal which indicates that fibrils are not seeded by stable oligomers(**Figure 21**). All of these suggest that stable oligomers are off the fibril formation pathway.

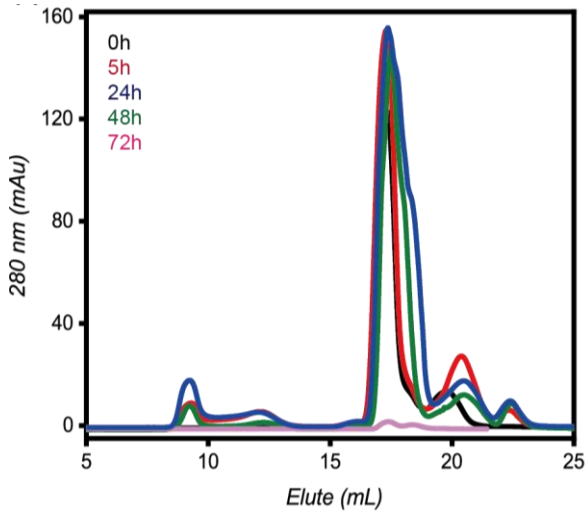

Figure 20. SEC profile of 10mg/mL protein incubated for different times. Similar amounts of big and small oligomers were formed by different incubation time.

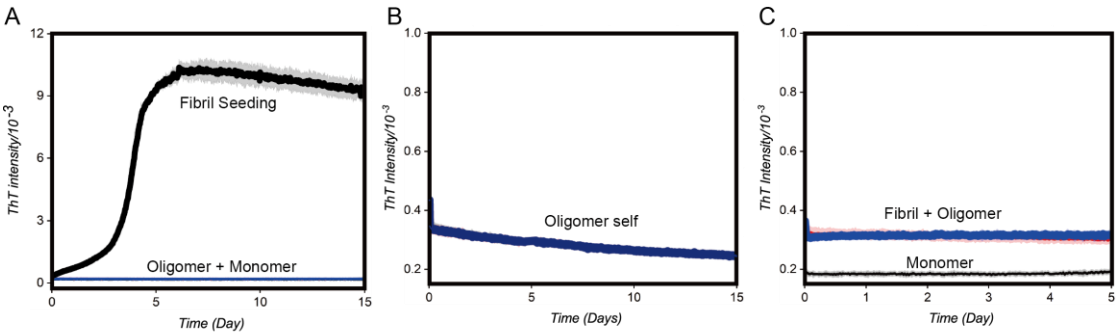

Figure 21. Characterization of the conversion between monomer, stable oligomers and fibril. (A) Thioflavin T (ThT) assay shows that fibril can seed monomer aggregation and form more fibrils while stable oligomers cannot. (B) Stable oligomers incubate at 37°C by itself monitored by ThT assay shows no increased ThT signal indicate stable oligomers can't convert into fibrils. (C) Fibril seeds added into stable oligomers incubate for 5 days do not show an increased ThT signal which indicates that fibrils can not seed stable oligomers into fibrils.

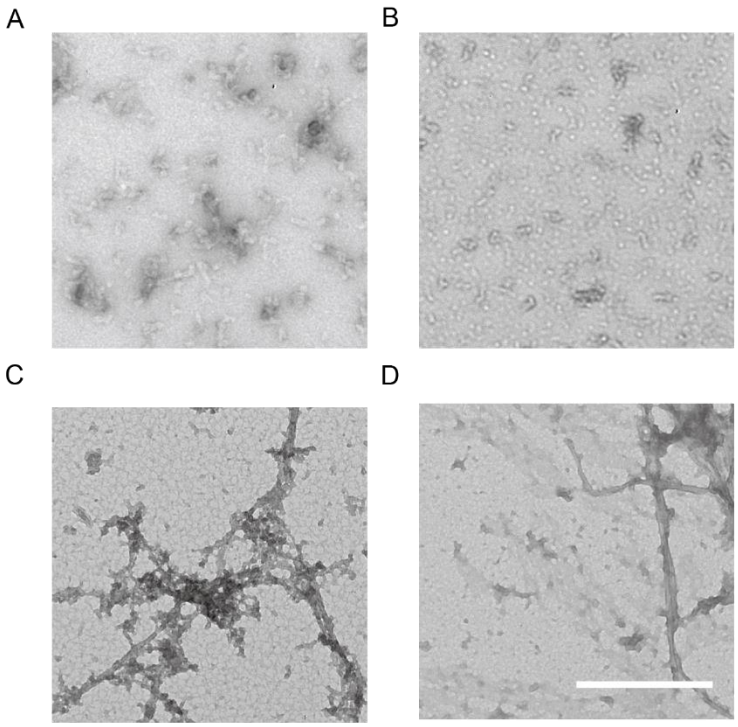

Figure 22. After incubation under 37°C for 6 weeks, big oligomers (A) and small oligomers (B) did not convert into larger aggregates or disaggregate completely into monomers. Big oligomers (C) and small oligomers (D) incubated with fibril seeds for 4 weeks. Stable oligomers cannot be seeded by fibrils to form more fibrils and they are likely to co-localize with fibril in TEM images. Scale bar is 500nm.

Stable oligomers inhibit fibril seeding in a dose dependent manner by interfering with fibril and monomer interactions.

It is shown in the literature that some similar type of oligomers can lead to a longer lag phase in a concentration dependent manner for αs monomer aggregation(*181*). In this work, we test how stable oligomers influence the fibril seeding process. In this set of experiments, we added fibril seeds (1uM) into a monomer pool (40uM) to initiate the seeding process

and tested with different concentration of stable oligomers (0,2,5,10 uM). By adding stable oligomers into the fibril seeding monomer aggregation system, the seeding processes can be suppressed dramatically. With 2 uM of stable oligomers added, a significant delay of ThT intensity increase was shown compared with the sample absent of stable oligomers; with 5uM and 10uM stable oligomers added, no significant ThT intensity increase was detected after 5 days (**Figure 23**). The stoichiometry between stable oligomers and fibrils may suggest that stable oligomers may primarily interact with fibril seeds to interfere with the seeding process. In order to test out how stable oligomers influence seeding processes, we first checked the inhibition effect under different monomer concentrations. Under the same fibril seeds and stable oligomer concentration, we could not detect any increased ThT intensity in the lower monomer concentration sample (20uM). With increasing monomer concentration, we can detect increasing ThT signal at longer incubation time (**Figure 25**). Next, we tested the inhibition effect with different lengths of seeds. It has been shown in the literature that at neutral pH elongation is the predominant seeding process. Under the same protein concentration, the shorter the fibril seeds are the more "elongation sites" will be provided which will result in a faster ThT signal increase. We keep fibril seeds at 1 μM, monomer at 40 μM and stable oligomers at 2 μM in this set of experiments and we sonicate fibril with different time to generate different length seeds. The longer the sonication time the shorter fibril seeds will be. The inhibition effect of seeding processes by stable oligomers are decreased with shorter seeds. Without sonication, fibril seeds and stable oligomers showed 2 days in delay of increased ThT signal; with sonicated fibril seeds, the delay time was dramatically decreased to several hours (**Figure 24**). By enhancing the monomer – fibril interaction,increasing monomer concentration or shorter seeds, the

inhibition effect by stable oligomers is decreased which suggests that stable oligomers interfere with the interactions between monomers and fibrils to inhibit the seeding processes.

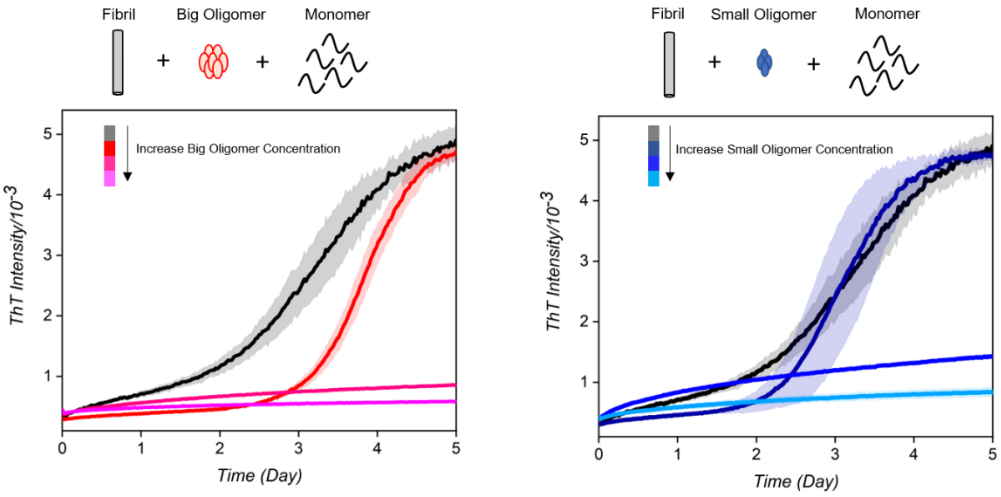

Figure 23. Stable oligomers inhibit the fibril seeding process in a dose dependent manner. 1 uM fibril seeds are added into 40 uM monomer with different stable oligomers concentration (2uM, 5uM and 10uM). Big oligomers (left), small oligomers (right). Seeding processes are monitored by ThT signal changes.

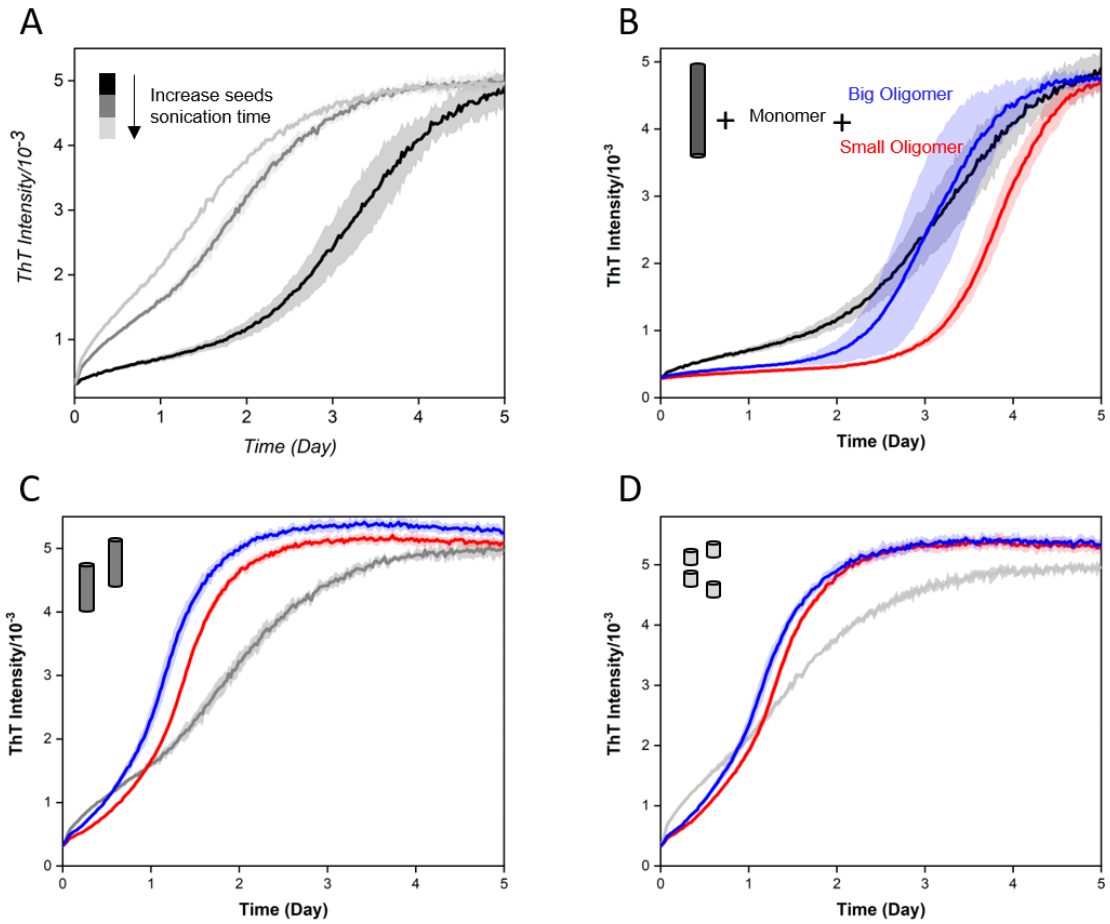

Figure 24. Increasing sonication time of fibril seeds will accelerate seeding processes (A). Non-sonicated seeds (B), 15s sonicated seeds (C) and 120s sonicated seeds (D) were added into 40μM monomer and 2μM big oligomer (blue) or 2μM small oligomer (red). The inhibition effect by stable oligomer is reduced with increasing sonication time of fibrils.

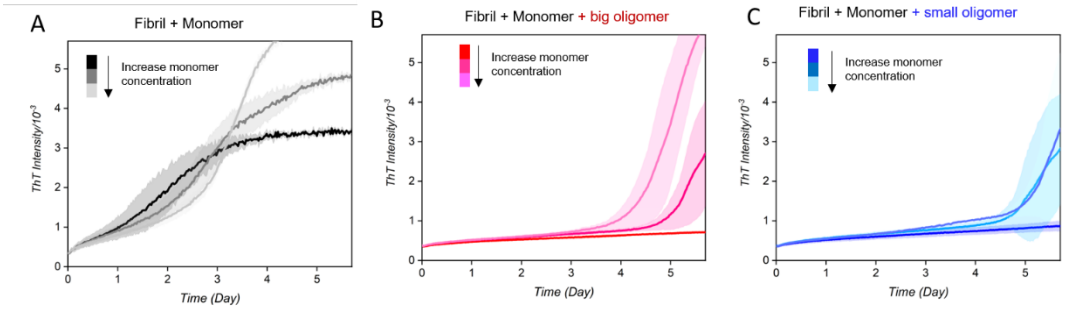

Figure 25. Seeding experiments with different monomer concentration. 1uM fibril seeds with 2uM stable oligomers (A – no oligomers, B- Big oligomers, C – small oligomers) were added into different monomer concentrations (20uM, 40uM and 80uM). The more monomer added, the less the inhibition effect which suggests stable oligomers interact with monomers to influence the seeding process.

Characterization of stable oligomers – monomer and fibrils - monomer interaction by NMR.

NMR is a technique that can detect interactions between proteins at different time scales(*182*). In order to understand the interaction between monomers and different aggregates, we ^{15}N labelled αS monomer and compared pure αS monomer and αS monomer plus monomer equivalent aggregate samples in terms of chemical shift, peak intensity and R2 relaxation changes. By adding fibrils or stable oligomers into ^{15}N labelled monomer, no chemical shifts were observed. But for fibrils added sample, the overall peak intensity is decreased by 15% compared with the pure monomer sample which indicates certain interaction between monomer and fibrils. For stable oligomers added sample, no significant overall peak intensity decrease was observed compared with pure monomer sample, however small peak intensity decreased was shown in NAC region. No significant differences between big and small oligomers were observed (**Figure 26**). Next, we use R_2 relaxation experiments to characterize fast motion interaction between αS monomer and aggregates. Compared with the pure monomer sample, added fibrils and stable oligomers samples showed increased R_2 value at first 20 residue which suggest that both fibrils and stable oligomers interact with monomer through first 20 residues (**Figure 27**).

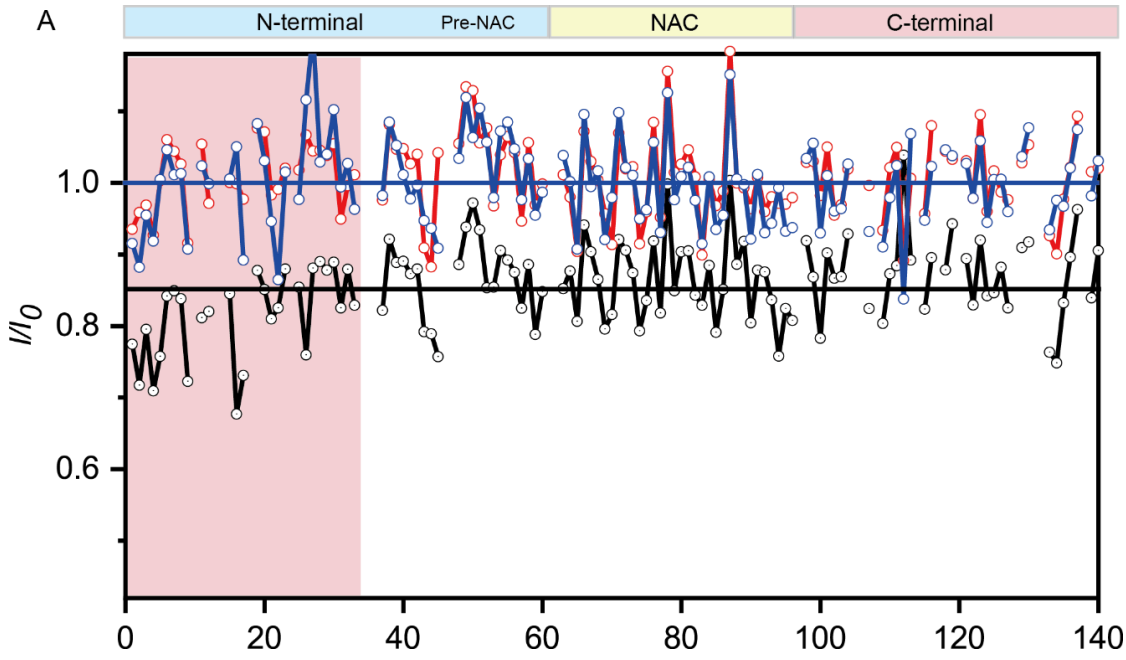

Figure 26. Characterization of alpha-synuclein monomer interaction with fibril seeds and stable oligomers by NMR. Ratio of peak intensity from HSQC spectrum of monomer added fibril (black), big oligomer (red) and small oligomers (blue) verse monomer control sample. Peak intensity differences are highlight in light pink.

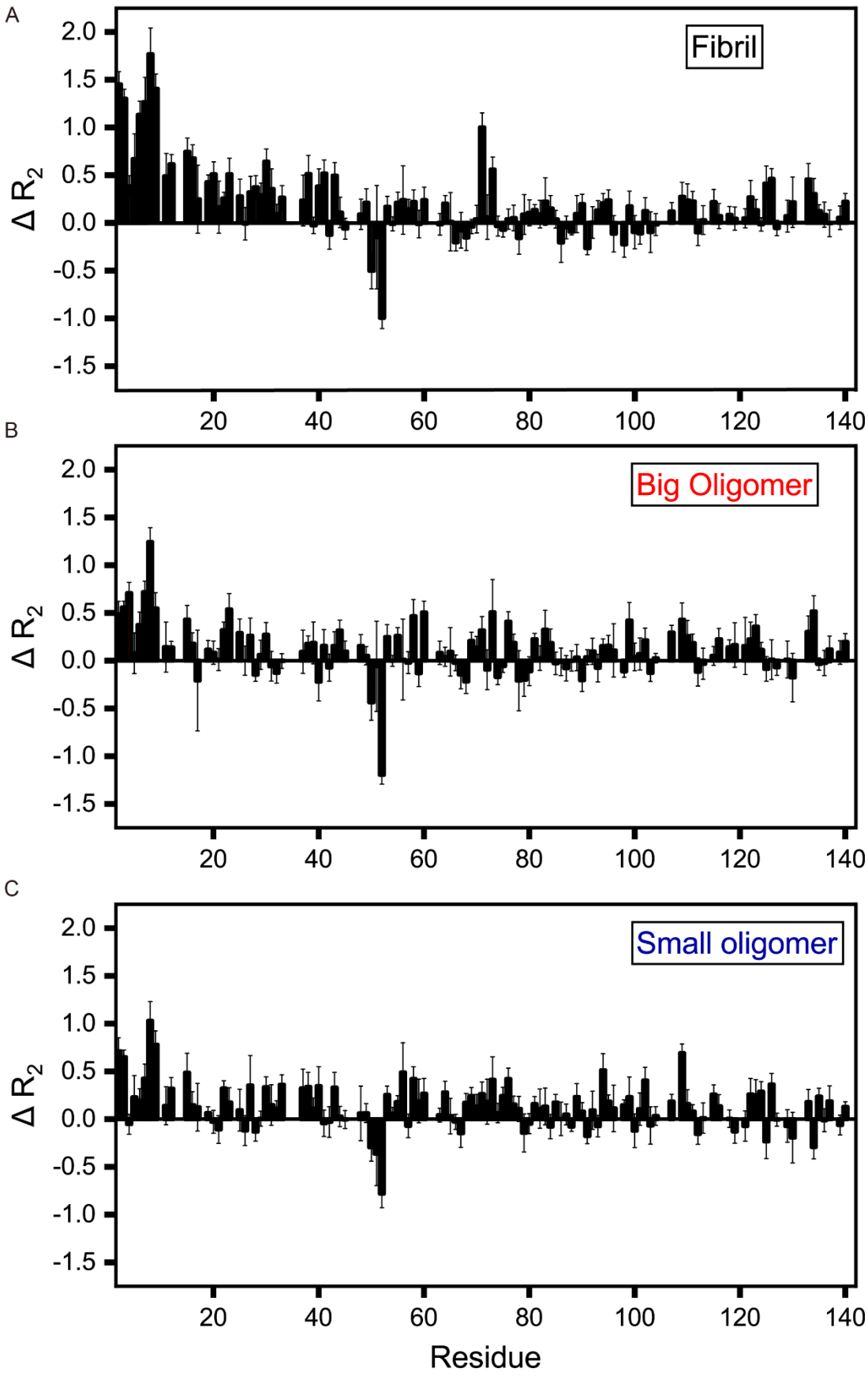
A
Fibril
B
Big Oligomer
C
Small oligomer
Δ R2
2.0
1.5
1.0
0.5
0.0
-0.5
-1.0
-1.5
20
40
60
80
100
120
140
Residue

Figure 27. Delta R_2 value between fibril – monomer(A), big oligomer -monomer (B) and small oligomer – monomer (C). By adding fibrils and stable oligomers into monomer, the monomer N-terminal first 20 residues show increase R_2 values.

Stable oligomers cannot induce cell toxicity as fibrils.

αS monomer misfolds and aggregates are associated with its toxicity(*170*). αS fibrils are shown to induce cell toxicity to human SH-SY5Y neuroblastoma as also demonstrated here by decreased MTS reduction when exposing cells with increasing concentration of fibrils. Under the same conditions, cells treated with the same monomer equivalent concentration of stable oligomers (big oligomers or small oligomers) have no decrease of MTS reduction compared with control cells, which suggests that stable oligomers cannot cause cell viability reducing as fibrils (**Figure 28**). A similar result was obtained by analyzing confocal images' fluorescence intensity of cells treated with αS monomer, big oligomers, small oligomers, and fibrils. All α-synuclein species left in cells were stained after 24h incubation with different aggregates. Fibril treated cells showed 3.3 times higher αS signal than monomer treated cells which suggests that fibrils induced endogenous αS to form aggregates. However for the big and small oligomers treated samples, 1.3 times and 1.7 times increased signal, respectively, was observed which suggests much less aggregates were present in the stable oligomers treated samples (**Figure 29, 30**). In order to rule out the possibility that αS signal increase in the stable oligomers and fibrils treated samples is only because of the treatment, we also labelled treatments with ATTO-488, which is an NHS ester used to label protein via conjugation to primary amine groups. By comparing the fluorescence intensity of ATTO-488, fibrils and small oligomers treated cells have 1.5

times higher intensity than the monomer control which indicates the increase signal of αS species in fibril treated cells is not only coming from the treatment while for small oligomers we cannot rule out the possibility that increase αS is only from added oligomers. Big oligomers treated cells showed 3.2 times higher ATTO - 488 fluorescence intensity than control while the overall αS intensity is only 1.3 times which may suggest that the dye to protein labelling ratio between big oligomers and small oligomers or fibrils are different. Taken all together, the data indicates that stable oligomers cannot induce a decrease in cell viability as fibrils.

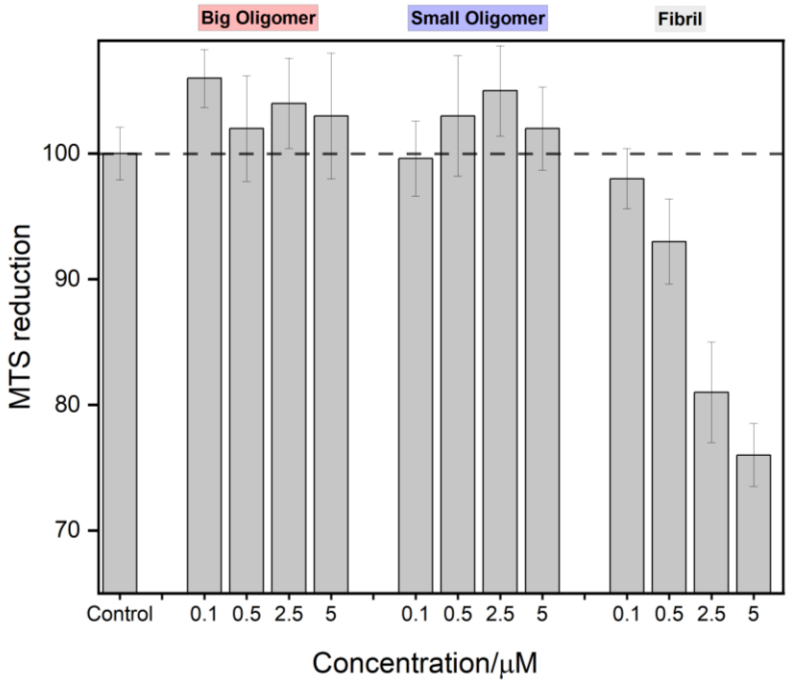

Figure 28. Viability of SH-SY5Y cells assessed by MTS assay after treatment for 48 hours with different concentrations of big oligomer, small oligomers, and fibril. Only fibrils treated cells show reduced MTS reduction.

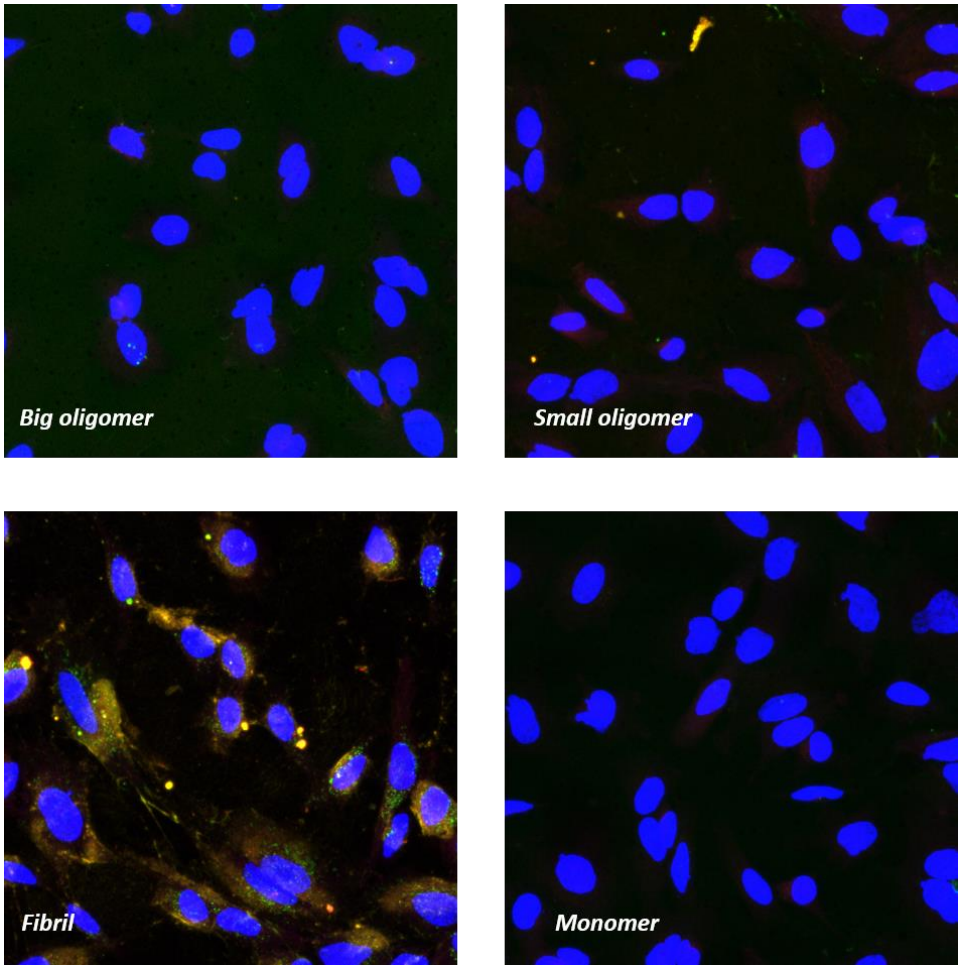

Figure 29. Representative confocal images of SH-SY5Y cells treated with 3µM of big oligomers, small oligomers, fibrils, and monomers. Treatments were labelled with ATTO-488 fluorescence dyes (green); α-synuclein was stained with SYN-1 (red) and nucleus were visualized by DAPI (blue).

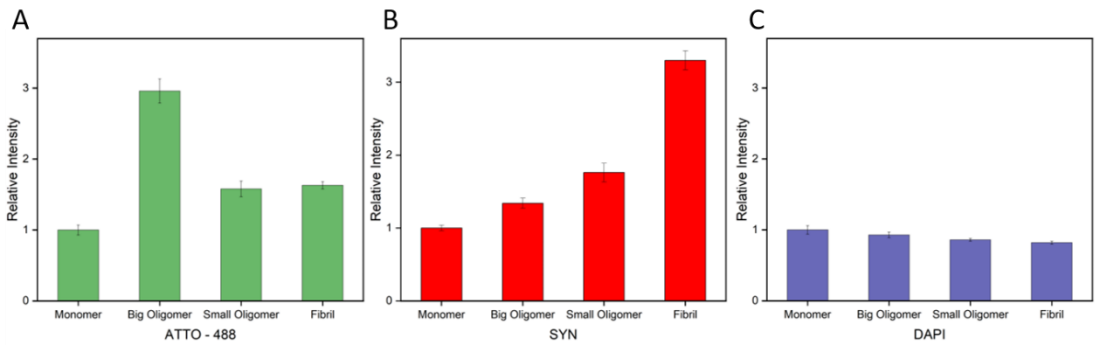

Figure 30. Fluorescence intensity from confocal images averaged from 220 cells form each sample. (A) ATTO-488 labeled treatment, (B) synuclein antibody signal, (C) DAPI signal.

4.3 Discussion

α-synuclein fibril seeding monomer aggregation is a process highly related to synucleinopathy. Once fibril seeds are formed, the autocatalytic reaction is very hard to inhibit which will induce severe cell loss(*183*). A lot of small molecules, antibodies, and polymers have been designed to interact with monomers to delay or inhibit the aggregation by interfering with the primary nucleation; but once fibril seeds have formed the self-seeding processes cannot be efficiently inhibited by those molecules which only act on monomers(*175, 184, 185*). Here, we characterized two types of off-fibril formation pathway oligomers which can inhibit fibril seeding amyloid formation by interfering with the monomer – fibril interactions.

First, we set out to answer the question "what is the role these oligomers play in the fibril formation pathway?" Oligomers can be intermediates between monomers and fibrils or they can be on another pathway which is different from the fibril formation pathway(*181, 186, 187*). In a series of ThT experiments these stable oligomers show off-fibril formation pathway properties – they cannot convert into fibrils, seed monomers to form fibrils, or be seeded by fibrils. The condition that can make these stable oligomers is also a fibril formation condition, suggesting that multiple aggregation pathways can happen simultaneously under this physiological condition. We then asked, "how does this off-fibril

formation pathway stable oligomer influence the fibril seeding processes?" Stable oligomers are on another aggregation pathway, will the aggregates formed on different pathways influence each other or not? By adding different concentrations of stable oligomers into fibril seeding monomer aggregation environments, the seeding reaction is greatly suppressed with stoichiometry ratio between fibrils and stable oligomers. Strengthening the monomer – fibril interaction by increasing monomer concentration or by providing more "fibril ends" in this system will weaken the inhibition effect by stable oligomers which suggests that stable oligomers can interfere with the monomer – fibril interactions. In order to have residue specific information about the interaction between monomers and aggregates, we used NMR to characterize the interaction between them. By analyzing peak intensity changes and R_2 relaxation data, we found that monomers interact with both stable oligomers and fibrils primarily through the first 20 residues at the N-terminus in a similar way which may result in competing interactions between monomer – stable oligomers and monomer -fibrils. This competing interaction may contribute to the inhibition effect. The profiles of peak intensity changes and delta R_2 across the sequence of monomer plus stable oligomers or fibrils are not the same. These subtle differences may be the reason that fibrils can seed monomer aggregation while stable oligomers cannot. The interaction between stable oligomers and fibrils may also contribute to the inhibition effect. These aggregates are solution NMR invisible; we cannot characterize the interaction between them and get residue specific information. But the stoichiometry between stable oligomers and fibrils and sub-stoichiometry between oligomers and monomers in ThT data suggest that certain interactions between stable oligomers and fibrils result in the inhibition phenomenon.

The big and small stable oligomers share a similar inhibition effect and secondary structure, but they have different morphologies. Are they the same types of oligomers with different sizes or are they different oligomers species? Our data suggest that big and small oligomers cannot inter-convert and that they interact with monomers in a similar way but with several differences. These indicate that big and small oligomers may form on the same aggregation pathway, but they are different species. Understanding the similarities and differences in structure and dynamic of these two types of oligomers may give us valuable information for the critical interactions that inhibit the seeding reaction.

Our work provides a new perspective α-synuclein aggregation inhibition which is using the interactions between different forms of α-synuclein to inhibit the gain-of-toxic seeding amyloid formation process. Understanding the interactions between monomers, oligomers, and fibrils is critical for any drug design. Future work can focus on designing molecules that can mimic the interactions of stable oligomers with fibrils and monomers or push the aggregation towards the off-fibril formation pathway.

4.4 Method

Protein expression and purification

Expression of N-terminal acetylate αS (Ac-αS) was done by co-expression with pNatB plasmid in *E. coli* BL21(DE3) cells. ^{15}N labeled Ac-αS was expressed in M9 minimal media with ^{15}N-ammonium chloride as the only nitrogen source. Purification was done as previously described(*188*). Protein purity and molecular weight were confirmed by ESI-MS. Protein was stored as lyophilized powder in -20°C until usage.

Stable oligomers and fibrils preparation

Stable oligomers were prepared by dissolving 10mg protein powder in 1mL 10 mM PBS buffer (pH =7.4) and incubated at 37°C for 5 hours with 300 rpm shaking speed. The sample was then loaded on a Superose 6 size exclusion column (GE) and eluted with PBS buffer at a flow rate of 0.3ml/min. Oligomer samples were concentrated with 3kDa centrifuge units when needed. Oligomer samples were kept in 4°C until use and all oligomer samples were used for different experiments within 24 hours. Fibrils were prepared as previous described(*189*). Probe sonication was applied to fibril seeds and fibrils used for cell toxicity treatment with 30% power. Sonication fibrils' morphology and length distribution were confirmed by TEM. Oligomer and fibril concentrations were measured by UV 280 nm after denatured with 4M guanidine hydrochloride.

Thioflavin T seeding experiments

α-synuclein protein powder was dissolved in PBS (pH = 7.4) buffer and used 50kDa centrifuge units to remove large aggregates formed during lyophilization. Different concentrations of fibril seeds or stable oligomers were added into monomer solutions with 20 μM ThT. 100 μL solution was added into 96-well plate and sealed with Axygen sealing tape. Plate was incubated at 37 °C in a POLARstar Omega fluorimeter under quiescent condition. Fluorescence was monitored every 33 mins for at least 5 days.

Transmission Electron Microscope (TEM)

3.5 μL samples were applied on a carbon coated cooper gird and incubated for 90s. Excessive solution was removed by taping dry with filter paper. 3.5 μL 3% uranyl acetate solution was added on the grid and incubated for 60s followed by washing with 3.5 μL

MilliQ water twice. Images were recorded with a JEOL 1200EX electron microscope with 80k voltage.

Circular Dichroism (CD)

Far-UV wavelength spectra of stable oligomers and fibrils were measured by an AVIV420SF circular dichroism spectrophotometer (Biomedical Inc., Lakewood, NJ) in a 1mm cuvette at 25 °C. The averaging time was 10 seconds and measured from 200 – 260 nm at a step size of 1 nm. Samples were diluted in 100mM phosphate buffer (pH=7.4)

Time dependent Proteinase K digestion

70μM monomer equivalent samples were incubated with 1μg/ml proteinase K in PBS (pH=7.4) buffer at 37 °C for different times. Digestion reactions were stopped by heating on a water bath (100°C) for 5 mins and mixed with 4x SDS-PAGE loading buffer. Samples were loaded on precast gel and run at 120V for 1h.

Cell culture

Human SH-SY5Y neuroblastoma cells were cultured in DMEM/F12 (GE Healthcare) with 10% fetal bovine serum (FBS) and kept in a 5% CO_2 humidified atmosphere at 37°C. For cell viability assay and immunocytochemistry, cells were placed into 96-well plate or 12-well plate (Cellvis, Mountain View, CA) and waited for at least 24 hours for recovery.

Cell viability MTS reduction assay

Cells were treated with different concentrations of fibrils or oligomers for 48 hours. Cell Viability was measured by adding 3-(4, 5-dimethylthiazol-2-yl)-5-(3-

carboxymethoxyphenol)-2-(4-sulfophenyl)-2H-tetrazolium (MTS, Promega, USA) and incubated for 2 hours at 37°C. Absorbance was measured at 490 nm which is directly proportional to the number of living cells in the culture.

Preparation of ATTO-488 Labelled samples

Samples (monomer, stable oligomers and fibrils) were labeled with the fluorescent ATTO488-NHS-ester (ATTO-TEC GmbH) per the manufacturer's procedure. In brief, samples were incubated with a 2 M excess of ATTO448-NHS-ester in labeling buffer (pH 8.3 PBS/sodium bicarbonate solution) for 1 hour at room temperature. Conjugated ATTO488-fibrils were then separated from unreacted fluorophore by centrifugation at 16k rpm for 30 min and resuspension of the ATTO488-fibril pellet in pH 7.4 PBS; this centrifugation/resuspension wash was repeated twice. Monomers and stable oligomers were using 3kDa centrifuge units to remove unbound fluorophore by washing 3 times with PBS (pH = 7.4) buffer.

Immunocytochemistry

Cells were fixed with 10% formalin (Sigma Aldrich, St. Louis, MO) and permeabilized in PBS buffer with 0.5% Triton. Before incubated with antibodies, cells were blocking by incubating with 5% Donkey Serum solution for 30min at 37°C. Cells were incubated with primary antibody (SYN-1) at 4°C overnight and protected from light. Afterwards cells were washed with PBS for 15 min and incubated with fluorophore-conjugated secondary antibody (TRITC antibody, Sigma Aldrich) for 1h. Cell nuclei were visualized by 4', 6-diamidino-2-phenylindole (DAPI). All samples were imaged by a Zeiss LSM 780 confocal laser scanning microscope.

Nuclear Magnetic Resonance (NMR) Experiments

All NMR experiments were performed in 10 mM PBS (pH = 7.4) with 10% D_2O at 4℃. Monomer samples were prepared by dissolve protein powder in PBS buffer and removing large aggregates by 50kDa centrifuge unit, concentrated with 3kDa when needed. Fibrils used for NMR were sonicated for 2 mins with 30s on, 30s off at power 30% on ice before NMR measurement.

Chapter 5 Dynamic nature of αSynuclein oligomers and fibrils.

5.1 Introduction

αSynuclein fibrils and oligomers are two distinct species formed during the αSynuclein aggregation process. Amyloid fibrils are believed to be the "end product" of synuclein aggregation and deposit into Lewy bodies *in vivo(190, 191)*. Fibrils have shown the ability to interfere with different cellular activities and cause dopamine cell loss in extensive research(*181, 183, 192, 193*). Before sedimenting into Lewy bodies, fibrils can efficiently seed monomer aggregation and propagate between cells, making them a notorious species for causing and aggravating neurodegenerative diseases(*194-196*). Oligomers are a diverse group of aggregates, potentially having different sizes, structures, stability and other properties(*179*). The wide definition and heterogeneous nature of oligomers makes them harder to study and understand. However, based on the role oligomers play during the aggregation process, oligomers can be defined as either on-fibril or off-fibril formation pathways(*179*). On-fibril formation pathway oligomers can convert into fibrils under certain conditions and are the intermediates between monomers and fibrils. Off-fibril formation pathway oligomers are often stable, and sometimes show inhibitory ability(*181*). Oligomers acquired with different protocols have shown toxicity in different cell models and can permeabilize into vesicles better than monomers and fibrils (*197, 198*).

Both fibrils and oligomers may be related to dopamine loss(*178, 198*). A lot of work has been done to characterize the structure, toxicity, and seeding ability of both fibrils and oligomers.(*199-202*). cryo-EM and ssNMR studies have revealed the reserved "Greek-key" motif structure in different αSynuclein fibrils (formed by different familial mutations,

under different buffer conditions, and with different post-translational modifications) and the two filament packing of αSynuclein fibrils plays a critical role in their ability to seed aggregation.(*203-205*). FRET work has captured the conversion between non-PK resistant oligomers and PK resistant oligomers, which reveals the structural build-up during the aggregation pathway(*186*). AFM, SAXS and Cryo-EM studies have characterized oligomers isolated via different methods that may share common structures(*181, 199, 202, 206*).

However, fibrils and oligomers are dynamic molecules in solution(*155, 207*). Based on the static structure alone, it is very hard to get a comprehensive understanding of these aggregates and design effective therapies. It has been shown that monomers in amyloid fibrils are in equilibrium with free monomers, which is a molecular recycling mechanism(*155, 208*). Oligomers can also interconvert with each other or with monomers. These dynamic properties of fibrils and oligomers may contribute to their toxicity and ability to propagate or seed aggregation. Thus, having a detailed characterization of the dynamics of fibrils and oligomers in solution will provide valuable information for therapeutic design. Because of the large molecular weight and heterogeneity of fibrils and oligomers, it is very hard to characterize them by the standard methods used to identify soluble protein interactions and varying equilibration states. In this work, we take advantage of solution NMR to probe disordered proteins and characterize the monomer-aggregate equilibration, which possess the same interactions that govern the seeding or oligomer formation processes.

In chapter 4, we have set up protocols for making samples of sonicated fibrils and stable oligomers for solution NMR. In this chapter, we use this sample preparation protocol and characterize the dynamic behavior of these oligomers and fibrils. For solution NMR, oligomers and fibrils are large molecules that are beyond the detection limits, but because of the equilibration with the monomeric form, we can always detect monomer – aggregate equilibration and interactions(*208*). By analyzing the ^{15}N labelled fibrils and oligomers, we determined the aggregates are in equilibration with monomers and equilibration monomers interact with aggregates through N-terminal residues. Adding excess monomers into this equilibration system shifts the reaction direction towards fibril formation, which occurs via the seeding process. Overall, by utilizing solution NMR experiments, we characterized the dynamic equilibration of fibrils and oligomers which will further our understanding of seeded aggregation.

5.2 Result

Stable oligomers and fibrils are in equilibration with monomers in solution.

First, we prepared ^{15}N labelled stable oligomers and fibrils and carried out ^{1}H-^{15}N HSQC experiments. When using solution NMR, it is very hard to get structural information on large protein complexes, such as oligomers (over 260kDa on SDS-PAGE) and fibrils, but we can get information on any flexible region in the oligomers or fibrils. The HSQC spectrum of both stable oligomers and fibrils overlap with the monomer spectrum nicely, which means the IDP state of the monomer is present in the sample. This is consistent with

SEC data, where stable oligomers re-injected revealed that small amounts of monomer will shed from oligomers once all the monomers are removed. For αS fibrils, it is already well-established in the literature that monomers can be released from amyloid fibrils when the monomer concentration in the system is lower than a certain critical number(*209*). Taken together, both stable oligomers and fibrils are in equilibration with monomers in solution.

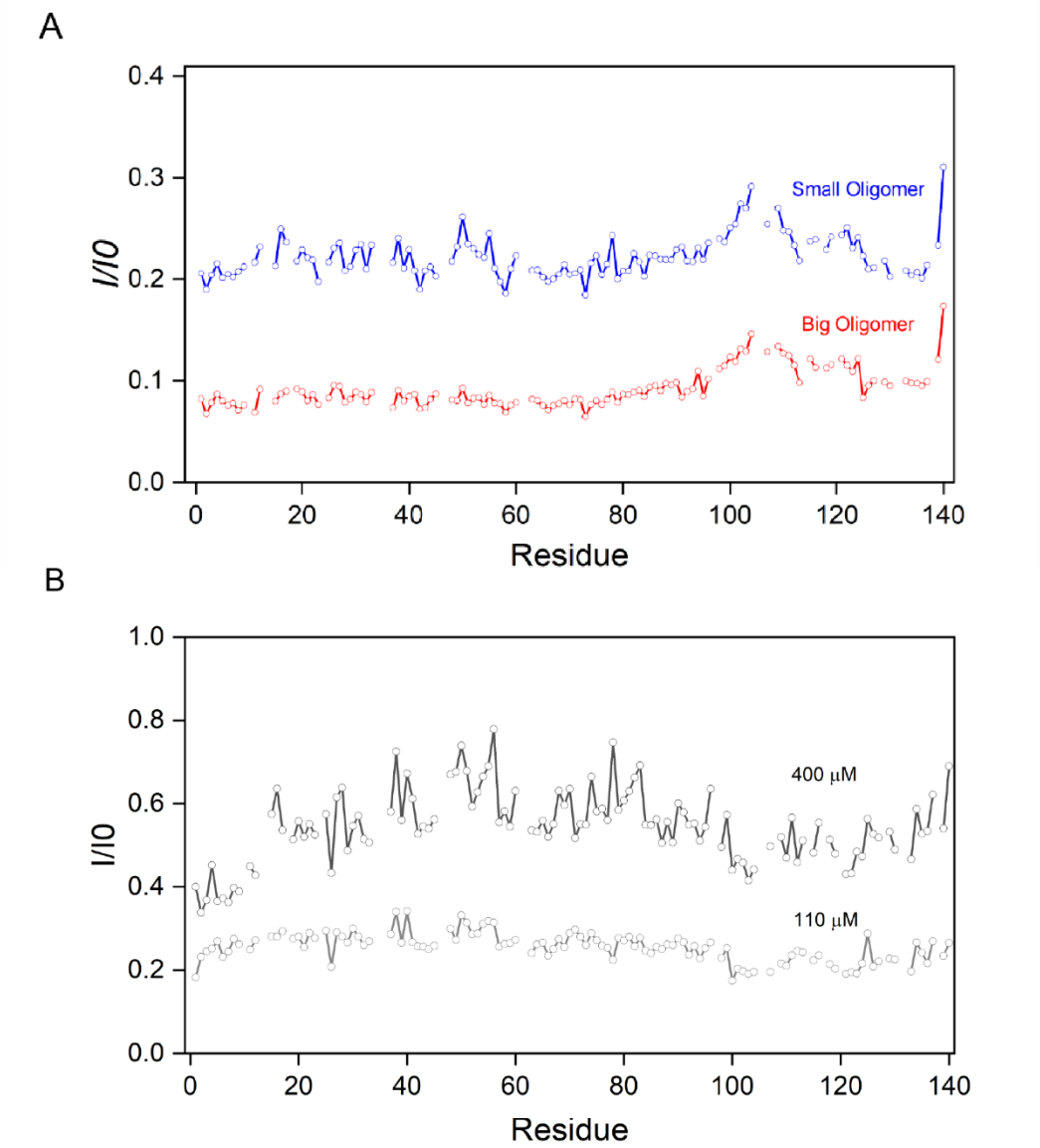

Figure 31. Peak intensity ratio of big or small oligomers (A) / monomer; sonicatied fibril (B) / monomer. Stable oligomers and fibrils are in equilibration with monomers. Stable oligomers showed increased C- terminus peak intensity and fibrils sample shows decreased peak intensity in both the N- and C- terminus. Reducing total protein concentration in sonicatied fibril sample from 400μM to 110 μM, the peak intensity differences across the sequence are decreased**.**

Stable oligomers show increased C-terminal peak intensity in solution NMR.

The HSQC spectrum of stable oligomers are overlaid with the monomers' spectrum, and by comparison, the peak intensity of pure monomer sample with the oligomer sample suggests that around 4% of the big oligomer and 8.5% of the small oligomer samples are in the monomeric state. For both big oligomers and small oligomers, the C-terminal peak intensity is slightly higher than the N-terminal and NAC region which may suggest that certain C-terminal residues in the oligomers are still flexible or some monomers are tightly bound to oligomers through the N – terminal and NAC region (**Figure 31**). This is consistent with the literature, where Otzen and co-workers have shown via solution NMR that some type of oligomers have a flexible C-terminal(*210*). The profile differences of peak intensity ratios between big and small oligomers are mainly at N- and NAC region – small oligomers show more bumpiness within those regions than big oligomers.

Equilibration monomer from stable oligomers shows different relaxation dynamic than free monomer.

R_2 relaxation experiments have been performed on big and small oligomers. Because of the equilibration nature of oligomers, we are monitoring the equilibration monomer and flexible region of oligomers in this set of experiments. For both stable oligomers, the overall R_2 value increased and has a different profile than the monomeric form, which suggests that the equilibration monomer from oligomers are not "free" monomers. The R_2 value of the C-termini in both oligomer samples have increased a lot, which could indicate a flexible C-terminal region in the oligomers. For big and small oligomers, the first 12 residues in the N-terminal showed increased R_2 values which is consistent with the data from labelled monomers added into non-labelled oligomer samples in Chapter 4, which suggests that both equilibration and added monomers interact with stable oligomers in a similar way (**Figure 32**). For the small oligomer sample, an increased R2 value also can be observed around residues 40-50. Again, we can't distinguish if the increased peak intensity (increased R_2 value) in the C-terminal is from oligomers themselves or monomers that are tightly bound on the oligomer surface, but the increased R_2 values in the N-terminal indicates the presence of interactions between large molecular weight oligomers and the equilibration monomers.

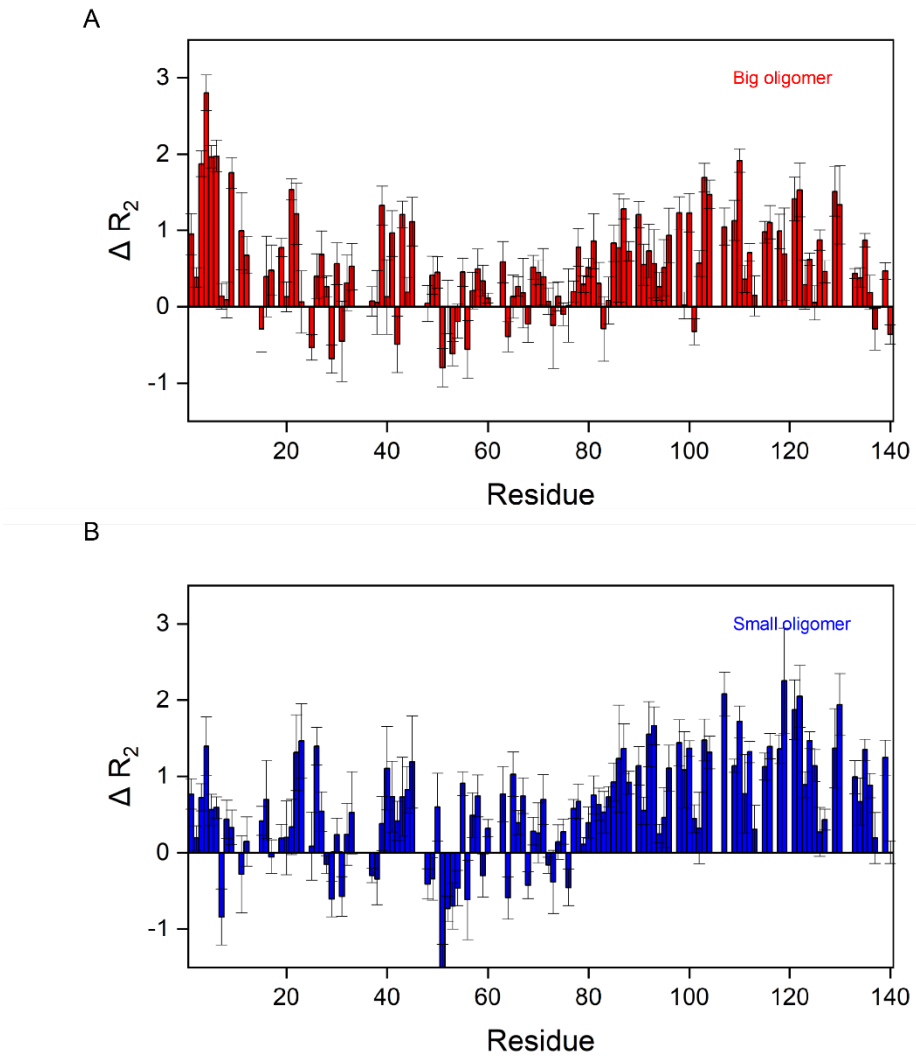

Figure 32. Comparison of the ΔR_2 value between monomer and big oligomers (A) and small oligomer (B). For both samples, the C-terminals have significant increased R_2 values compared to the monomeric form. The first 12 residues of the N-terminal showed increased R_2 values, which is consistent with adding excess monomer into stable oligomers.

Equilibration monomers from fibrils interact with fibril primarily through N- and C-terminus.

Fibrils are not visible in solution NMR, but we can monitor the equilibration monomers via fibrils to get information about the equilibration monomers and their interactions. By analyzing the peak intensity ratio of fibrils and sample of pure monomer, both the N- (0-20) and C- (100-120) termini shows decreased peak intensity, which suggests that equilibration monomers interact with fibrils through these two termini. When the total protein concentration in the sample is decreased from 400 μM to 100 μM, the peak intensity differences between the N-, NAC and C- termini are reduced, which suggests the equilibration process and interactions may be concentration related.

We also preformedR_2 relaxation experiments on the fibril samples. For both 700 and 800 MHz NMR, a large increase in the R_2 value is present in the first 20 residues of the N-terminal, which is consistent with the R_2 data of adding excessive monomer to fibril. Residues 20-40 also showed an increased R_2 value, but not as large as the first 20 residues. Although the C-terminal showed a similar peak intensity decrease as the N-terminal, the R_2 value along the C-terminal didn't change to the same degree, only a 1 or 2 Hz difference was observed which indicates the interactions happening in the N- or C- terminal are different. The relaxation experiments done with different NMR fields shows differences in ΔR_2 values from residue 48 to 123, which includes the preNAC and NAC regions. For the 800 MHz NMR data, the ΔR_2 values in residues 48 to 123 are all within 2 Hz. Residues 51 – 56 and residues 98 – 103 have shown negative delta R_2 values. For the same fibril sample, R_2 relaxation experiments also done on a 700 MHz NMR, residues 48 to 123

showed no negative ΔR_2 values. Slightly increased R_2 values were shown across the preNAC and NAC regions (**Figure 33**). The consistency of ΔR_2 data in the early N-terminus and late C-terminus on different field NMRs indicates that these changes are coming from interactions or conversion with NMR invisible aggregates, the fibril form. The different ΔR2 values in the preNAC and NAC region may suggest that exchange between different states of these regions may occur.

We also investigated how concentration influences the dynamic equilibration between monomer and fibrils. By lowering the concentration to 110 μM, the R_2 values also decreased, but we can still see increased R_2 values on the first 12 residues. The negative ΔR_2 around residues 51 – 56 and 98 - 103 are consistent with a high concentration sample. The changes in R_2 values in different concentration samples suggests that the equilibration process is influenced by monomer or total protein concentration.

Overall, in the mixture of fibril and equilibration monomer system, no chemical shift was observed, and peak intensity decreases are not uniform across the entire sequence, indicating that a higher fraction of N- and C- terminus residues are immobilized on fibrils. The R_2 value increase was inconsistent across the entire sequence and was influenced by different NMR fields, suggesting multiple, long-lived states of fibril – bound or interacting with αSynuclein monomer.

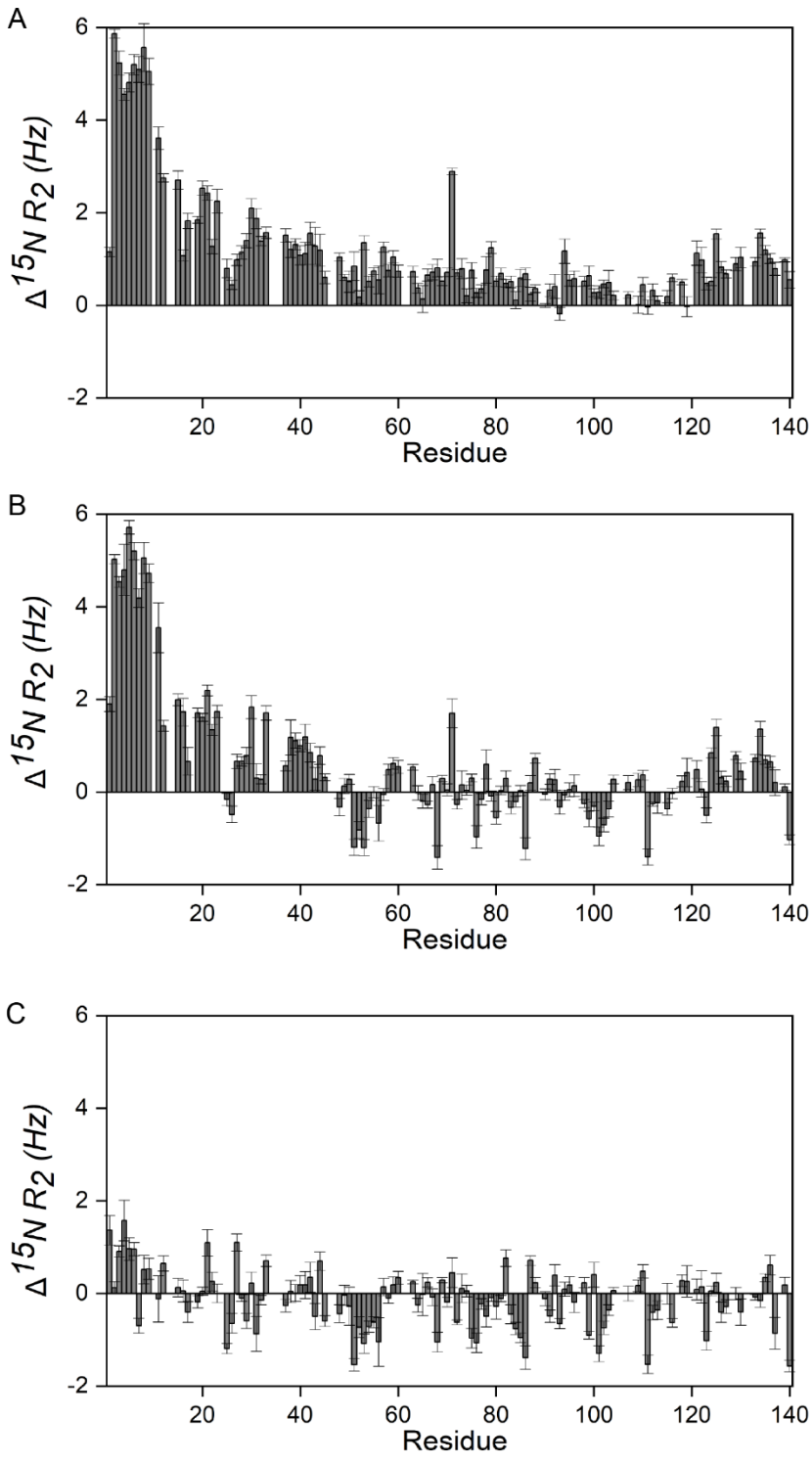

Figure 33. Characterizing interactions between fibrils and the equilibration monomers. R_2 relaxation experiments were done on 800 MHz NMR of 400µM (B) and 110µM (C)

sonicated fibrils. ΔR_2 values were calculated by subtracting the R_2 value of the 150μM monomer sample. R_2 relaxation experiments of 400μM sonicated fibril samples also performed on a 700 MHz NMR(A). Compared with "free" monomers, equilibration monomers interact with fibrils through multiple sites. The first 45 residues in the N-terminal shows the largest changes in R_2 values and residues 120 -140 of the C-terminal shows slightly increased ΔR_2 values for both the 700 MHz and 800 MHz NMR data. Lower protein concentration sample(C) doesn't show as large of a ΔR_2 compared to the high concentration sample.

R_2 values of αSynuclein monomers are influences by different NMR fields.

R_2 data is usually used to characterize protein dynamics, where higher R_2 values usually indicate a more rigid region. In our ΔR_2 data, which compared the monomer and fibril samples from the 800 MHz NMR, negative ΔR_2 values of some residues was observed. With the fibrils present, monomers are supposed to be more rigid than when they are in the "free" state. The negative value indicates that certain residues are more dynamic or flexible than pure monomer, but we didn't observe the same negative values on the 700 MHz NMR. We do not quite understand what negative ΔR_2 values really means. More detailed analyses and experiments need to be done to answer this question. However, we compared the R_2 profile of monomer in different NMR fields and found out the R_2 value from the 800 MHz NMR is overall slightly higher than the 700 MHz NMR with more bumpiness (**Figure 34**). The magnetic field differences may contribute to the negative ΔR_2 values.

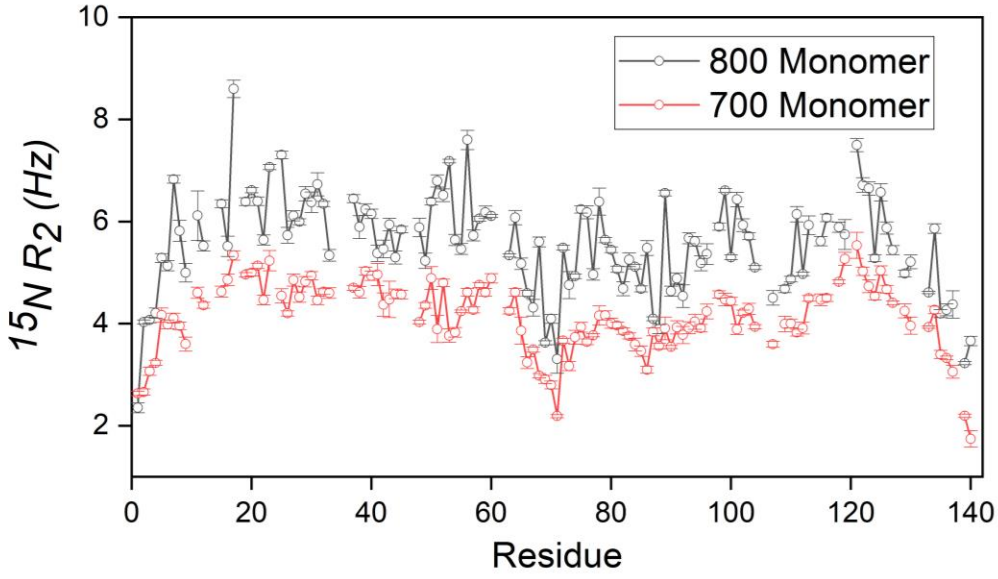

Figure 34. Relaxation dynamics of αSynuclein monomer in PBS buffer at 4 °C acquired on different NMR fields. Black – 800 MHz NMR; red – 700 MHz NMR. Monomer concentration is 150 μM.

5.3 Discussion

Fibrils and oligomers are aggregates formed during the progression of PD(*208*). Abundant work has been focusing on inhibiting the formation of aggregates or the clearance of oligomers and fibrils(*211*). Increased levels of oligomers can be found in PD or other synucleinopathies patients' blood and saliva, which indicates they may form in the early stage and accumulate during the progression of diseases(*212-214*). αS fibrils are the main protein accumulated in Lewy bodies that are found postmortem(*191*). Oligomers and fibrils made via *in vitro* methods have been characterized in terms of structure, toxicity and seeding ability, providing more information for therapeutic design. However, oligomers

and fibrils are dynamic species in solution or in cellular environments, which are missing in the literature. In this chapter, we characterize the equilibration between aggregates and monomers and the interactions between oligomers or fibrils with their equilibration monomers. This information on their dynamics provides another aspect of properties of amyloid aggregates that are critical to understanding their role in neurodegenerative diseases.

Based on our solution NMR data, both stable oligomers and fibrils are in equilibration with monomers. No "pure" oligomer or fibril samples have been made in solution, with around 10% of the total protein concentration in the monomeric form(*210*). The presence of low equilibration monomer concentrations may corelate with literature, which indicates that below a certain critical monomer concentration, aggregation cannot happen. It has been shown in the literature that amyloid fibrils undergo a molecular recycling process where monomers associate and dissociate from fibrils. Adding excess monomers into "equilibrated" fibril samples will break the monomer – fibril equilibration and move the reaction towards the fibril direction, which is the seeding process. The interaction between fibrils and equilibration monomers may provide us with information about the seeding interaction. Based on the peak intensity ratio of the "fibril" sample versus the monomer sample, both the N- (1-20) and C- (100-120) termini of equilibration monomers are decreased compared to the other regions, which suggests equilibration monomers interact with fibrils through these two regions. By comparing the R_2 relaxation data of "fibril" samples with pure monomer, the N- (1-45) and C- (125-138) termini residues of equilibration monomers show significant increased R_2 values. Within this region, the first

12 residue have the largest increased R_2 value, which suggests this region is much more rigid compared to its monomeric state. The C-terminal residues have similar levels of peak intensity decreases, but their R_2 values only show slight increases, which suggests the interactions in the C- terminal region are different from the N-terminal region. Overall, our data suggests that the equilibration monomers interact with fibrils through the N- and C-termini, which may be critical interactions for the seeding process. More work is needed to characterize the interaction fibrils and monomers in equilibration and in the seeding reaction. The next step could be adding different concentrations of ^{15}N labelled monomer or non-labelled monomer into fibrils to investigate the interaction changes by adding excess monomer.

Stable oligomers are also dynamic species in solution. They share some similarity with fibrils, but stable oligomers are not completely invisible to solution NMR. The increased C-terminal peak intensity suggests that some monomer C-terminal region is still in an IDP state in the oligomers, which may be consistent with the increased R_2 values in the C-terminal. Because we cannot distinguish between equilibration monomers and the IDP-like part in oligomers, it is very hard to get detailed information about how oligomers interact with equilibration monomers.

We demonstrated in this chapter that both stable oligomers and fibrils are dynamic species and are in equilibration with monomers. For future therapeutic design, the dynamic nature

should be considered. Approaches can be used to push aggregate – monomer equilibration towards the monomer direction, which will disaggregate fibrils or stable oligomers.

5.4 Method

Protein expression and purification

Expression of N-terminal acetylation αS (Ac-αS) was done by co-expression with pNatB plasmid in *E. coli* BL21(DE3) cells. ^{15}N labeled Ac-αS was expressed in M9 minimal media with ^{15}N-ammonium chloride as the only nitrogen sources. Purification was done as previously described(*188*). Protein purity and molecular weight was confirmed by ESI-MS. Protein was stored as lyophilized powder in -20°C until usage.

Nuclear Magnetic Resonance (NMR) Experiments

All NMR experiments were performed in 10 mM PBS (pH = 7.4) with 10% D_2O at temperature below 4°C. Monomer samples were prepared by dissolving protein powder in PBS buffer and removing large aggregates by 50kDa centrifuge unit, concentrated with 3kDa when needed. Fibrils used for NMR were prepared as previously described and followed by sonication for 2 mins with 30s on, 30s off at power 30% on ice before NMR measurement.

Chapter 6 What makes an amyloid fibril a good seeder? – A comparison of αSynuclein and βSynuclein fibrils

6.1 Introduction

βSynuclein has been recognized as a natural αSynuclein aggregation inhibitor(*215*). The amino acid sequence similarity between αSynuclein and βSynuclein is about 78%. Relative to αSynuclein the N- terminal domain of βSynuclein contains only 8 residue substitutions, while there is an 11 residue deletion in the NAC region(*188, 216*). Both synucleins are co-localized at the pre-synapse, but only αSynuclein is found in Lewy bodies(*217*). No evidence has shown that βSynuclein aggregates and forms amyloid fibrils *in vivo* or *in vitro* under cytoplasmic physiological conditions(*218*). There are two mutations of βSynuclein (V70M and P123H) that are associated with LB Dementia, suggesting a role for βSynuclein in the pathophysiology of neurodegeneration(*219, 220*). But no evidence has shown that these two βSynuclein mutations can form amyloid aggregates in a similar manner as αSynuclein. All these facts lead to one question – why can't βSynuclein aggregate like αSynuclein? Extensive research has been done to compare the differences between αSynuclein and βSynuclein in terms of structure, aggregation ability, aggregate formation and physiological functions at the monomer level. Yet we still don't know what key factors differentiate aggregation ability while maintaining high similarity in sequence.

As discussed in chapter 2, recent work has shown that over expression of βSynuclein can lead to neurotoxicity, but to a lesser extent than overexpressing αSynuclein in neurons(*221*). Understanding βSynuclein's aggregation pathway, and its relationship to toxicity, is critical to reveal a general mechanism for synuclein pathology. Under physiological conditions,

βSynuclein only forms oligomers and mostly stays in the monomer stage(*218*). A lot of work has been done to investigate under what conditions βSynuclein can form amyloid fibrils. For example, an acidic environmental pH, adding metal ions and certain pesticides, the presence of lipid vesicles at elevated temperatures, and a single mutation at residue 61 will result in βSynuclein fibril formation(*188, 222*). This information suggests that under physiological conditions, βSynuclein does not have the same fibril formation propensity as αSynuclein, but we can "push" it to form amyloid fibrils. However, since we can induce fibril formation of βSynuclein, the question then becomes: Are fibrils formed by βSynuclein the same as αSynuclein fibrils in terms of structure, seeding aggregation ability, toxicity and dynamics?

In this chapter, we compare the fibrils formed by βSynuclein at pH = 5.8 and fibrils formed by αSynuclein at pH = 7.4, and discover that βSynuclein fibrils under lower pH conditions have a reduced stability and reduced ability to seed monomer aggregations relative to αSynuclein fibrils. However, both αSynuclein fibrils and βSynuclein fibrils can decrease SH-SY5Y cell viability at similar levels, which suggests that beside seeding aggregation of endogenous monomer, other factors also contribute to the toxicity of amyloid fibrils. Further work to investigate the structure and dynamics of βSynuclein fibrils may reveal an underlying reason why αSynuclein fibrils can seed aggregation better than βSynuclein.

6.2 Results

βSynuclein forms “Ribbons” Under low pH conditions.

First, we used ThT aggregation assays to characterize aggregation kinetics of αSynuclein and βSynuclein under pH 7.4 and 5.8. Consistent with the literature, βSynuclein only forms ThT positive aggregates at lower pH while αSynuclein can form amyloid fibrils at both pH (**Figure 35 a, b**)(*188*). The morphology of aggregates formed during the ThT assay was confirmed by TEM. αSynuclein fibrils formed under pH 7.4 showed straight or twisted morphology and have a width around 10 nm to 15 nm, consistent with previous research (**Figure 35 c, d**)(*204*). αSynuclein fibrils formed under lower pH have different morphology than at pH 7.4, where they are clumped together and harder to get images of single fibrils by TEM (data not shown). For βSynuclein fibrils, they show “Ribbon” like morphology which is wider than a typical αSynuclein fibril and there is no twisted pattern(*180*). The ThT intensity from the aggregation assay also confirmed that under the same protein concentration, βSynuclein fibrils only show 10% of the maximum ThT fluorescence intensity of αSynuclein fibrils. Therefore, the TEM morphology and ThT intensity suggest that βSynuclein form “Ribbon” fibrils at pH 5.8.

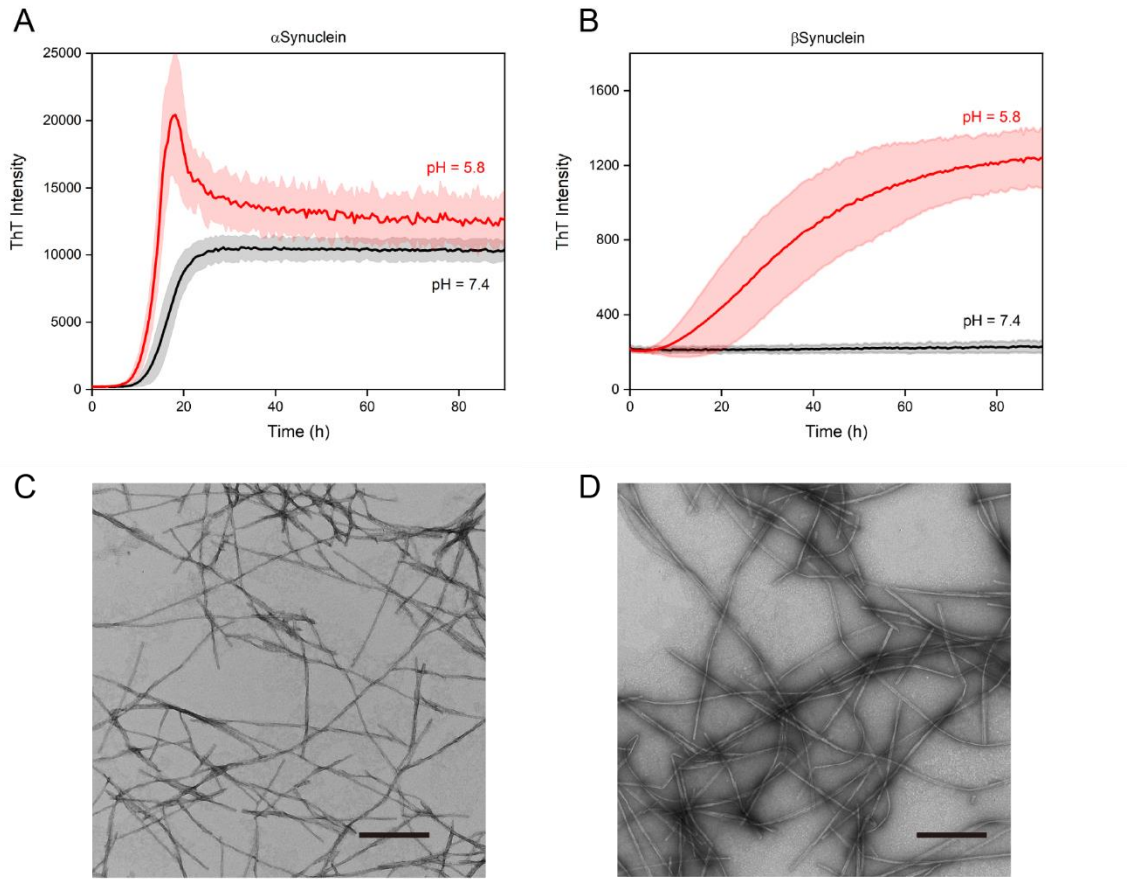

Figure 35. αSynuclein (A) and βSynuclein (B) aggregation kinetics under both pH 7.4 (black) and 5.8 (red). βSynuclein forms ThT positive aggregates under low pH, while αSynuclein can form ThT positive aggregates at both pH. TEM image of (C) αSynuclein fibril (pH 7.4) and (D) βSynuclein fibril (pH 5.8). Scale bar is 500 nm.

βSynuclein fibrils do not induce monomer aggregation like αSynuclein fibrils.

By adding αSynuclein fibrils into an αSynuclein monomer solution, the lag time of the aggregation process can be abolished, and the monomer will convert into fibrils quickly. This process is called "seeding" (*174*). With an increase in the fibril concentration added into the monomer solution, the faster the aggregation processes will be. Here, we tested out

if βSynuclein fibrils can seed βSynuclein monomer or αSynuclein monomer aggregation under different pH conditions. By adding αSynuclein fibrils into αSynuclein monomer, we can see that the ThT intensity increased immediately. After 3 days of incubation, the fibril formation reaches its plateau (raw fluorescence intensity increased from 350 to 5800). Adding βSynuclein fibrils into βSynuclein monomer under pH 5.8 or 7.4, we didn't detect ThT intensity increases under either condition. After 5 days incubation, the ThT intensity only showed a slightly increased (raw fluorescence intensity increased from 220 to 280) intensity under low pH conditions, which suggests that βSynuclein fibrils are not a good template for seeding. We also tested if αSynuclein fibrils can seed βSynuclein monomer aggregation. Adding αSynuclein fibrils into βSynuclein monomer at pH 7.4 showed no increase in ThT intensity. When αSynuclein fibrils are added into βSynuclein monomer under low pH (5.8), a slightly increased ThT intensity (raw fluorescence intensity increased from 360 to 400) was observed (**Figure 36 a**). This suggests that αSynuclein can seed βSynuclein aggregation weakly. We also tried to use βSynuclein fibrils to seed αSynuclein monomer aggregation under pH 7.4. No increased fluorescence intensity was observed, suggesting that βSynuclein fibrils may have a different structure or packing interface which can't result in an αSynuclein seeding processes (**Figure 36 b**).

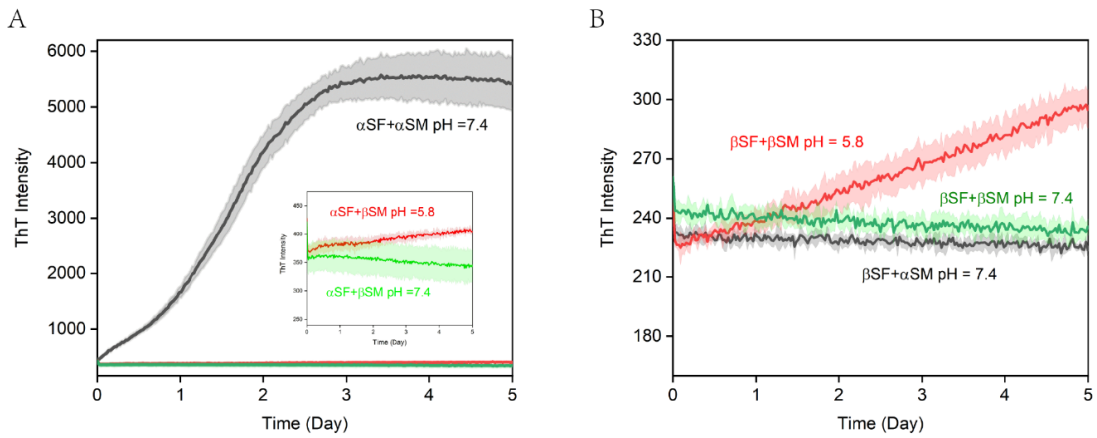

Figure 36. ThT aggregation assay monitoring αSynuclein fibril (A) and βSynuclein (B) seeding monomer aggregation under different conditions. αSynuclein fibrils can seed αSynuclein monomer (pH 7.4) aggregation immediately, and can weakly seed βSynuclein monomer at pH 5.8 (A). βSynuclein fibrils can't seed either αSynuclein or βSynuclein at pH 7.4, but can induce slight ThT intensity increase for βSynuclein at pH 5.8.

βSynuclein fibrils can cause similar levels of cell viability decrease like αSynuclein fibrils.

Amyloid fibrils formed by different protein have shown toxicity to cells(*183*). Here, we investigated if βSynuclein can cause cell toxicity or not. We treated SH-SY5Y neuroblastoma cells (purchased from ATCC) with increased concentrations of βSynuclein fibrils. Up to 5μM βSynuclein fibrils, we observed around 20% decreased cell viability compared with untreated cells, while for αSynuclein fibril treated cells 25% decreased cell viability was observed (**Figure 37 a, b**). This data indicates that both βSynuclein and αSynuclein fibrils can cause cell toxicity. We also tested how βSynuclein and αSynuclein fibrils influence the cell viability of SH-SY5Y cells overexpressing αSynuclein. Compared

with regular SH-SY5Y cells, both βSynuclein and αSynuclein fibrils cause a decrease in cell viability and don't follow a simple linear concentration dependent pattern which suggests that multiple mechanisms for fibril cell toxicity may be occuring (**Figure 37 c, d**).

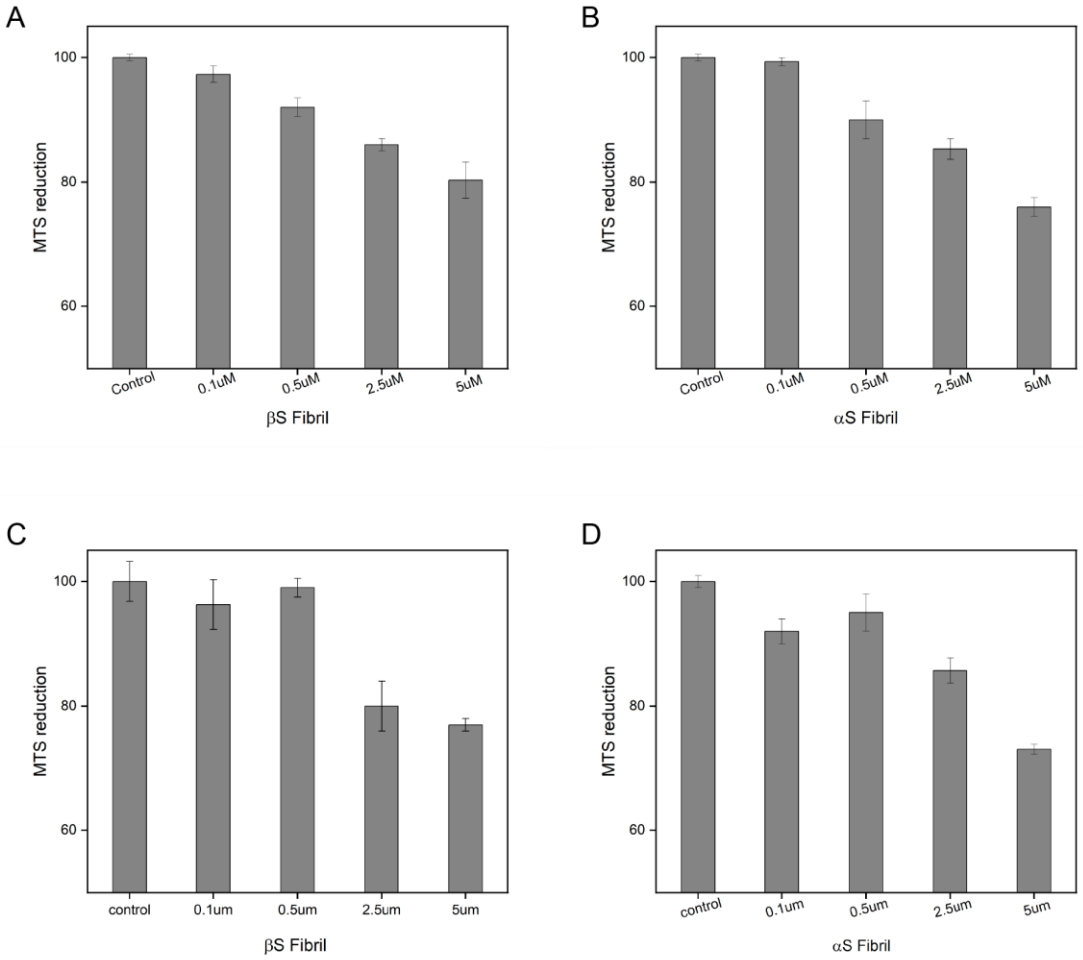

Figure 37. MTS cell viability assay of regular SH-SY5Y cells treated with (A) βSynuclein fibrils and (B) αSynuclein fibrils at different concentrations. (C) βSynuclein fibrils and (D) αSynuclein fibrils also cause reduced viability in over expressing αSynuclein SH-SY5Y cells.

βSynuclein fibrils are not proteinase K and SDS resistant.

Previous research has shown that αSynuclein fibrils are proteinase K (PK) and SDS resistant(*180*). For αSynuclein fibrils both made *in vitro* and extracted from postmortem tissue, proteinase K can't get access to the fibril core. The enzyme can only digest the flanking regions of the αSynuclein fibril, the early N- terminal and the C-terminal regions, which result in residues 31-109 being left in the fibril core(*223*). In this work, we checked the PK digestion profile of βSynuclein fibrils and compared it with the PK digestion profile of αSynuclein fibrils (**Figure 38**). βSynuclein or αSynuclein fibrils were incubated with 2 µg/mL PK for various times at 37 °C, and the reaction was then quenched by adding SDS-PAGE running buffer and heated at 100 °C. The digestion profile was revealed by running an SDS-PAGE gel of the quenched reaction mixture. αSynuclein fibril samples were consistent with literature, in that large fibril aggregates didn't run through the gel and at long incubation times the monomer band intensity decreased. However, βSynuclein fibril samples showed no large aggregates left at the top of the gel even without incubation with proteinase K. This suggests that these aggregates are not SDS-resistant nor heat-resistant like αSynuclein fibrils. βSynuclein oligomer (between 40kDa and 70kDa) bands were observed on SDS-PAGE gel without incubatation with proteinase K, which suggests that these oligomer species may be the stable form for βSynuclein. With increased incubation time with proteinase K, βSynuclein oligomer and monomer bands showed decreased intensities. After 60 minute incubation, almost no βSynuclein monomer or oligomer bands were visible.

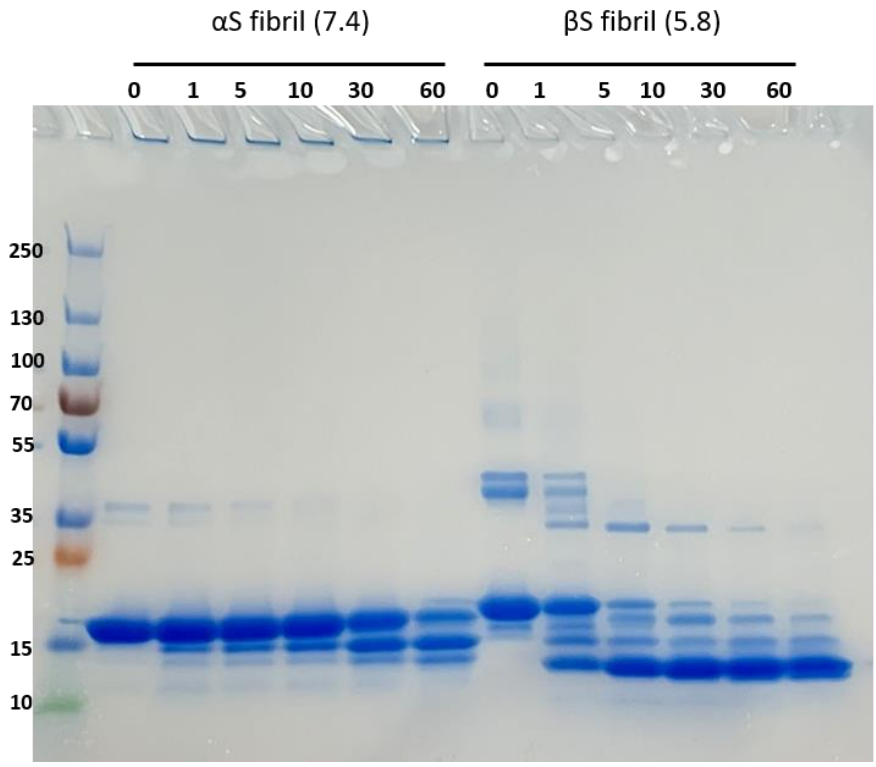

Figure 38. Proteinase K digestion of αSynuclein and βSynuclein fibrils with different incubation times.

6.3 Discussion

In this chapter, we compared αSynuclein and βSynuclein fibrils from the perspective of their morphology, seeding aggregation ability, toxicity and stability. The concept of polymorphism of αSynuclein fibrils is well established. Under different buffer conditions, αSynuclein can form "rod", "twisted fibril" and "ribbon" morphologies(*180*). The structure of αSynuclein rod and twisted fibrils have been solved by cryo-EM, and the primary difference between them is the packing interface between two filaments(*204*). No high-resolution structure of αSynuclein ribbons are available. There are more differences

between ribbon and twisted fibril than rod. Ribbons bind ThT much lower than rod and twisted fibril (around 10%), and they are wider as observed by TEM. It's clear that the fibrils formed by βSynuclein could be defined as "ribbon" based on the ThT and TEM data presented in this chapter(*180*). Rod, twisted fibril and ribbon αSynuclein can seed monomer aggregation efficiently and cause cell viability decreases. However, no matter the pH, βSynuclein fibrils can't efficiently seed βSynuclein monomer aggregation. The reason that βSynuclein fibrils can't seed may be because the ribbon fibril is not a good template, or that βSynuclein monomer itself is harder to be seeded. But pH 5.8 is the condition that βSynuclein monomers can aggregate, and αSynuclein fibrils (a generally good seeder) can slightly seed βSynuclein monomer aggregation, which may suggest that the βSynuclein fibrils are not good seeders.

In order to understand why βSynuclein fibrils can't seed aggregation efficiently, we compared the PK digestion profiles of αSynuclein and βSynuclein fibrils. The gel suggests that αSynuclein fibrils have a more stable structure than βSynuclein fibrils. Incubation with proteinase K, SDS and heat at 100 °C can't disaggregate αSynuclein fibrils completely into monomer or smaller fragments, but for βSynuclein fibril SDS and heating will disaggregate into monomers and a small number of oligomers. This may suggests that having a stable structure as a template may be critical for the seeding process. For future work, the structure of βSynuclein fibrils needs to be resolved and compared with αSynuclein fibrils to have a better understanding of what makes αSynuclein/βSynuclein fibrils either a good or bad seeder.

The *in vitro* ThT data suggest that βSynuclein fibrils can't seed monomer (both α and β) aggregation efficiently, we so wanted to test if they can still cause cellular toxicity similar to that of αSynuclein fibrils. Based on MTS reduction assays, βSynuclein fibrils can induce similar cell toxicity as αSynuclein fibrils, which suggests that seeding aggregation formation is not the only reason for amyloid fibril toxicity. This can be confirmed with fibril treated over-expressing αSynuclein SH-SY5Y cells; αSynuclein fibrils cause similar cell viability decrease for these over-expressing cells compared with cells having a regular expression level. However, the over-expressing cell line data doesn't follow a nice linear concentration dependence like the regular cell line for βSynuclein fibril treated samples, which may suggest different cell lines have different resistance to certain toxins or the mechanism for causing cell toxicity by αSynuclein fibrils and βSynuclein fibrils is different.

Because of the similarity between αSynuclein and βSynuclein monomers and their differences in the aggregation process and role in neurodegenerative diseases, having a detailed structure and property comparison will provide valuable information for answering questions like: 1) What makes αSynuclein fibrils a good seeding template? 2) How does crossing-seeding between αSynuclein and βSynuclein happen? 3) Why are amyloid fibrils toxic to neuronal cells? Using NMR, cryo-EM and other techniques will help us to develop a comprehensive understanding of βSynuclein fibrils.

6.4 Method

Making βSynuclein fibrils

Making βSynuclein fibril used the protocol as describe previously with minor adaption(*188*). N-terminal acetylated βSynuclein protein powder was dissolved in 20 mM phosphate buffer with 100 mM NaCl at pH 5.8. Large protein aggregates were removed by 50kDa filter. Protein concentration was determined by UV absorbance at 280 nm. 100 µl of 70 µM protein was place into 96-well plate with Teflon beads. The plate was incubated at 37°C and with 600 rpm shaking. Fibrils were harvested after at least 100h incubation by centrifugation at 14k rpm for 1h, and followed by washing 3 times with buffer.

Time dependence of Proteinase K digestion

70µM monomer equivalent samples were incubated with 2µg/ml proteinase K in PBS (pH=7.4) buffer at 37 °C for different times. Digestion reactions were stopped by heating on a water bath (100°C) for 5 mins and mixed with 4x SDS-PAGE loading buffer. Samples were loaded on precast gels and run at 120V for 1h.

Cell culture and MTS reduction assay

Human SH-SY5Y neuroblastoma cells were cultured in DMEM/F12 (GE Healthcare) with 10% fetal bovine serum (FBS) and kept in a 5% CO_2 humidified atmosphere at 37°C. For cell viability assay, cells were plated into 96-well plate and waited for at least 24 hours for recovery. Cells were treated with different concentration of fibrils for 48 hours. Cell viability was measured by adding 3-(4, 5-dimethylthiazol-2-yl)-5-(3-carboxymethoxyphenol)-2-(4-sulfophenyl)-2H-tetrazolium (MTS, Promega, USA) and incubated for 2 hours at 37°C. Absorbance was measured at 490 nm which is directly

proportional to the number of living cells in the culture. Fibril concentration was determined by denaturation with 4M guanidine hydrochloride for measuring concentration at 280 nm.

Reference

1. V. Csizmok, A. V. Follis, R. W. Kriwacki, J. D. Forman-Kay, Dynamic Protein Interaction Networks and New Structural Paradigms in Signaling. *Chem. Rev.* **116**, 6424-6462 (2016).
2. J. P. Brady *et al.*, Structural and Hydrodynamic Properties of an Intrinsically Disordered Region of a Germ Cell-Specific Protein on Phase Separation. *Proc. Natl. Acad. Sci. U.S.A.* **114**, E8194-E8203 (2017).
3. S. F. Banani, H. O. Lee, A. A. Hyman, M. K. Rosen, Biomolecular Condensates: Organizers of Cellular Biochemistry. *Nat. Rev. Mol. Cell Biol.* **18**, 285-298 (2017).
4. P. E. Wright, H. J. Dyson, Intrinsically Unstructured Proteins: Re-assessing the Protein Structure-Function Paradigm. *J. Mol. Biol.* **293**, 321-331 (1999).
5. H. J. Dyson, P. E. Wright, Intrinsically Unstructured Proteins and their Functions. *Nat. Rev. Mol. Cell Biol.* **6**, 197-208 (2005).
6. P. J. Knowles, M. Vendruscolo, C. M. Dobson, The Amyloid State and its Association with Protein Misfolding Diseases. *Nat. Rev. Mol. Cell Biol.* **15**, 384-396 (2014).
7. F. Chiti, C. M. Dobson, Protein misfolding, functional amyloid, and human disease. *Annu. Rev. Biochem.* **75**, 333-366 (2006).
8. Y. Naranjo, M. Pons, R. Konrat, Meta-structure correlation in protein space unveils different selection rules for folded and intrinsically disordered proteins. *Mo. BioSyst.* **8**, 411-416 (2012).
9. J. M. Beitz, Parkinson's Disease: A Review. *Front. Biosci.* **S6**, 65-74 (2014).
10. I. V. J. Murray, V. M. Y. Lee, J. Q. Trojanowski, Synucleinopathies: A Pathological and Molecular Review. *Clin. Neurosci. Res.* **1**, 445-455 (2001).
11. M. Ferreira, J. Massano, An Updated Review of Parkinson's Disease Genetics and Clinicopathological Correlations. *Acta Neurol. Scand.* **135**, 273-284 (2017).
12. M. Goedert, R. Jakes, M. G. Spillantini, The Synucleinopathies: Twenty Years On. *J. Parkinsons Dis.* **7**, S51-S69 (2017).
13. W. Poewe *et al.*, Parkinson Disease. *Nat. Rev. Dis. Primers* **3**, 17013 (2017).
14. D. F. Clayton, J. M. Geroge, The Synucleins: A Family of Proteins Involved in Synaptic Function, Plasticity, Neurodegeneration and Disease. *Trends Neurosci.* **21**, 249-254 (1998).
15. R. Jakes, M. G. Spillantini, M. Goedert, Identification of Two Distinct Synucleins from Human Brain. *FEBS Lett.* **345**, 27-32 (1994).
16. D. D. Murphy, S. M. Rueter, J. Q. Trojanowski, V. M. Y. Lee, Synucleins are Developmentally Expressed, and α-Synuclein Regulates the Size of the Presynaptic Vesicular Pool in Primary Hippocampal Neurons. *J. Neurosci.* **20**, 3214-3220 (2000).

17. M. Hashimoto, E. Rockenstein, M. Mante, M. Mallory, E. Masliah, β-Synuclein Inhibits α-Synuclein Aggregation: A Possible Role as an Anti-Parkinsonian Factor. *Neruon* **32**, 213-223 (2001).
18. M. K. Janowska, K.-P. Wu, J. Baum, Unveiling Transient Protein-Protein Interactions that Modulate Inhibition of Alpha-Synuclein Aggregation by Beta-Synuclein, a Pre-Synaptic Protein that Co-localizes with Alpha-Synuclein. *Sci. Rep.* **5**, 15164 (2015).
19. D. H. Brookes, T. Head-Gordon, Experimental inferential structure determination of ensembles for intrinsically disordered proteins. *J. Am. Chem. Soc.* **138**, 4530-4538 (2016).
20. J. Kragelj, M. Blackledge, M. R. Jensen, Ensemble Calculation for Intrinsically Disordered Proteins Using NMR Parameters. *Adv. Exp. Med. Biol.* **870**, 123-147 (2015).
21. N. Salvi, A. Abyzov, M. Blackledge, Multi-timescale dynamics in intrinsically disordered proteins from NMR relaxation and molecular simulation. *J. Phys. Chem. Lett.* **7**, 2483-2489 (2016).
22. S.-H. Chong, P. Chatterjee, S. Ham, Computer simulations of intrinsically disordered proteins. *Annu. Rev. Phys. Chem.* **68**, 117-134 (2017).
23. P. Sormanni *et al.*, Simultaneous Quantification of Protein Order and Disorder. *Nat. Chem. Biol.* **13**, 339-342 (2017).
24. C. Narayanan, D. S. Weinstock, K.-P. Wu, J. Baum, R. M. Levy, Investigation of the Polymeric Properties of α-Synuclein and Comparison with NMR Experiments: A Replica Exchange Molecular Dynamics Study. *J. Chem. Theory Comput.* **8**, 3929-3942 (2012).
25. R. K. Das, R. V. Pappu, Conformations of Intrinsically Disordered Proteins are Influenced by Linear Sequence Distributions of Oppositely Charged Residues. *Proc. Natl. Acad. Sci. U.S.A.* **110**, 13392-13397 (2013).
26. J. R. Allison, R. C. Rivers, J. C. Christodoulou, M. Vendruscolo, C. M. Dobson, A Relationship Between the Transient Structure in the Monomeric State and the Aggregation Propensities of α-Synuclein and β-Synuclein. *Biochemistry* **53**, 7170-7183 (2014).
27. D. Eliezer, E. Kutluay, R. Bussell, G. Browne, Conformational Properties of α-Synclein in its Free and Lipid-Associated States. *J. Mol. Biol.* **307**, 1061-1073 (2001).
28. Y. Sung, D. Eliezer, Residual Structure, Backbone Dynamics, and Interactions within the Synuclein Family. *J. Mol. Biol.* **372**, 689-707 (2007).
29. Y.-H. Sung, D. Eliezer, Secondary Structure and Dynamics of Micelle Bound β- and γ-Synuclein. *Prot. Sci.* **15**, 1162-1174 (2006).
30. C. W. Bertoncini *et al.*, Structural Characterization of the Intrinsically Unfolded Protein β-Synuclein, a Natural Negative Regulator of α-Synuclein Aggregation. *J. Mol. Biol.* **372**, 708-722 (2007).
31. S. L. Bernstein *et al.*, α-Synuclein: Stable Compact and Extended Monomeric Structures and pH Dependence of Dimer Formation. *J. Am. Soc. Mass Spectrom.* **15**, 1435-1443 (2004).

32. J. A. Marsh, V. K. Singh, Z. Jia, J. D. Forman-Kay, Sensitivity of Secondary Structure Propensities to Sequence Differences Between α- and γ-synuclein: Implications for Fibrillation. *Prot. Sci.* **15**, 2795-2804 (2006).
33. K.-P. Wu, D. S. Weinstock, C. Narayanan, R. M. Levy, J. Baum, Structural Reorganization of α-Synuclein at Low pH Observerd by NMR and REMD Simulations. *J. Mol. Biol.* **391**, 784-796 (2009).
34. C. A. Waudby *et al.*, In-Cell NMR Characterization of the Secondary Structure Populations of a Disordered Conformation of α-Synuclein within E. coli Cells. *PLoS One* **8**, e72286 (2013).
35. H. McWilliam *et al.*, Analysis Tool Web Services from the EMBL-EBI. *Nucleic Acids Res.* **41**, W597-W600 (2013).
36. A. K. Buell *et al.*, Solution Conditions Determine the Relative Importance of Nucleation and Growth Processes in α-Synuclein Aggregation. *Proc. Natl. Acad. Sci. U.S.A.* **111**, 7671-7676 (2014).
37. R. Gaspar *et al.*, Seconday Nucleation of Monomers on Fibril Surface Dominates α-Synuclein Aggregation and Provides Autocatalytic Amyloid Amplification. *Q. Rev. Biohpys.* **50**, e6 (2017).
38. T. D. Romo, A. K. Lewis, A. R. Braun, A. Grossfield, J. N. Sachs, Minimal Nucleation State of α-Synuclein is Stabilized by Dynamic Threonine-Water Networks. *ACS Chem. Neurosci.* **8**, 1859-1864 (2017).
39. A. K. Buell, C. M. Dobson, T. P. J. Knowles, The Physical Chemistry of the Amyloid Phenomenon: Thermodynamics and Kinetics of Filamentous Protein Aggregation. *Essays Biochem.* **56**, 11-39 (2014).
40. P. Arosio, R. Cukalevski, B. Frohm, T. P. J. Knowles, S. Linse, Quantification of the concentration of Aβ42 propagons during the lag phase by an amyloid chain reaction assay. *J. Am. Chem. Soc.* **136**, 219-225 (2014).
41. P. Arosio, T. P. J. Knowles, S. Linse, On the lag phase in amyloid fibril formation. *Phys. Chem. Chem. Phys.* **17**, 7606-7618 (2015).
42. V. N. Uversky *et al.*, Biophysical Properties of the Synucleins and Their Propensities to Fibrillate. *J. Biol. Chem.* **277**, 11970-11978 (2002).
43. L. Kang, M. K. Janowska, G. M. Moriarty, J. Baum, Mechanistic Insight into the Relationship between N-Terminal Acetylation of a-Synclein and Fibril Formation Rates by NMR and Fluorescence. *PLoS ONE* **8**, e75018 (2013).
44. S. P. Braithwaite, J. B. Stock, M. M. Mouradian, α-Synuclein Phosphorylation as a Therapeutic Target in Parkinson's Disease. *Rev. Neurosci.* **23**, 191-198 (2012).
45. T. Abeywardana, M. R. Pratt, Extent of Inhibition of α-Synuclein Aggregation in Vitro by SUMOylation is Conjugation Site- and SUMO Isoform-Selective. *Biochemistry* **54**, 959-961 (2015).
46. J. Li, M. Zhu, S. Rajamani, V. N. Uversky, A. L. Fink, Rifampicin Inhibits α-Synuclein Fibrillation and Disaggregates Fibrils. *Chem. Biol.* **11**, 1513-1521 (2004).
47. K. Ubhi *et al.*, Rifampicin Reduces α-Synuclein in a Transgenic Mouse Model of Multiple System Atrophy. *Neuroreport.* **19**, 1271-1276 (2008).
48. T. J. Collier *et al.*, Nortiptyline Inhibits Aggregation and Neurotoxicity of Alpha-Synuclein by Enhancing Reconfiguration of the Monomeric Form. *Neruobiol. Dis.* **106**, 191-204 (2017).

49. M. Perni *et al.*, A Natural Product Inhibits the Initiation of α-Synuclein Aggregation and Suppresses its Toxicity. *Proc. Natl. Acad. Sci. U.S.A.* **114**, E1009-E1017 (2017).
50. I. B. Bruinsma *et al.*, Inhibition of α-Synuclein Aggregation by Small Heat Shock Proteins. *Proteins* **79**, 2956-2967 (2011).
51. A. Rekas, L. Jankova, D. C. Thorn, R. Cappai, J. A. Carver, Monitoring the Prevention of Amyloid Fibirl Formation by α-Crystallin. *FEBS J.* **274**, 6290-6305 (2007).
52. J. Klucken, Y. Shin, E. Masliah, B. T. Hyman, P. J. McLean, Hsp70 Reduces α-Synuclein Aggregation and Toxicity. *J. Biol. Chem.* **279**, 25497-25502 (2004).
53. D. Cox *et al.*, The Small Heat Shock Protein Hsp27 Binds α-Synuclein Fibrils, Preventing Elongation and Cytotoxicity. *J. Biol. Chem.* **293**, 4486-4497 (2018).
54. F. A. Aprile *et al.*, Inhibition of α-Synuclein Fibril Elongation by Hsp70 is Governed by a Kinetic Binding Competition between α-Synuclein Species. *Biochemistry* **56**, 1177-1180 (2017).
55. G. Toth *et al.*, Targeting the Intrinsically Disordered Structural Ensemble of α-Synuclein by Small Molecules as a Potential Therapeutic Strategy for Parkinson's Disease. *PLoS One* **9**, e87133 (2014).
56. G. T. Heller, M. Bonomi, M. Vendruscolo, Structural Ensemble Modulation upon Small-Molecule Binding to Disordered Proteins. *J. Mol. Biol.* **430**, 2288-2292 (2018).
57. A. Borgia *et al.*, Extreme Disorder in an Ultrahigh-Affinity Protein Complex. *Nature* **555**, 61-66 (2018).
58. S. Wu *et al.*, The Dynamic Multisite Interactions between Two Intrinsically Disordered Proteins. *Angew. Chem. Int. Ed.* **56**, 7515-7519 (2017).
59. G. M. Moriarty *et al.*, A pH-dependent switch promotes β-synuclein fibril formation via glutamate residues. *J. Biol. Chem.* **292**, 16368-16379 (2017).
60. G. Yamin *et al.*, Forcing Nonamyloidogenic β-Synuclein to Fibrillate. *Biochemistry* **44**, 9096-9107 (2005).
61. J. W. P. Brown *et al.*, Kinetic barriers to α-synuclein protofilament formation and conversion into mature fibrils. *Chem. Commun.* **54**, 7854-7857 (2018).
62. Y. Fan *et al.*, β-Synuclein Modulates α-Synuclein Neruotoxicity by Reducing α-Synuclein Protein Expression. *Hum. Mol. Gen.* **15**, 3002-3011 (2006).
63. J.-Y. Park, P. T. Lansbury, β-Synuclein Inhibits Formation of α-Synuclein Protofibrils: A Possible Therapeutic Strategy Against Parkinson's Disease. *Biochemistry* **42**, 3696-3700 (2003).
64. J. W. P. Brown *et al.*, β-Synuclein Suppresses Both the Initiation and Amplification Steps of α-Synuclein Aggregation via Competitive Binding to Surfaces. *Sci. Rep.* **6**, 36010 (2016).
65. A. Leitao, A. Bhumkar, D. J. B. Hunter, Y. Gambin, E. Sierecki, Unveiling a Selective Mechanism for the Inhibition of α-Synuclein Aggregation by β-Synuclein. *Int. J. Mol. Sci.* **19**, 334 (2018).
66. H. Ohtake *et al.*, Beta-Synuclein Gene Alterations in Dementia with Lewy Bodies. *Neurology* **63**, 805-811 (2004).

67. M. Fujita *et al.*, A β-Synuclein Mutation Linked to Dementia Produces Neurodegeneration when Expressed in Mouse Brain. *Nat. Commun.* **1**, 110 (2010).
68. M. Fujita, A. Sekigawa, K. Sekiyama, Y. Takamatsu, M. Hashimoto, Possible Alterations in β-Synuclein, the Non-Amyloidogenic Homologue of α-Synuclein, during Progression of Sporadic α-Synucleinopathies. *Int. J. Mol. Sci.* **13**, 11584-11592 (2012).
69. H. Mirbaha *et al.*, Inert and seed-competent tau monomers suggest structural origins of aggregation. *eLife* **7**, e36584 (2018).
70. M. K. Janowska, J. Baum, The Loss of Inhibitory C-Terminal Conformations in Disease Associated P123H β-Synuclein. *Prot. Sci.* **25**, 286-294 (2016).
71. G. Taschenberger *et al.*, β-Synuclein Aggregates and Induces Neurodegeneration in Dopaminergic Neurons. *Ann. Neurol.* **74**, 109-118 (2013).
72. S. Tenreiro *et al.*, Yeast Reveals Similar Molecular Mechanisms Underlying Alpha- and Beta-Synuclein Toxicity. *Hum. Mol. Gen.* **25**, 275-290 (2016).
73. B. Popova *et al.*, Sumoylation Protects Against β-Synuclein Toxicity in Yeast. *Front. Mol. Neurosci.* **11**, 94 (2018).
74. T. Lee, C. R. Moran-Gutierrez, A. A. Deniz, Probing protein disorder and complexity at single-molecule resolution. *Semin. Cell Dev. Biol.* **37**, 26-34 (2015).
75. A. C. M. Ferreon, C. R. Moran, Y. Gambin, A. A. Deniz, Single-molecule fluorescence studies of intrinsically disordered proteins. *Methods Enzymol.* **472**, 179-204 (2010).
76. M. Aznauryan *et al.*, Comprehensive structural and dynamical view of an unfolded protein from the combination of single-molecule FRET, NMR, and SAXS. *Proc. Natl. Acad. Sci. U.S.A.* **113**, E5389-E5398 (2016).
77. C. Tang, R. Ghirlando, G. M. Clore, Visualization of Transient Ultra-Weak Protein Self-Association in Solution Using Paramagnetic Relaxation Enhancement. *J. Am. Chem. Soc.* **130**, 4048-4056 (2008).
78. G. M. Clore, J. Iwahara, Theory, Practice, and Applications of Paramagnetic Relaxation Enhancement for the Characterization of Transient Low-Population States of Biological Macromolecules and Their Complexes. *Chem. Rev.* **109**, 4108-4139 (2009).
79. M. D. Tuttle *et al.*, Solid-State NMR Structure of a Pathogenic Fibril of Full-Length Human α-Synuclein. *Nat. Struct. Mol. Biol.* **23**, 409-415 (2016).
80. J. K. Williams *et al.*, Multi-Pronged Interactions Underlie Inhibition of α-Synuclein Aggregation by β-Synuclein. *J. Mol. Biol.* **430**, 2360-2371 (2018).
81. A. Sanjeev, R. K. Sahu, V. S. K. Mattaparthi, Potential of Mean Force and Molecular Dynamics Study on the Transient Interactions Between α and β Synuclein that Drive Inhibition of α-Synuclein Aggregation. *J. Biomol. Struct. Dynam.* **35**, 3342-3353 (2017).
82. Y. Zhang, I-TASSER Server for Protein 3D Structure Prediction. *BMC Bioinformatics* **9**, 40 (2008).
83. T. S. Ulmer, A. Bax, N. B. Cole, R. L. Nussbaum, Structure and Dynamics of Micelle-Bound Human α-Synuclein. *J. Biol. Chem.* **280**, 9595-9603 (2005).

84. I. F. Tsigelny *et al.*, Dynamics of α-Synuclein Aggregation and Inhibition of Pore-like Oligomer Development by β-Synuclein. *FEBS J.* **274**, 1862-1877 (2007).
85. K. Ono, The Oligomer Hypothesis in α-Synucleinopathy. *Neurochem. Res.* **42**, 3362-3371 (2017).
86. L. Rodriguez, M. M. Marano, A. Tandon, Import and export of misfolded α-synuclein. *Front. Neurosci.* **12**, 344 (2018).
87. M. L. Choi, S. Gandhi, Crucial Role of Protein Oligomerization in the Pathogenesis of Alzheimer's and Parkinson's Diseases. *FEBS J.*, In Press (2018).
88. J. Bendor, T. Logan, R. H. Edwards, The Function of α-Synuclein. *Neuron* **79**, 1044-1066 (2013).
89. G. Fusco *et al.*, Structural Basis of Membrane Disruption and Cellular Toxicity by α-Synuclein Oligomers. *Science* **358**, 1440-1443 (2017).
90. E. Israeli, R. Sharon, β-Synuclein Occurs in vivo in Lipid Associated Oligomers and Forms Hetero Oligomers with α-Synuclein. *J. Neurochem.* **108**, 465-474 (2009).
91. V. C. Ducas, E. Rhoades, Quantifying Interactions of β-Synuclein and γ-Synuclein with Model Membranes. *J. Mol. Biol.* **423**, 528-539 (2012).
92. G. Fusco *et al.*, Direct Observation of the Three Regions in α-Synuclein that Determine its Membrane-Bound Behavior. *Nat. Commun.* **5**, 3827 (2014).
93. T. P. J. Knowles *et al.*, An Analytical Solution to the Kinetics of Breakable Filament Assembly. *Science* **326**, 1533-1537 (2009).
94. H. Snyder *et al.*, Aggregated and Monomeric α-Synuclein Bind to the S6' Proteasomal Protein and Inhibit Proteasomal Function. *J. Biol. Chem.* **278**, 11753-11759 (2003).
95. H. Snyder *et al.*, β-Synuclein Reduces Proteasomal Inhibition by α-Synuclein But Not γ-Synuclein. *J. Biol. Chem.* **280**, 7562-7569 (2005).
96. O.-B. Tysnes, A. Storstein, Epidemiology of Parkinson's disease. *J. Nerual. Transm.* **124**, 901-905 (2017).
97. C. A. Ross, M. A. Poirier, Protein aggregation and neurodegenerative disease. *Nat. Med.* **10**, S10-S17 (2004).
98. K. Vekrellis, M. Xilouri, E. Emmanouilidou, H. J. Rideout, L. Stefanis, Pathological roles of α-synuclein in neurological disorders. *Lancet Neurol.* **10**, 1015-1025 (2011).
99. L. A. Volpicelli-Daley *et al.*, Exogenous α-synuclein fibrils induce Lewy body pathology leading to synaptic dysfunction and neuron death. *Neuron* **72**, 57-71 (2011).
100. L. Pieri, K. Madiona, L. Bousset, R. Melki, Fibrillar α-synuclein and huntingtin exon 1 assemblies are toxic to the cells. *Biophys. J.* **102**, 2894-2905 (2012).
101. L. Bousset *et al.*, Structural and functional characterization of two α-synuclein strains. *Nat. Commun.* **4**, 2575 (2013).
102. N. Mammadova *et al.*, Accelerated accumulation of retinal α-synuclein (pSer129) and tau, neuroinflammation and autophagic dysregulation in a seeded mouse model of Parkinson's disease. *Neurobiol. Dis.* **121**, 1-16 (2019).
103. E. C. Freundt *et al.*, Neuron-to-neuron transmission of α-synuclein fibrils through axonal transport. *Ann. Neurol.* **72**, 517-524 (2012).

104. F. Longhena *et al.*, The contribution of α-synuclein spreading to Parkinson's disease synaptopathy. *Neural. Plast.* **2017**, 5012129 (2017).
105. X. Mao *et al.*, Pathological α-synuclein transmission initiated by binding lymphocyte-activation gene 3. *Science* **353**, aah3374 (2016).
106. R. Yan *et al.*, Synergistic neuroprotection by coffee components eicosanoyl-5-hydroxytryptamide and caffeine in models of Parkinson's disease and DLB. *Proc. Natl. Acad. Sci. U.S.A.* **In Press**, 10.1073/pnas.1813365115 (2018).
107. B. Li *et al.*, Cryo-EM of full-length α-synuclein reveals fibril polymorphs with a common structural kernel. *Nat. Commun.* **9**, 3609 (2018).
108. M. Vilar *et al.*, The fold of α-synuclein fibrils. *Proc. Natl. Acad. Sci. U.S.A.* **105**, 8637-8642 (2008).
109. W. Peelaerts *et al.*, α-Synuclein strains cause distinct synucleinopathies after local and systemic administration. *Nature* **522**, 340-344 (2015).
110. C. Peng *et al.*, Cellular milieu imparts distinct pathological α-synuclein strains in α-synucleinopathies. *Nature* **557**, 558-563 (2018).
111. K. W. Tipping *et al.*, pH-induced molecular shedding drives the formation of amyloid fibril-derived oligomers. *Proc. Natl. Acad. Sc.i U.S.A.* **112**, 5691-5696 (2015).
112. N. Cremades *et al.*, Direct observation of the interconversion of normal and toxic forms of α-synuclein. *Cell* **149**, 1048-1059 (2012).
113. A. Tarutani *et al.*, The effect of fragmented pathogenic α-synuclein seeds on prion-like propagation. *J. Biol. Chem.* **291**, 18675-18688 (2016).
114. R. J. Karpowicz *et al.*, Selective imaging of internalized proteopathic α-synucelin seeds in primary neurons reveals mechanistic insight into transmission of synucleinopathies. *J. Biol. Chem.* **292**, 13482-13497 (2017).
115. B. B. Holmes *et al.*, Heparan sulfate proteoglycans mediate internalization and propagation of specific proteopathic seeds. *Proc. Natl. Acad. Sci. U.S.A.* **110**, E3138-E3147 (2013).
116. A. N. Shrivastava *et al.*, α-Synuclein assemblies sequester neuronal α3-Na+/K+-ATPase and impair Na+ gradient. *EMBO J.* **34**, 2408-2423 (2015).
117. D. Freeman *et al.*, Alpha-synuclein induces lysosomal rupture and cathepsin dependent reactive oxygen species following endocytosis. *PLoS ONE* **8**, e62143 (2013).
118. W. P. Flavin *et al.*, Endocytic vesicle rupture is a conserved mechanism of cellular invasion by amyloid proteins. *Acta Neuropathol.* **134**, 629-653 (2017).
119. F. Samuel *et al.*, Effects of serine 129 phosphorylation on α-synuclein aggregation, membrane association, and internalization. *J. Biol. Chem.* **291**, 4374-4385 (2016).
120. S. A. Tanik, C. E. Schultheiss, L. A. Volpicelli-Daley, K. R. Brunden, V. M. Y. Lee, Lewy body-like α-synuclein aggregates resist degradation and impair macroautophagy. *J. Biol. Chem.* **288**, 15194-15210 (2013).
121. S. Abounit *et al.*, Tunneling nanotubes spread fibrillar α-synuclein by intercellular trafficking of lysosomes. *EMBO J.* **35**, 2120-2138 (2016).
122. K. Beyer, L. Ispierto, P. Latorre, E. Tolosa, A. Ariza, Alpha- and beta-synuclein expression in Parkison disease with and without dementia. *J. Neruol. Sci.* **310**, 112-117 (2011).

123. E. Rockenstein *et al.*, Altered expression of the synuclein family mRNA in Lewy body and Alzheimer's disease. *Brain Res.* **914**, 48-56 (2001).
124. M. Hashimoto, E. Rockenstein, M. Mante, M. Mallory, E. Masliah, β-Synuclein inhibits α-synuclein aggregation: a possible role as an anti-parkinsonian factor. *Neuron* **32**, 213-223 (2001).
125. S. Chartier, C. Duyckaerts, Is Lewy pathology in the human nervous system chiefly an indicator of neuronal protection or of toxicity? *Cell Tissue Res.* **373**, 149-160 (2018).
126. K. Wakabayashi *et al.*, The Lewy body in Parkinson's disease and related neurodegenerative disorders. *Mol. Neurobiol.* **47**, 495-508 (2013).
127. M. K. Janowska, K. P. Wu, J. Baum, Unveiling transient protein-protein interactions that modulate inhibition of alpha-synuclein aggregation by beta-synuclein, a pre-synaptic protein that co-localizes with alpha-synuclein. *Sci. Rep.* **5**, 15164 (2015).
128. V. N. Uversky *et al.*, Biophysical properties of the synucleins and their propensities to fibrillate: inhibition of α-synuclein assembly by β- and γ-synucleins. *J. Biol. Chem.* **277**, 11970-11978 (2002).
129. H. A. Lashuel, C. R. Overk, A. Oueslati, E. Masliah, The many faces of α-synulcein: From structure and toxicity to therapeutic target. *Nat. Rev. Neurosci.* **14**, 38-48 (2013).
130. M. Birol, S. P. Wojcik, A. D. Miranker, E. Rhoades, Identification of N-linked glycans as specific mediators of neuronal uptake of acetylated α-synuclein. *PLoS Biol.* **17**, e3000318 (2019).
131. Y. Li *et al.*, Amyloid fibril structure of α-synuclein determined by cryo-electron microscopy. *Cell Res.* **28**, 897-903 (2018).
132. R. Guerrero-Ferreira *et al.*, Cryo-EM structure of alpha-synuclein fibrils. *eLife* **7**, e36402 (2018).
133. M. D. Tuttle *et al.*, Solid-state NMR structure of a pathogenic fibril of full-length human α-synuclein. *Nat. Struct. Mol. Biol.* **23**, 409-415 (2016).
134. E. L. Ulrich *et al.*, BioMagResBank. *Nuc. Acids Res.* **36**, D402-D408 (2008).
135. G. Comellas *et al.*, Structured regions of α-synuclein fibrils include the early-onset Parkinson's disease mutation sites. *J. Mol. Biol.* **411**, 881-895 (2011).
136. J. Gath *et al.*, Solid-state NMR sequential assignments of α-synuclein. *Biomol. NMR Assign.* **6**, 51-55 (2012).
137. G. Comellas, L. R. Lemkau, D. H. Zhou, J. M. George, C. M. Rienstra, Structural intermediates during α-synuclein fibrillogenesis on phospholipid vesicles. *J. Am. Chem. Soc.* **134**, 5090-5099 (2012).
138. D. H. Zhou *et al.*, Solid-state NMR analysis of membrane proteins and protein aggregates by proton detected spectroscopy. *J. Biomol. NMR* **54**, 291-305 (2012).
139. J. Verasdonck *et al.*, Further exploration of the conformational space of α-synuclein fibrils: Solid-state NMR assignment of a high-pH polymorph. *Biomol. NMR Assign.* **10**, 5-12 (2016).
140. A. M. Barclay, D. D. Dhavale, J. M. Courtney, P. T. Kotzbauer, C. M. Rienstra, Resonance assignements of an α-synuclein fibril prepared in Tris buffer at moderate ionic strength. *Biomol. NMR Assign.* **12**, 195-199 (2018).

141. A. Krushelnitsky *et al.*, Expanding the frequency range of the solid-state T1r experiment for heteronuclear dipolar relaxation. *Solid State Nucl. Magn. Reson.* **22**, 423-438 (2002).
142. O. C. Andronesi *et al.*, Characterization of Alzheimer's-like paired helical filaments from the core domain of tau protein using solid-state NMR spectroscopy. *J. Am. Chem. Soc.* **130**, 5922-5928 (2008).
143. J. K. Williams, M. Hong, Probing membrane protein structure using water polarization transfer solid-state NMR. *J. Magn. Reson.* **247**, 118-127 (2014).
144. J. K. Williams, D. Tietze, M. Lee, J. Wang, M. Hong, Solid-state NMR investigation of the conformation, proton conduction, and hydration of the influenza B virus M2 transmembrane proton channel. *J. Am. Chem. Soc.* **138**, 8143-8155 (2016).
145. M. R. Elkins *et al.*, Structural polymorphism of Alzheimer's beta-amyloid fibrils as controlled by an E22 switch: A solid-state NMR study. *J. Am. Chem. Soc.* **138**, 9840-9852 (2016).
146. T. Wang, H. Jo, W. F. DeGrado, M. Hong, Water distribution, dynamics and interactions with Alzheimer's beta-amyloid fibrils investigated by solid-state NMR. *J. Am. Chem. Soc.* **139**, 6242-6252 (2017).
147. M. D. Gelenter *et al.*, The peptide hormone glucagon forms amyloid fibrils with two coexisting β-strand conformations. *Nat. Struct. Mol. Biol.* **26**, 592-598 (2019).
148. D. M. Smith, Could a common mechanism of protein degradation impairment underlie many neurodegenerative diseases? *J. Exp. Neurosci.* **12**, 1179069518794675 (2018).
149. F. Opazo, A. Krenz, S. Heermann, J. B. Schulz, B. H. Falkenburger, Accumulation and clearance of α-synuclein aggregates demonstrated by time-lapse imaging. *J. Neurochem.* **106**, 529-540 (2008).
150. D. Vilchez, I. Saez, A. Dillin, The role of protein clearance mechanisms in organismal ageing and age-related diseases. *Nat. Commun.* **5**, 5659 (2014).
151. E. S. Luth, I. G. Stavrovskaya, T. Bartels, B. S. Kristal, D. J. Selkoe, Soluble, prefibrillar a-synuclein oligomers promote complex I-dependent, Ca2+ -induced mitochondrial dysfunction. *J. Biol. Chem.* **289**, 21490-21507 (2014).
152. N. K. Polinski *et al.*, Best practices for generating and using alpha-synuclein pre-formed fibrils to model Parkinson's disease in rodents. *J. Parkinsons Dis.* **8**, 303-322 (2018).
153. W. F. Xue *et al.*, Fibril fragmentation enhances amyloid cytotoxicity. *J Biol Chem* **284**, 34272-34282 (2009).
154. M. Tanaka *et al.*, Aggresomes formed by α-synuclein and synphilin-1 are cytoprotective. *J. Biol. Chem.* **279**, 4625-4631 (2004).
155. N. Carulla *et al.*, Molecular recycling within amyloid fibrils. *Nature* **436**, 554-558 (2005).
156. K. J. Fritzsching, M. Hong, K. Schmidt-Rohr, Conformationally selective multidimensional chemical shift ranges in proteins from a PACSY database purged using intrinsic quality criteria. *J. Biomol. NMR* **64**, 115-130 (2016).

157. H. Miake, H. Mizusawa, T. Iwatsubo, M. Hasegawa, Biochemical characterization of the core structure of α-synuclein filaments. *J. Biol. Chem.* **277**, 19213-19219 (2002).
158. J. W. Brown *et al.*, beta-Synuclein suppresses both the initiation and amplification steps of alpha-synuclein aggregation via competitive binding to surfaces. *Sci Rep* **6**, 36010 (2016).
159. E. Israeli, R. Sharon, Beta-synuclein occurs in vivo in lipid-associated oligomers and forms hetero-oligomers with alpha-synuclein. *J Neurochem* **108**, 465-474 (2009).
160. M. Tornquist *et al.*, Secondary nucleation in amyloid formation. *Chem. Commun.* **54**, 8667-8684 (2018).
161. R. Gaspar *et al.*, Secondary nucleation of monomers on fibril surface dominates a-synuclein aggregation and provides autocatalytic amyloid amplification. *Q. Rev. Biophys.* **50**, e6 (2017).
162. A. K. Buell *et al.*, Solution conditions determine the relative importance of nucleation and growth processes in α-synuclein aggregation. *Proc. Natl. Acad. Sci. U.S.A.* **111**, 7671-7676 (2014).
163. L. Kang *et al.*, N-terminal acetylation of α-synuclein induces increased transient helical propensity and decreased aggregation rates in the intrinsically disordered monomer. *Prot. Sci.* **21**, 911-917 (2012).
164. D. Necas, P. Kapetek, Gwyddion: an open-source software for SPM data analysis. *Cent. Eur. J. Phys.* **10**, 181-188 (2012).
165. K. Takegoshi, S. Makamura, T. Terao, 13C-1H dipolar-assisted rotational resonance in magic-angle spinning NMR. *Chem. Phys. Lett.* **344**, 631-637 (2001).
166. M. Hong, R. G. Griffin, Resonance assignments for solid peptides by dipolar-mediated 13C/15N correlation solid-state NMR. *J. Am. Chem. Soc.* **120**, 7113-7114 (1998).
167. J. Schindelin *et al.*, Fiji: an open-source platform for biological-image analysis. *Nat. Methods* **9**, 676-682 (2012).
168. K. Vekrellis, M. Xilouri, E. Emmanouilidou, H. J. Rideout, L. Stefanis, Pathological roles of alpha-synuclein in neurological disorders. *Lancet Neurol* **10**, 1015-1025 (2011).
169. W. H. Oertel, Recent advances in treating Parkinson's disease. *F1000Res* **6**, 260 (2017).
170. H. Braak, E. Braak, Pathoanatomy of Parkinson's disease. *J Neurol* **247 Suppl 2**, II3-10 (2000).
171. M. Karampetsou *et al.*, Phosphorylated exogenous alpha-synuclein fibrils exacerbate pathology and induce neuronal dysfunction in mice. *Sci Rep* **7**, 16533 (2017).
172. H. A. Lashuel, C. R. Overk, A. Oueslati, E. Masliah, The many faces of alpha-synuclein: from structure and toxicity to therapeutic target. *Nat Rev Neurosci* **14**, 38-48 (2013).
173. Y. Chu *et al.*, Intrastriatal alpha-synuclein fibrils in monkeys: spreading, imaging and neuropathological changes. *Brain* **142**, 3565-3579 (2019).

174. D. Pinotsi *et al.*, Nanoscopic insights into seeding mechanisms and toxicity of alpha-synuclein species in neurons. *Proc Natl Acad Sci U S A* **113**, 3815-3819 (2016).
175. J. Pujols *et al.*, Small molecule inhibits alpha-synuclein aggregation, disrupts amyloid fibrils, and prevents degeneration of dopaminergic neurons. *Proc Natl Acad Sci U S A* **115**, 10481-10486 (2018).
176. A. K. Buell *et al.*, Solution conditions determine the relative importance of nucleation and growth processes in alpha-synuclein aggregation. *Proc Natl Acad Sci U S A* **111**, 7671-7676 (2014).
177. R. Gaspar *et al.*, Secondary nucleation of monomers on fibril surface dominates alpha-synuclein aggregation and provides autocatalytic amyloid amplification. *Q Rev Biophys* **50**, e6 (2017).
178. N. Bengoa-Vergniory, R. F. Roberts, R. Wade-Martins, J. Alegre-Abarrategui, Alpha-synuclein oligomers: a new hope. *Acta Neuropathol* **134**, 819-838 (2017).
179. P. Alam, L. Bousset, R. Melki, D. E. Otzen, alpha-synuclein oligomers and fibrils: a spectrum of species, a spectrum of toxicities. *J Neurochem* **150**, 522-534 (2019).
180. L. Bousset *et al.*, Structural and functional characterization of two alpha-synuclein strains. *Nat Commun* **4**, 2575 (2013).
181. N. Lorenzen *et al.*, The role of stable alpha-synuclein oligomers in the molecular events underlying amyloid formation. *J Am Chem Soc* **136**, 3859-3868 (2014).
182. N. Nishida, I. Shimada, An NMR method to study protein-protein interactions. *Methods Mol Biol* **757**, 129-137 (2012).
183. L. Pieri, K. Madiona, L. Bousset, R. Melki, Fibrillar alpha-synuclein and huntingtin exon 1 assemblies are toxic to the cells. *Biophys J* **102**, 2894-2905 (2012).
184. G. Grelle *et al.*, Black tea theaflavins inhibit formation of toxic amyloid-beta and alpha-synuclein fibrils. *Biochemistry* **50**, 10624-10636 (2011).
185. X. Li *et al.*, Naturally occurring antibodies isolated from PD patients inhibit synuclein seeding in vitro and recognize Lewy pathology. *Acta Neuropathol* **137**, 825-836 (2019).
186. N. Cremades *et al.*, Direct observation of the interconversion of normal and toxic forms of alpha-synuclein. *Cell* **149**, 1048-1059 (2012).
187. W. Paslawski, S. Mysling, K. Thomsen, T. J. Jorgensen, D. E. Otzen, Co-existence of two different alpha-synuclein oligomers with different core structures determined by hydrogen/deuterium exchange mass spectrometry. *Angew Chem Int Ed Engl* **53**, 7560-7563 (2014).
188. G. M. Moriarty *et al.*, A pH-dependent switch promotes beta-synuclein fibril formation via glutamate residues. *J Biol Chem* **292**, 16368-16379 (2017).
189. X. Yang, J. K. Williams, R. Yan, M. M. Mouradian, J. Baum, Increased Dynamics of alpha-Synuclein Fibrils by beta-Synuclein Leads to Reduced Seeding and Cytotoxicity. *Sci Rep* **9**, 17579 (2019).
190. K. Beyer, M. Domingo-Sabat, A. Ariza, Molecular pathology of Lewy body diseases. *Int J Mol Sci* **10**, 724-745 (2009).
191. C. W. Shults, Lewy bodies. *Proc Natl Acad Sci U S A* **103**, 1661-1668 (2006).

192. K. Nakamura *et al.*, Direct membrane association drives mitochondrial fission by the Parkinson disease-associated protein alpha-synuclein. *J Biol Chem* **286**, 20710-20726 (2011).
193. M. S. Celej *et al.*, Toxic prefibrillar alpha-synuclein amyloid oligomers adopt a distinctive antiparallel beta-sheet structure. *Biochem J* **443**, 719-726 (2012).
194. S. Gribaudo *et al.*, Propagation of alpha-Synuclein Strains within Human Reconstructed Neuronal Network. *Stem Cell Reports* **12**, 230-244 (2019).
195. S. J. Lee, P. Desplats, H. J. Lee, B. Spencer, E. Masliah, Cell-to-cell transmission of alpha-synuclein aggregates. *Methods Mol Biol* **849**, 347-359 (2012).
196. A. Tarutani *et al.*, The Effect of Fragmented Pathogenic alpha-Synuclein Seeds on Prion-like Propagation. *J Biol Chem* **291**, 18675-18688 (2016).
197. G. Fusco *et al.*, Structural basis of membrane disruption and cellular toxicity by alpha-synuclein oligomers. *Science* **358**, 1440-1443 (2017).
198. M. Ingelsson, Alpha-Synuclein Oligomers-Neurotoxic Molecules in Parkinson's Disease and Other Lewy Body Disorders. *Front Neurosci* **10**, 408 (2016).
199. N. Cremades, S. W. Chen, C. M. Dobson, Structural Characteristics of alpha-Synuclein Oligomers. *Int Rev Cell Mol Biol* **329**, 79-143 (2017).
200. A. Rekas *et al.*, The structure of dopamine induced alpha-synuclein oligomers. *Eur Biophys J* **39**, 1407-1419 (2010).
201. C. Dong *et al.*, Structural characteristics and membrane interactions of tandem alpha-synuclein oligomers. *Sci Rep* **8**, 6755 (2018).
202. S. W. Chen *et al.*, Structural characterization of toxic oligomers that are kinetically trapped during alpha-synuclein fibril formation. *Proc Natl Acad Sci U S A* **112**, E1994-2003 (2015).
203. M. D. Tuttle *et al.*, Solid-state NMR structure of a pathogenic fibril of full-length human alpha-synuclein. *Nat Struct Mol Biol* **23**, 409-415 (2016).
204. B. Li *et al.*, Cryo-EM of full-length alpha-synuclein reveals fibril polymorphs with a common structural kernel. *Nat Commun* **9**, 3609 (2018).
205. R. Guerrero-Ferreira *et al.*, Cryo-EM structure of alpha-synuclein fibrils. *Elife* **7**, (2018).
206. M. M. Apetri, N. C. Maiti, M. G. Zagorski, P. R. Carey, V. E. Anderson, Secondary structure of alpha-synuclein oligomers: characterization by raman and atomic force microscopy. *J Mol Biol* **355**, 63-71 (2006).
207. S. Mysling, C. Betzer, P. H. Jensen, T. J. Jorgensen, Characterizing the dynamics of alpha-synuclein oligomers using hydrogen/deuterium exchange monitored by mass spectrometry. *Biochemistry* **52**, 9097-9103 (2013).
208. H. Yu, Extending the size limit of protein nuclear magnetic resonance. *Proc Natl Acad Sci U S A* **96**, 332-334 (1999).
209. K. Afitska, A. Fucikova, V. V. Shvadchak, D. A. Yushchenko, alpha-Synuclein aggregation at low concentrations. *Biochim Biophys Acta Proteins Proteom* **1867**, 701-709 (2019).
210. N. Lorenzen *et al.*, How epigallocatechin gallate can inhibit alpha-synuclein oligomer toxicity in vitro. *J Biol Chem* **289**, 21299-21310 (2014).
211. S. K. Singh, A. Dutta, G. Modi, alpha-Synuclein aggregation modulation: an emerging approach for the treatment of Parkinson's disease. *Future Med Chem* **9**, 1039-1053 (2017).

212. C. Tian *et al.*, Erythrocytic alpha-Synuclein as a potential biomarker for Parkinson's disease. *Transl Neurodegener* **8**, 15 (2019).
213. W. Kang *et al.*, Salivary total alpha-synuclein, oligomeric alpha-synuclein and SNCA variants in Parkinson's disease patients. *Sci Rep* **6**, 28143 (2016).
214. G. Vivacqua *et al.*, Abnormal Salivary Total and Oligomeric Alpha-Synuclein in Parkinson's Disease. *Plos One* **11**, e0151156 (2016).
215. M. Hashimoto, E. Rockenstein, M. Mante, M. Mallory, E. Masliah, beta-Synuclein inhibits alpha-synuclein aggregation: a possible role as an anti-parkinsonian factor. *Neuron* **32**, 213-223 (2001).
216. M. K. Janowska, K. P. Wu, J. Baum, Unveiling transient protein-protein interactions that modulate inhibition of alpha-synuclein aggregation by beta-synuclein, a pre-synaptic protein that co-localizes with alpha-synuclein. *Sci Rep* **5**, 15164 (2015).
217. K. M. Fung, L. B. Rorke, B. Giasson, V. M. Lee, J. Q. Trojanowski, Expression of alpha-, beta-, and gamma-synuclein in glial tumors and medulloblastomas. *Acta Neuropathol* **106**, 167-175 (2003).
218. V. N. Uversky *et al.*, Biophysical properties of the synucleins and their propensities to fibrillate: inhibition of alpha-synuclein assembly by beta- and gamma-synucleins. *J Biol Chem* **277**, 11970-11978 (2002).
219. J. Wei *et al.*, Enhanced lysosomal pathology caused by beta-synuclein mutants linked to dementia with Lewy bodies. *J Biol Chem* **282**, 28904-28914 (2007).
220. M. Fujita *et al.*, A beta-synuclein mutation linked to dementia produces neurodegeneration when expressed in mouse brain. *Nat Commun* **1**, 110 (2010).
221. B. Popova *et al.*, Sumoylation Protects Against beta-Synuclein Toxicity in Yeast. *Front Mol Neurosci* **11**, 94 (2018).
222. G. Yamin *et al.*, Forcing nonamyloidogenic beta-synuclein to fibrillate. *Biochemistry* **44**, 9096-9107 (2005).
223. M. Neumann, V. Muller, H. A. Kretzschmar, C. Haass, P. J. Kahle, Regional distribution of proteinase K-resistant alpha-synuclein correlates with Lewy body disease stage. *J Neuropathol Exp Neurol* **63**, 1225-1235 (2004).

Acknowledgments of published work in this thesis

Published work in Chapter 2 - Williams, J. K., Yang, X., Baum, J., *Proteomics* 2018, 18, 1800109. https://doi.org/10.1002/pmic.201800109

The work is available on-line at -

https://onlinelibrary.wiley.com/doi/abs/10.1002/pmic.201800109

RightsLink one-time use license for this dissertation: License Number 4730870043988

Published work in Chapter 3 - Yang, X., Williams, J.K., Yan, R. *et al.* Increased Dynamics of α-Synuclein Fibrils by β-Synuclein Leads to Reduced Seeding and Cytotoxicity. *Sci Rep* **9,** 17579 (2019) doi:10.1038/s41598-019-54063-8